

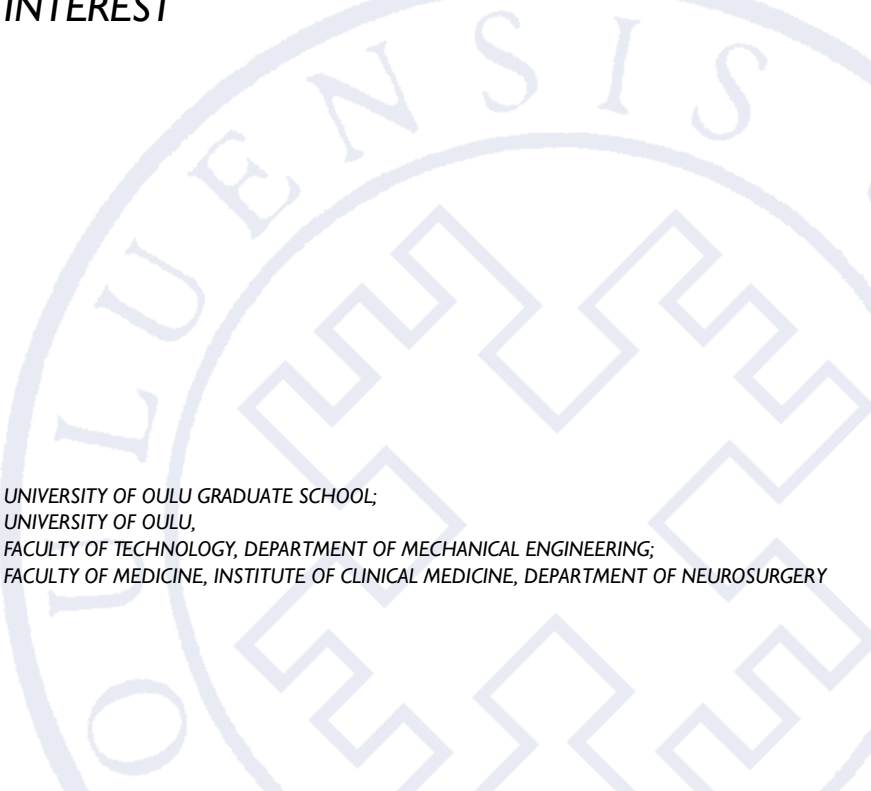
ACTA

UNIVERSITATIS OULUENSIS

Tapani Koivukangas

METHODS FOR
DETERMINATION OF
THE ACCURACY OF SURGICAL
GUIDANCE DEVICES

A STUDY IN THE REGION OF NEUROSURGICAL
INTEREST



UNIVERSITY OF OULU GRADUATE SCHOOL;
UNIVERSITY OF OULU,
FACULTY OF TECHNOLOGY, DEPARTMENT OF MECHANICAL ENGINEERING;
FACULTY OF MEDICINE, INSTITUTE OF CLINICAL MEDICINE, DEPARTMENT OF NEUROSURGERY



ACTA UNIVERSITATIS OULUENSIS
C Technica 427

TAPANI KOIVUKANGAS

**METHODS FOR DETERMINATION
OF THE ACCURACY OF SURGICAL
GUIDANCE DEVICES**

A study in the region of neurosurgical interest

Academic dissertation to be presented with the assent
of the Doctoral Training Committee of Technology
and Natural Sciences of the University of Oulu for
public defence in OP-sali (Auditorium L10), Linnanmaa,
on 21 September 2012, at 12 noon

UNIVERSITY OF OULU, OULU 2012

Copyright © 2012
Acta Univ. Oul. C 427, 2012

Supervised by
Professor Kalervo Nevala

Reviewed by
Doctor Erkki Vahala
Doctor Jani Virtanen

ISBN 978-951-42-9903-2 (Paperback)
ISBN 978-951-42-9904-9 (PDF)

ISSN 0355-3213 (Printed)
ISSN 1796-2226 (Online)

Cover Design
Raimo Ahonen

JUVENES PRINT
TAMPERE 2012

Koivukangas, Tapani, Methods for determination of the accuracy of surgical guidance devices. A study in the region of neurosurgical interest

University of Oulu Graduate School; University of Oulu, Faculty of Technology, Department of Mechanical Engineering; Faculty of Medicine, Institute of Clinical Medicine, Department of Neurosurgery, P.O. Box 5000, FI-90014 University of Oulu, Finland

Acta Univ. Oul. C 427, 2012

Oulu, Finland

Abstract

Minimally invasive surgery (MIS) techniques have seen rapid growth as methods for improved operational procedures. The main technology of MIS is based on image guided surgery (IGS) devices, namely surgical navigators, surgical robotics and image scanners. With their widespread use in various fields of surgery, methods and tools that may be used routinely in the hospital setting for “real world” assessment of the accuracy of these devices are lacking.

In this thesis the concept of accuracy testing was developed to meet the needs of quality assurance of navigators and robots in a hospital environment. Thus, accuracy was defined as the difference between actual and measured distances from an origin, also including determination of directional accuracy within a specific volume. Two precision engineered accuracy assessment phantoms with assessment protocols were developed as advanced materials and methods for the community. The phantoms were designed to include a common region of surgical interest (ROSI) that was determined to roughly mimic the size of the human head. These tools and methods were utilized in accuracy assessment of two commercial navigators, both enabling the two most widely used tracking modalities, namely the optical tracking system (OTS) and the electromagnetic tracking system (EMTS). Also a study of the accuracy and repeatability of a prototype surgical interactive robot (SIRO) was done. Finally, the phantoms were utilized in spatial accuracy assessment of a commercial surgical 3D CT scanner, the O-Arm.

The experimental results indicate that the proposed definitions, tools and methods fulfill the requirements of quality assurance of IGS devices in the hospital setting. The OTS and EMTS tracking modalities were nearly identical in overall accuracy but had unique error trends. Also, the accuracy of the prototype robot SIRO was in the range recommended in the IGS community. Finally, the image quality of the O-Arm could be analyzed using the developed phantoms. Based on the accuracy assessment results, suggestions were made when setting up each IGS device for surgical procedures and for new applications in minimally invasive surgery.

Keywords: accuracy assessment phantom, accuracy assessment protocol, image-guided surgery, medical imaging, region of surgical interest (ROSI), surgical navigation, surgical robotics

Koivukangas, Tapani, Kirurgisten paikannuslaitteiden tarkkuudenmääritysmenetelmiä. Tutkimus neurokirurgisessa kohdealueessa

Oulun yliopiston tutkijakoulu; Oulun yliopisto, Teknillinen tiedekunta, Konetekniikan osasto; Lääketieteellinen tiedekunta, Klinisen lääketieteen laitos, Neurokirurgia, PL 5000, 90014 Oulun yliopisto

Acta Univ. Oul. C 427, 2012

Oulu

Tiivistelmä

Mini-invastiivisen eli täsmäkirurgian tekniikoita ja teknologioita on alettu hyödyntää viime aikoina yhä enemmän. Tavoitteena on ollut parantaa kirurgisten operaatioiden tarkkuutta ja turvallisuutta. Täsmäkirurgiassa käytetyt teknologiat pohjautuvat kuvaohjattuihin kirurgisiin paikannuslaitteisiin. Kuvaohjattuihin laitteisiin kuuluvat navigaattorit, kirurgiset robotit ja kuvantalaitteet. Näiden laitteistojen kehittyminen on mahdollistanut tekniikkoiden hyödyntämisen monialaisessa kirurgiassa. Paikannuslaitteistojen ja robottien yleistyminen on kuitenkin nostanut sairaaloissa esiin yleisen ongelman paikannustarkkuuden määrittämisessä käytännön olosuhteissa.

Tässä väitöskirjassa esitetään kirurgisten yksiköiden käyttöön menetelmä sekä kaksi uutta fantomia ja protokollaa käytössä olevien paikannuslaitteistojen tarkkuuden määrittämiseen. Fantomit suunniteltiin sisältämään ennalta määritetty kirurginen kohdealue, mikä rajattiin käsittämään ihmisen kallon tilavuus. Fantomeita ja protokollaa hyödynnettiin kahden kaupallisen paikannuslaitteen tarkkuuden määrittyksessä. Navigaattorit käyttivät optiseen ja elektromagneettiseen paikannukseen perustuvaa tekniikkaa. Lisäksi työssä kehitetyillä menetelmillä tutkittiin prototyypivaiheessa olevan kirurgisen robotin paikannus- ja toistotarkkuutta sekä tietokonetonografialaitteen O-kaaren kuvan tarkkuuden määrittystä.

Kokeellisten tulosten perusteella työssä kehitetyt fantomit ja protokollat ovat luotettavia ja tarkkoja menetelmiä kirurgisten paikannuslaitteistojen tarkkuuden määrittämiseen sairaalaoloissa. Kirurgisten navigaattoreiden tarkkuuden määrittystulokset osoittivat optisen ja elektromagneettisen paikannustekniikan olevan lähes yhtä tarkkoja. Prototyppirobotin tarkkuus oli tulosten perusteella kirjallisudessa esitettyjen suosituksien mukainen. Lisäksi O-kaaren kuvanlaatua voitiin tutkia kehitetyillä fantomeilla. Tarkkuudenmäärittystulosten perusteella työssä ehdotetaan menetelmiä laitteistojen optimaalisesta käytöstä leikkaussalissa sekä laajennetaan niiden käyttömahdolisuksia. Tuloksia voidaan hyödyntää myös paikannuslaitteistojen kehittämistyössä.

Asiasanat: kirurginen kohdealue, kirurginen navigointi, kirurginen robotiikka, kuvaohjattu kirurgia, lääketieteellinen kuvantaminen, tarkkuudenmääritysfantomi, tarkkuudenmääritysprotokolla

To my family

Acknowledgments

This research work was carried out at the Departments of Neurosurgery and Mechanical Engineering, University of Oulu, and the Neurosurgical Research Unit, Oulu University Hospital, during 2008–2011 and completed in 2012.

I wish to express my warmest thanks to my supervisor, Professor Kalervo Nevala, D.Sc. (Tech), for his valuable support and advice in the process of this research and my doctoral studies in the field of mechanical engineering.

My sincerest thanks are due to hospital physicist Jani Katisko, Ph.D., from the Department of Neurosurgery and the Neurosurgical Research Unit for his invaluable help and advice throughout this entire project. His guidance especially in the designing of the phantoms and in assessing the accuracies of the surgical guidance devices with the phantoms proved indispensable.

The research sites of this work have pioneered intra-operative ultrasound imaging, neuronavigation and intraoperative MRI. I am grateful to the people who have been involved in this work and the staff of the Research Unit for providing the tools and facilities for this thesis. I wish to thank Senior Lecturer Yrjö Louhisalmi, Lic.Sc. (Tech), and Tomi Makkonen, M.Sc., from the Department of Mechanical Engineering, for their support in this research and in article preparation.

My thesis reviewers, Erkki Vahala, Ph.D., and Jani Virtanen, Ph.D., are also thanked for their valuable advice and guidance in finalizing this thesis.

My warmest thanks are due to my parents, my father, Professor of Neurosurgery John Koivukangas, M.D., Ph.D., and my mother, Docent of Health Economics Pirjo Koivukangas, Ph.D. (Econ), for their advice in this project and throughout my studies at the University of Oulu and the University of Minnesota in Minneapolis, USA. Unnoticeably they provided me with the basis for research especially in the field of biomedical engineering by taking me together with my siblings along on their many conference and research trips abroad since early childhood.

My siblings and friends are also warmly thanked for their continual support and interest in this research work.

Also my colleagues at Lewel Group Finland Oy, especially Mr. Jukka Kangas, CEO, and Kari Auranaho, President, are thanked in particular for providing me with necessary time for completing this thesis and for providing me with an inspiring work environment in the development of medical devices.

I am grateful to the Graduate School of Concurrent Mechanical Engineering, Academy of Finland, University of Oulu Graduate School, and University of Oulu Research and Innovation Services for financial support in finishing this thesis work. This research work was also financially supported by the following foundations: The Finnish Cultural Foundation, Emil Aaltonen Foundation, Finnish Foundation for Technology Promotion, Finnish Society of Electronics Engineers, Elektronikkainsinöörien Seura ry and the Riitta ja Jorma J. Takasen säätiö.

Most importantly I wish to thank my dear wife, Minna, and my two sons, Gabriel and Rudolf for their continual support for my work and studies and also for providing me the most important aspects of life. Their understanding on daddy's long work days, short holidays and necessary conference trips away from home has been appreciated.

Oulu, 21.9.2012

Tapani Koivukangas

Symbols and Abbreviations

3D	Three dimensional
AISI	Stainless steel
AlSiMg	Aluminum alloy
ANSI	American National Standards Institute
ASTM	American Society for Testing Materials
B0	Magnetic flux density of static magnetic field
CAD	Computer aided design
CAOS	International Society for Computer Assisted Orthopedic Surgery
CAS	Computer assisted surgery
CNC	Computed numeric control
CPU	Central processing unit
CT	Computed tomography
CTA	Computed tomography angiography
DH	Denavit-Hartenberg parameters
DOF	Degree of freedom
DTI	Diffusion tensor imaging
EMTS	Electromagnetic tracking system
FDA	Food and Drug Administration
FDA QSR-21	Quality System (QS) Regulation/Medical Device
CFR-820	Good Manufacturing Practices
fMRI	Functional magnetic resonance imaging
iCT	Interactive computed tomography
IEC	International Electrotechnical Commission
IEEE	Institute of Electrical and Electronics Engineers
IGS	Image guided surgery
IIGS	Interactive image guided surgery
iMRI	Interactive magnetic resonance imaging
IR	Infra-red
ISO	International Organization for Standardization
ISO 13485	Standard for Medical Devices quality management systems - Requirements for regulatory purposes
ISO 5725-1	Standard for Accuracy (trueness and precision) of measurement methods and results
ISO 9238	Standard for Manipulating industrial robots – Performance criteria and related test methods

kHz	kilohertz
kVp	peak kilo-voltage
LED	Light emitting diode
mAs	milliampere second
MAUDE	The Manufacturer and User Facility Experience Database, an online database of the FDA
MIS	Minimally invasive surgery
MR	Magnetic resonance
MRA	Magnetic resonance angiography
MRI	Magnetic resonance imaging
MRS	Magnetic resonance spectroscopy
mT	millitesla
NBS	Navigated brain stimulation
NDI	Northern Digital Inc., Waterloo, ON, Canada
OTS	Optical tracking system
PET	Positron emission tomography
PMMA	Thermoplastic – polymethylmethacrylate
PT	Patient tracker
PubMed	A database for biomedical literature, produced by the National Library of Medicine, USA
RF	Radio frequency
RMS	Root mean square
ROSI	Region of surgical interest
SIRO	Surgical interactive robot developed into MRI
SPECT	Single photon emission computed tomography
T	Tesla
TMS	Transcranial magnetic stimulation
TOF	Time-of-flight
X-Ray	Electromagnetic radiation

Symbols

ϵ	Root mean square error (RMS)	mm
σ	Standard Deviation	mm
μ	Variance	mm
95% CI	Confidence interval of 95%	mm
E_{ij}	Error at each corresponding accuracy assessment point	mm
E_{MAX}	Maximum error	mm

E_{MEAN}	Mean error	mm
FLE	Fiducial localization error	mm
FRE	Fiducial registration error	mm
SD	Standard deviation	mm
TRE	Target registration error	mm
X_{ij}	Error of X-component at each accuracy assessment point	mm
Y_{ij}	Error of Y-component at each accuracy assessment point	mm
Z_{ij}	Error of Z-component at each accuracy assessment point	mm

Trademarks

StealthStation Treon plus, StealthStation S7 and O-arm are registered trademarks of Medtronic Navigation Inc., Louisville, CO, USA.

Contents

Abstract	
Tiivistelmä	
Acknowledgments	9
Symbols and Abbreviations	11
Contents	15
1 Introduction	17
1.1 Background	17
1.2 Research problem and objectives.....	19
1.3 Research scope and approach.....	21
1.4 Contribution	21
2 Review of the literature	23
2.1 Surgical guidance devices in IGS.....	23
2.1.1 General definitions of surgical guidance devices	23
2.1.2 Surgical navigation.....	24
2.1.3 Surgical robotics.....	32
2.1.4 Medical imagers	37
2.2 Accuracy assessment of surgical guidance devices	39
2.2.1 Definition of accuracy of surgical guidance devices.....	39
2.2.2 Accuracy assessment of surgical guidance devices.....	46
2.2.3 Instrument tracking error theory.....	50
3 Development of advanced materials and methods based on statistical formulation for the region of surgical interest	53
3.1 Accuracy assessment tools.....	53
3.2 Accuracy assessment analysis.....	58
4 Results of accuracy assessment	63
4.1 Accuracy assessment of OTS.....	63
4.2 Accuracy assessment of EMTS.....	70
4.3 Comparison of the OTS and EMTS	74
4.4 Accuracy assessment of the SIRO	75
4.5 Spatial accuracy results of the O-Arm	80
4.6 Summary of the research contributions.....	86
5 Discussion	87
5.1 Accuracy assessment tools and methods for periodic testing of IGS devices	87
5.2 Accuracy assessment of surgical navigators	89

5.3	Accuracy assessment of the SIRO	91
5.4	Spatial accuracy of the O-Arm.....	94
6	Conclusions	95
	References	99

1 Introduction

1.1 Background

Minimally invasive surgery (MIS) has been developed especially during the last 20 years for use in the operating room. It is largely based on navigation, that is, it uses virtual imaging data registered to the patient to guide surgical procedures (Howe & Matsuoka 1999, Zoppi *et al.* 2010, Stiehl *et al.* 2007, West & Maurer Jr. 2004).

The technological advance of computers and surgical planning has rapidly increased the routine use of surgical guidance devices. Especially the period of last few decades has been an era of major breakthrough inventions for safer operations. Image guided surgery (IGS) is now a routinely used technique in operations linking image data to the patient anatomy or, in the case of endoscopic devices, following visual images displayed by these instruments.

Surgical guidance devices covered in this thesis are navigational tracking systems, robots and an imaging scanner. The main advantage reached with these surgical guidance devices is that the surgeon can perform operations closer to sensitive structures in the patient. Also the incisions can be minimized and tailored to the operation zone. This has led to more error-free operations and to shorter postoperative recovery times (Alexander *et al.* 1995, Knappe *et al.* 2003, Koivukangas *et al.* 1993, Simon 1997, Russell & Joskowicz 2009). The adaptation of these surgical navigational techniques to operations has also led to the concept of image guided surgery (IGS). IGS is usually based on preoperative image data sets (Knappe *et al.* 2003) meaning that the surgeon has to account for changes that occur during operation. To make these errors smaller another method has also been developed. This method is called IIGS (Interactive Image Guided Surgery) (Beaulieu *et al.* 2008). This technique is otherwise similar to IGS, but during operation new images of the patient are taken as many times as necessary (Knappe *et al.* 2003). With IIGS, the survival rates have been reported to increase significantly (Hill *et al.* 2000, Hosoda *et al.* 2011, Kubben *et al.* 2011, McGirt *et al.* 2009, Nimsky 2011, Sanai & Berger 2008).

Prior to the adoption of IGS, operations were performed with the aid of pre-operative images on a light box viewer or computer screen for finding the disorders in human anatomy. The first major discovery in medical imaging was the research done by Wilhelm Conrad Röntgen on November 8, 1895, when he

found the feasibility of X-ray imaging by unintentionally scanning his wife's hand (Fig. 1.). The use of X-ray imaging was later adapted to finding anatomical disorders, e.g. fractured bones, in the human anatomy. After this experiment, it took a few decades for professionals to understand the great possibilities and importance of pre-operative images. This led to the development of the new imaging modalities. The later advancement of image scanners, such as computed tomography (CT) and magnetic resonance imaging (MRI), was a key step in the development of IGS systems. Even though the images could be retrieved and scanned on a computer display, there still remained the problem of linking this image data to the human anatomy.



Fig. 1. The first X-Ray image of human anatomy taken by Wilhelm Conrad Röntgen in 1895 (NASA 2012).

Surgical navigation can be described as a method for linking a 3D object (the patient) and the surgical instrument to image data. This image registration to the object is the basis for surgical navigation. Through this linkage any instrument used can be precisely bound to the navigational setting. The view of the 3D-model of the patient data refreshes as the navigator is moved on or within the patient. Thus the surgeon can locate the disorder e.g. brain tumor inside the skull

before opening the head. This has been a great achievement, e.g., in patient operations. For example in tumor removing operations, the size of the surgical opening has often diminished from the size of a fist to the size of a fingertip (Fischer 2005, Knappe *et al.* 2003, Wiles *et al.* 2004).

As the use of surgical guidance devices rapidly increased, a variety of technologies enabling this procedure were developed (Grunert *et al.* 2003, Kwartowitz *et al.* 2006, Simon 1997). These guidance devices may be divided to three main categories, namely surgical navigators, surgical robots, and medical imagers.

Surgical navigators are classified by their instrument tracking system. The basis for current surgical navigators has been the classical stereotactic frame (Grunert *et al.* 2003). Navigators based on mechatronic digitizers were the first devices that were used for operation guidance (Watanabe *et al.* 1987, Koivukangas *et al.* 1993). Since then navigators based on the electromagnetic tracking system (EMTS) and the optical tracking system (OTS) have been adopted as the main tracking modalities.

Surgical robots are categorized using a functional classification and technological classification depending on the nature of the manipulator. The functional classification includes the following three classes: dexterity enhancement, precision localization and precision manipulation. The technological classification is divided into the following three aspects: autonomous, supervisory and teleoperated (Madhavan *et al.* 2002).

Modern volumetric surgical imaging for IGS is primarily based on three imaging techniques, CT (computed tomography), MRI (magnetic resonance imaging) and US (ultrasound). These imaging modalities have complementary rather than competing features (Alakuijala 2001, Chen & Pelizzari 1995). CT clearly shows skeletal anatomy, while MRI and US provide information on the soft tissues (Katisko 2012).

Quality regulations such as the ISO 13485 and FDA QSR-21CFR-820 together with local and international laws have been set for the medical device industry. New medical devices undergo extensive testing and approval processes before the use of these devices is actually approved for the market.

1.2 Research problem and objectives

Because of the large variation in guidance device technologies and applications, manufacturers have not agreed on standardized methods for accuracy assessment

of surgical guidance devices (Clarke *et al.* 2008, Haidegger *et al.* 2010, Kroneif *et al.* 2011, Stiehl *et al.* 2007, West & Maurer Jr. 2004, Wiles *et al.* 2004). Research on accuracy analysis and standardization has been called for by international groups and standardization organizations (Stiehl *et al.* 2007, Wiles *et al.* 2004). Some accuracy assessment methods can be found in the literature, but they all have their own protocols and accuracy assessment tools for unique applications. Thus, the accuracies between the systems with these results are not directly comparable. Earlier studies related to this topic concentrated on the accuracies of these devices in general, providing information on the devices in the laboratory environment. The most relevant standard for the purpose of accuracy assessment of IGS devices was just recently published by the ASTM (American Society for Testing Materials) in January 2011 (ASTM 2011). Since the standard was focused on orthopedic procedures, there remain open questions for applying it to other fields, e.g. neurosurgical procedures, and to scanners, such as the O-Arm (Medtronic Inc., Louisville, CO, USA). Also, ASTM realized that their standardization protocol is preliminary and leaves open the questions of phantom design. Their assessment protocol is similar to that of the present study, which was started in 2008.

Also, based on the extensive development and accuracy testing of several surgical navigation methods at the Department of Neurosurgery, University of Oulu, the need for in-hospital accuracy assessment tools and methods was realized as each phase of development since the early 1990's required customized accuracy assessment methods.

This thesis concentrates on the technical accuracy assessment of surgical guidance devices in detail. It gathers information on the accuracies of the optical tracking system (OTS) and electromagnetic tracking system (EMTS) and the image quality of the O-arm. Also the development and testing of an MRI compatible robot is discussed. This thesis presents the tools and methods for universal accuracy assessment that can be applied for all surgical guidance devices enabling IGS.

IGS involves the following possible error sources: (Alakuijala 2001, Grunert *et al.* 2003)

1. Technical accuracy
2. Registration accuracy
3. Application accuracy.

Since this thesis concentrated on the technical accuracy of IGS devices, and registration accuracy dependence of the imager, specific objectives for this thesis were (1) to design an accuracy assessment phantom with enough test points for assessing the accuracies of the IGS guidance devices applied to the region of surgical interest (ROSI) and manufactured using imaging scanner compatible materials; (2) to design a technical accuracy assessment protocol according to which the devices are tested; (3) to analyze the technical accuracies of the optical tracking system (OTS), electromagnetic tracking system (EMTS), and a surgical robot that was developed in a joint research project between the Technical Research Center of Finland (VTT) and the University of Oulu (Heikkilä *et al.* 2012, Koivukangas *et al.* 2012, Virtanen 2006); and (4) to use the developed phantoms to detect the spatial accuracy of a commercial surgical 3D CT scanner, the O-arm.

1.3 Research scope and approach

This thesis addresses the issues regarding the different terminologies, definitions, validation methods and analysis of accuracy by evaluating the used surgical guidance devices with the developed accuracy assessment phantoms and protocols. The results are also presented in a uniform manner providing the means for quick and comprehensive comparison between the different IGS devices.

To address the objectives set for this thesis, the problems were approached by determining the region of surgical interest (ROSI) for which accuracy assessment phantoms and protocols were developed, and by investigating the accuracy patterns and trends using these tools and methods. This was done by analyzing the collected data from the devices and presenting the results in 3D-surfaces, histograms, sequence plots and directional analysis. Two special accuracy assessment phantoms and protocols for this purpose were designed and developed. The phantoms consisted of three levels and 147 accuracy assessment points each.

The analyzed data was collected during 2008–2011 in various experimental settings.

1.4 Contribution

This thesis presents methods for accuracy assessment of surgical guidance devices based on experiences with the advanced methods using two special phantoms and accuracy assessment protocols developed for this purpose

(Koivukangas *et al.* 2009, Koivukangas & Katisko 2010). The motivation of this study was to find a way to periodically verify, in the real-world hospital setting, the technical accuracy of surgical navigators and surgical robots in the region of surgical interest (ROSI). Specifically, the geometrical relation between the camera pair of OTS navigators and the scene was determined.

Two commercial navigators and a prototype surgical robot were used as the surgical guidance devices assessed using the presented methods and tools. The study showed the localization error trend of the assessed surgical navigators and prototype surgical robot, and the direction in which the error tended to be highest. Finally, a study of the spatial accuracy of a commercial CT scanner was conducted utilizing the developed phantoms.

These results are important when setting up the operating room (OR) for operations involving IGS devices. The accuracy assessment protocol together with the phantom also proved to be a suitable way for periodic accuracy analysis of the studied devices in the hospital setting.

The author of this thesis was primarily responsible for designing the accuracy assessment phantoms and protocols and for the accuracy analysis. The author was also a researcher in the robot project (SIRO), to which the technical accuracy assessment methods were applied (Koivukangas *et al.* 2012).

2 Review of the literature

“Medicine is a science of uncertainty and an art of probability.”

Sir William Osler, Canadian physician

This chapter introduces the basis of the thesis with state-of-the-art devices and methods. Section 2.1 is a general overview of image guided surgery devices. Section 2.2 concentrates on the accuracy assessment of surgical guidance devices.

2.1 Surgical guidance devices in IGS

This section deals with the basic equipment in surgical guidance devices, the phenomena behind the techniques, a comparison of the accuracies and the use of the systems as defined in the literature. Section 2.1.2 deals with surgical navigators and Section 2.1.3 with MRI compatible surgical robots in use today. Finally, Section 2.1.4 introduces the commonly used imaging scanners.

2.1.1 General definitions of surgical guidance devices

Surgical navigators and robots are considered as surgical guidance devices for image guided surgery (IGS) in this thesis. The use of these devices has seen rapid growth in users among surgeons. Surgical navigation can be described as a method of linking image data to a 3D object (the patient) and the surgical instrument. This image registration to the object is the basis for surgical navigation. Through this linkage the instrument used can be precisely bound to the navigational setting. The view of the 3D-model of the patient images refreshes as the navigator is used in the patient. The surgeon can locate the disorder, e.g., brain tumor inside the skull even before opening the head. This has been a great achievement in patient operations. For example, in tumor removing operations, the size of the surgical opening has often diminished from the size of a fist to the size of a fingertip (Fischer 2005, Knappe *et al.* 2003, Wiles *et al.* 2004).

The classification of surgical guidance devices studied in this thesis consists of three main categories:

1. Surgical navigators, which are classified by their method of determining the position of the instrument in space.
2. Surgical robots, which are categorized by their functional and technological classification.
3. Medical imagers, which are classified by the physics behind image scanning.

The development and integration of other operating room equipment, especially the surgical microscope (Adams *et al.* 1996) and imaging systems including ultrasound (Galloway *et al.* 1993, Koivukangas 1984) will also affect the choice of IGS localization modality (Alakuijala 2001).

2.1.2 *Surgical navigation*

Surgical navigators are also called frameless navigation systems. This term is adopted from earlier localization technologies, especially stereotactic localization, that uses a frame with position guides. The idea behind frameless IGS is to see the tip or axis of the navigated instrument in the corresponding image data without the need for a stereotactic frame for calculation (Grunert *et al.* 2003, West & Maurer 2004). The purpose of surgical navigators in intraoperative use is to provide the surgeon with real-time information on the location of the surgical tools with respect to the anatomy during surgery. The goal is to improve the surgeon's hand/eye coordination in the region of surgical interest (ROSI), thus improving the accuracy of surgical operations (Russell & Joskowicz 2009). The basic components of surgical navigation systems are (after Russell & Joskowicz 2009, Schneberger 2004):

1. A real-time tracking system that follows the surgical instruments with respect to the patient images
2. Surgical tools and reference frames that enable the tracking
3. Displays that show the intraoperative situation
4. A computer system that integrates the information.

Navigation uses images that are based on the surgical procedure. The images are transferred preoperatively in most cases, but as mentioned earlier, in the case of IIGS new image data may be taken intraoperatively (Galloway *et al.* 1993, Knappe *et al.* 2003). Figure 2 shows a common IGS procedure of the studied surgical navigators as a step-by-step diagram.

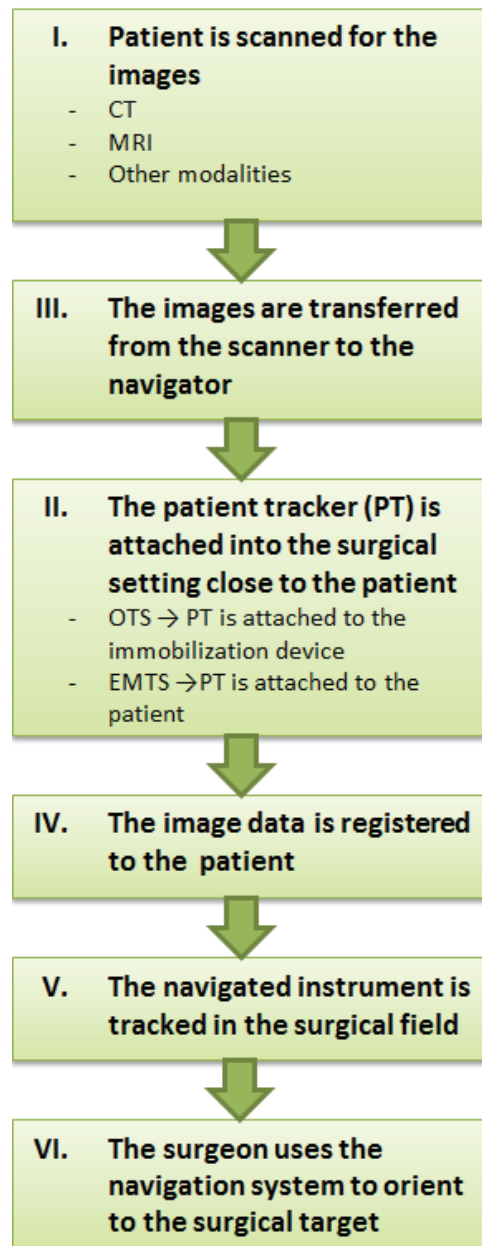


Fig. 2. The procedure of surgical navigation.

Navigators are classified by the nature of the tracking system. The optical tracking system is the most commonly used tracking modality (Fischer 2005, Schneider & Stevens 2008, Birkenfeller *et al.* 2008). In IGS it has become the method of choice for a variety of surgical procedures (Chung *et al.* 2004). The OTS consists of a receiver unit with two or more cameras and markers that are calibrated to the system. In the IR-based OTS technique, the infrared cameras are set to follow IR reflections from passive or IR emission from active markers on the instruments and the patient tracker (PT). An optical band-pass filter is set to eliminate all ambient light of other wavelengths, thus making identification of the markers reliably simple. As the distance between the markers and the cameras changes with respect to the PT, the place and the orientation of the instrument with respect to the patient is calculated and shown on the display. Usually the PT with the markers is attached to the patient directly or via the head holder, thus immobilizing the reference system (Chung *et al.* 2004, Katisko 2012, Taylor & Kazanzides 2007, West & Maurer Jr. 2004). This procedure is presented in Figure 3 (After Taylor & Kazanzides 2007).

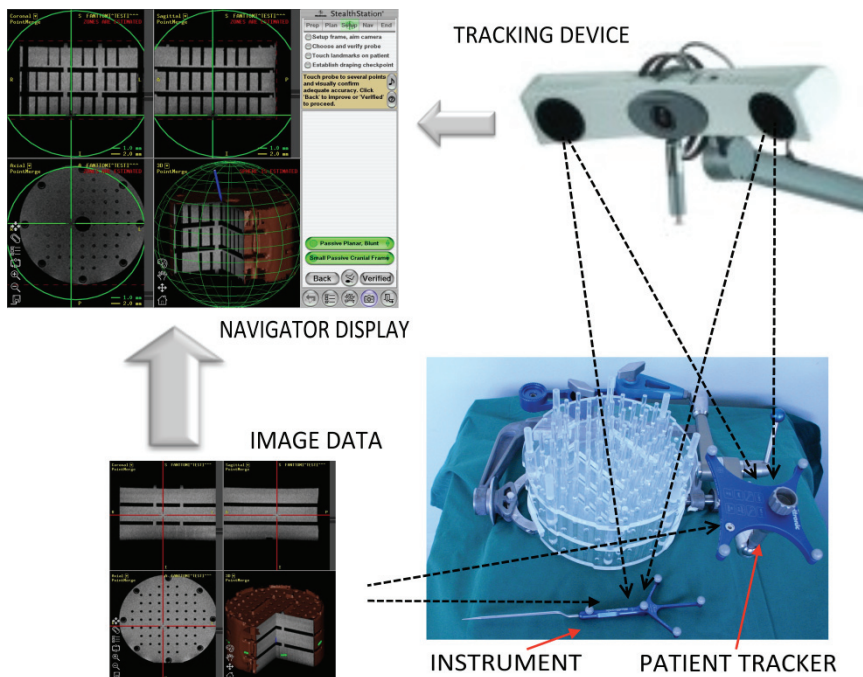


Fig. 3. Surgical navigation procedure setup.

A typical camera model with two infra-red cameras is illustrated in Figure 4. This figure shows the dependence on the camera placement of the area that the camera views cover. The larger the intersecting view area, the larger the working area and thus the more accurately the used instrument's movements may be followed using the markers. The image also shows the dependence between the two camera coordinate systems and the working volume. In the Figure, 'a' and 'b' represent the cameras' first nodal points to their common viewing center and ' α ' represents the angle between the cameras. The camera model is presented in Cartesian coordinates in such a way that the y-axes are coincident with the optical axes representing the longitudinal distance from the camera to the navigated objects; x-axes represent the lateral components in the camera coordinate systems. Z-axes represent the view up vectors and thus the vertical parameters in the accuracy assessment analysis.

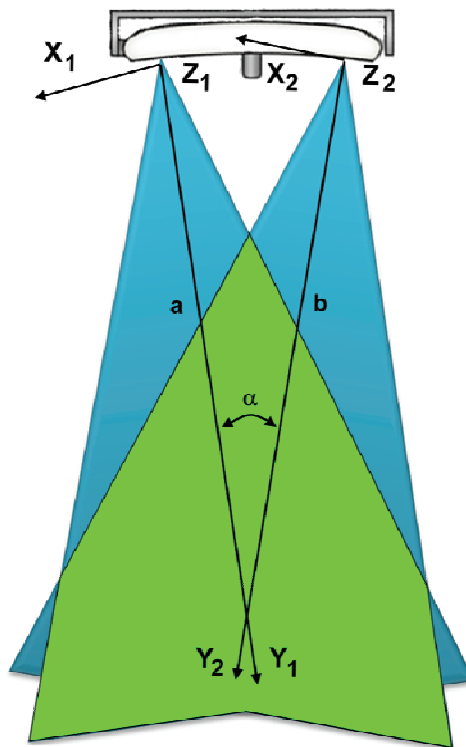


Fig. 4. A typical camera model of the OTS with two IR cameras (After Madritsch 1996).

There are two optical navigation tracking systems, the so-called active and passive systems. In the active system, tracking diodes generate light that is sensed by the camera. In the passive systems, reflecting spheres, called fiducials, reflect the light generated by the infra-red camera. The difference in the accuracies of these two methods has been shown to be minimal (Wiles *et al.* 2004). The setup for the active system involves wired connections to the patient tracker and the instrument. There are also tracking devices that merge both systems (Chung *et al.* 2004, Frantz *et al.* 2003, Katisko 2012, Schneberger 2002, Wiles *et al.* 2004). Figure 5A illustrates an optical tracking modality using passive markers. As seen in the picture, the fiducial markers reflect the infra-red waves produced by the receiver device. Figure 5B shows the tracking modality using active diodes that send their own light which the camera is set to follow.

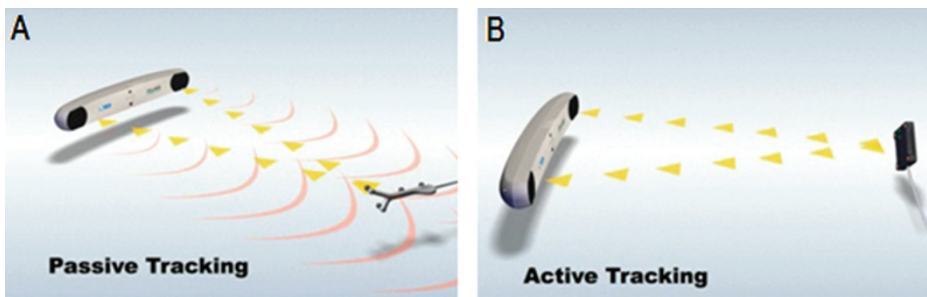


Fig. 5. Optical navigation techniques. The passive tracking system (A) where the infra-red waves produced by the camera reflect from the reflecting spheres, and the active tracking system (B) where the diodes of the patient tracker send their own waves that the camera is set to follow (NDI Digital 2012).

Superior maneuverability is gained with the passive optical tracking system, because the instrument used is wireless and frameless (Vahala *et al.* 2001, Birkenfeller *et al.* 2008). Also, lightness of weight together with linearity, stability and accuracy are clear advantages of the system (Birkenfeller *et al.* 2008, Katisko 2004, Vahala *et al.* 2001). This makes it possible for the surgeon to use the instruments more comfortably. The greatest setback with the optical tracking system is that the systems are obtrusive and require a clear line-of-sight between source and detector (Chung *et al.* 2004, Katisko 2004, Schneider & Stevens 2008). Possible error sources for the accuracy of the OTS include lens and imaging distortions and rough handling (Wiles *et al.* 2004). Most of the active OTS devices are partially wired because of the need of energy for the active LEDs.

Exceptions to the common active OTSSs are the navigators by Stryker Inc. (Kalamazoo, MI, USA). The Stryker navigators, while being active, are wireless.

Electromagnetic tracking system (EMTS) based navigation is another widely used method. It has been used increasingly within the last few years (Birkenfeller *et al.* 2008, Chung *et al.* 2004, Frantz *et al.* 2003, Hummel *et al.* 2006, Schicho *et al.* 2005, Schneider & Stevens 2005). The system consists of a field generator that produces a magnetic field and an instrument as a sensor with one or more coils that induce voltage in the presence of a changing magnetic field. The position and orientation of the instrument are calculated using these induced voltages by the measurement system of the device (NDI 2012). The system also has a computer control unit between the field generator and the sensor that calculates the relative position of the instrument with respect to the patient tracker. The coordinate space in which the sensor is moved is produced by a field generator. Sensors used for EMTS can provide three volumetric positions (XYZ) and depending on the number of coils, two or three orientation angles. Depending on the number of orientation angles, the system is referred to as a 5 DOF (degree of freedom) or 6 DOF tracking system. Figure 6 illustrates the basic concept of EMTS.

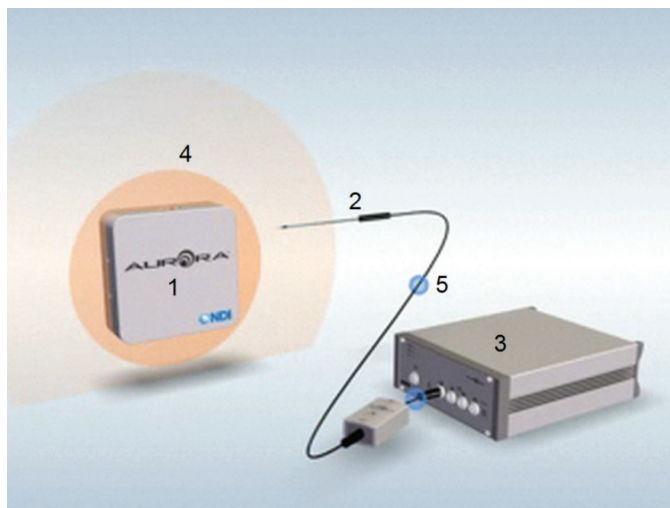


Fig. 6. An illustration of the concept of EMTS including the basic components of the system with the field generator (1), the tracked instrument (2) and the measurement unit (3). Also the produced magnetic field (4) and the detected pulses (5) of the instrument are shown (NDI Digital 2012).

The greatest advantage reached with EMTS is that it does not require a clear line-of-sight between the field generator and the sensor (Birkenfeller *et al.* 2008, Chung *et al.* 2004, Frantz *et al.* 2003, Schicho *et al.* 2005, Schneider & Stevens 2005). Another advantage over the OTS is that since the sensing coils are close to the tip of the tracked instrument, and thus closer to the point of interest, tracking inside the human body with a flexible instrument is made possible. The disadvantage with EMTS is that it is sensitive to errors especially with objects consisting of metals in the presence of the magnetic field and thus very challenging to make MRI compatible (Birkenfeller *et al.* 2008, Frantz *et al.* 2003, Schicho *et al.* 2005). This limits the widespread use of EMTS in surgical procedures. Miniaturization of the sensor coils has produced more applications to IGS in recent years (Birkenfeller *et al.* 2008, Hummel *et al.* 2006).

Figure 7 illustrates the pointer instruments of the OTS (1) and the EMTS (2). As can be seen, the basic difference in tracking of the instruments is highly affected by the tracking method. On the OTS instrument, the reflective spheres are located by the IR rays. Thus, depending on the length of the instrument, the located tip is relatively far away from the spheres that are followed by the system. On the hand, the located coils of the EMTS instrument are relatively close to the followed tip. This is the basic difference in the method of surgical navigation of the two most commonly used tracking methods.

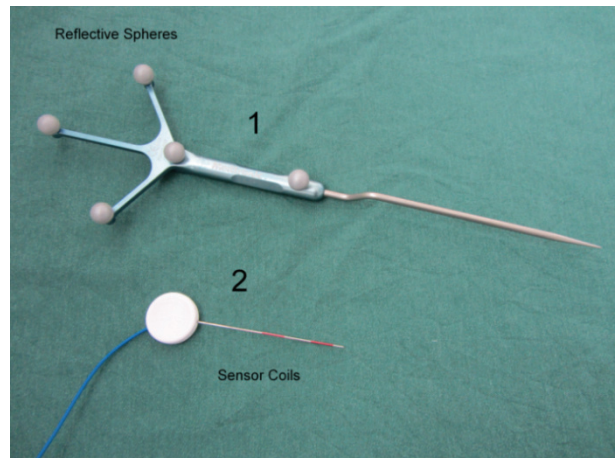


Fig. 7. The basic difference of the OTS and EMTS modalities. The instrument used in OTS modality (1) and the EMTS instrument (2).

The mechatronic tracking system is based on the so-called mechanical digitizer. The system consists of rigid segments and sensor encoded joints that are usually optical encoders or potentiometers. The sensors are calibrated so that the movement of the digitizer is sensed by the angular displacement of the segments (Watanabe *et al.* 1987, Koivukangas *et al.* 1993). The position of the base of the arm is rigid and known. As the instrument attached to the device is moved, the sensors detect the movement and thus, using forward kinematics, the location of the instrument tip (Watanabe *et al.* 1987) or the angular displacement and location of the instrument axis (Koivukangas *et al.* 1993) is known with respect to the base frame of the arm. This information is then graphically displayed on reformatted planar images.

The main advantages gained using the mechanical digitizer are accuracy with an error of 0.1–2.5 mm and no line-of-sight restriction. This makes it possible to navigate the object to the extent of the length of the arm (Schiffbauer 1997). The main setback with these systems is that they are relatively clumsy and heavy (Schiffbauer 1997). This type of tracking is the basis of most of the current surgical robots (Cleary & Nguyen 2001, Virtanen 2006). One of the newest is the MR-compatible robot prototyped at the Department of Mechanical Engineering, University of Oulu (Heikkilä *et al.* 2012, Koivukangas *et al.* 2012, Virtanen 2006).

Acoustic tracking typically uses a device that is based on ultrasound (US). It is the least used of the tracking systems. The frequencies for range detection are above the human hearing threshold at around 20 kHz. The simplest US device uses a pair of transmitter/receivers coupled to obtain distance measurement. For a 3D location the modality needs a system of three transmitters and one receiver or a system of one transmitter and three receivers (Birkenfeller *et al.* 2008, Hummel *et al.* 2006, Roberts *et al.* 1986, Wood *et al.* 2005). Acoustic tracking is based on either Time of Flight (TOF) or Phase Coherence technique for orientation and displacement determination. TOF technique uses a process of triangulation of the known speed of sound through the medium, the reflection delay and the distance difference of the receivers. The Phase Coherence technique measures the phase difference of the receiver and transmitter pulses (Wells 1977).

2.1.3 Surgical robotics

“I can't define a robot, but I know one when I see one.”

Joseph Engelberger, pioneer in industrial robotics

General overview

Surgical robotics is a field that has improved rapidly within the last 30 years (Heikkilä *et al.* 2012, Kwartowitz *et al.* 2006, Madhavan *et al.* 2002, Virtanen 2006). Within the last two decades a number of successful robotic systems have been adopted into surgical use (Haidegger *et al.* 2010, Heikkilä *et al.* 2012, Howe & Matsuoka 1999, MaRS 2010, Shiakolas *et al.* 2002, Virtanen 2006). In fact, medical robotics is the fastest growing segment in the robotics industry today (MaRS 2010). One reason for the rapid progression of robotics to surgical applications is the large technology base that has been developed in robotics research in the past three decades (Craig 1989, Khatib 1992).

Originally surgical robots were designed to perform simple tasks in ordinary operating rooms such as holding instruments and guiding them into correct positions. Robotics Institute of America has defined a robot as a re-programmable, multi-functional manipulator designed to move material, parts, tools, or specialized devices through various programmable motions for the performance of a variety of tasks (Madhavan *et al.* 2002). Another definition of a robot by Webster's Dictionary is “an automatic device that performs functions normally ascribed to humans or a machine in the form of a human.” In the beginning of robotics, the applications were for industrial use in the late 1950's and early 1960's. The robots were then adapted to other fields and most recently also to the medical device industry.

The development of robotics for surgery has experienced three main advancement waves (Madhavan *et al.* 2002). At the outset in the mid 1980's, the robots were modified from industrial robots for simple assistive manipulators. Then, at the end of 1980's new robotic applications and technologies were developed purely for the intention and needs of surgical procedures. Finally, the most recent advances in surgical robotics date back to the late 1990's as the robots were actually performing surgical procedures. The first published robot assisted closed chest bypass on the human heart was performed by surgeons at the London

Health Sciences Centre's University campus in London, UK, in 1999 (Madhavan *et al.* 2002).

The differences in human anatomy and machine characteristics are a way to understand the advantages of using robots in surgery. The improvement of robotics has led to unique capabilities for which the surgical robots may be used. The main differences between the human and a machine are accuracy, precision and repeatability to perform identical tasks (Alakuijala 2001, Ng *et al.* 1993, Howe & Matsuoka 1999). Another difference in the characteristics is that specialized manipulator design allows the robots to work through incisions that may be much smaller than those that a human would need. The robots used for IGS can accurately guide instruments deep in the human anatomy without causing harm to the body (Howe & Matsuoka 1999, Riviere *et al.* 1997). Robots may also be used for reducing the surgeon's involuntary hand movement during surgery (Riviere *et al.* 1997) and to improve manual accuracy (Alakuijala 2001, Howe & Matsuoka 1999, Kwartowitz *et al.* 2006, Riviere & Khosla 1997). The goal for the use of surgical robotics is to complement and enhance the surgeon's skills in IGS operations, but also to always leave them in control and never to replace them (Russell & Joskowicz 2009). "Surgical procedures need surgical robots – industrial robots could be hazardous" (Drake *et al.* 1991).

Surgical robots are categorized into functional and technological classifications by the nature of the manipulator (Madhavan *et al.* 2002). The functional classification includes the following three classes: (After Madhavan *et al.* 2002)

- Dexterity enhancement

The robots are controlled by a surgeon during surgery and are thus considered as slave manipulators. These types of robots may be controlled from a remote location

- Precision localization

The robots precisely locate a predetermined surgical target, for example, by using pre-operative images

- Precision manipulation

The robots perform preoperatively programmed functions instead of surgeon's direct control.

The technological classification is divided into the following key aspects: (After Madhavan *et al.* 2002)

- Autonomous
Robot control is based on preoperatively programmed plans and image data
- Supervisory
The robotic system guides the surgeon to accurately perform the operation
- Teleoperated
The robots may be controlled from a location geographically remote from the operating room.

The surgical robots may be designed and controlled under these classifications. The objectives for all surgical robotic systems are to provide better quality operations and to perform the tasks programmed accurately and safely. Some of the more specific objectives are minimal invasiveness and finer control.

As the imaging modalities have improved, so also the use of surgical robotics has been made more acceptable and the system control more accurate especially when preoperative or intraoperative images are used (Virtanen 2006).

The development of surgical robots for operational means is a potential growth area for image-guided treatment procedures. Even with the finest design and accuracy, the use of a robot for replacing a surgeon is highly unlikely to happen. Instead, the robots may be designed to serve as tools for some phases in a surgical procedure (Alakuijala 2001). Since robotic manipulators are able to do small, precise maneuvers, surgical robotic systems are a good match for MIS procedures (Kwartowitz *et al.* 2006).

The following Table includes the four most widely used surgical robotic systems and the numbers of devices sold.

Table 1. A representative list of surgical robots in clinical use. (According to Haidegger & Virk 2012).

Device and Manufacturer	Devices Sold	Intended Procedure
Neuromate, Renishaw plc., Gloucestershire, UK	~30	Stereotactic neurosurgery
MAKO RIO, MAKO Surgical Corp., Ft. Lauderdale, FL, USA	113 (07/2010)	Orthopedic procedures
CyberKnife, Accuray, Sunnyvale, CA, USA	220 (12/2010)	Non-invasive tumor procedures
da Vinci, Intuitive Surgical Inc., Sunnyvale, CA, USA	~2300 (3/2011)	Laparoscopic, thoracoscopic, endoscopic surgery

A prototype surgical interactive robot developed into MRI (SIRO)

A prototype surgical interactive robot (SIRO, Fig. 8.) was designed and developed as a 6 DOF (degree of freedom) articulated configuration manipulator with a working volume intended for use inside a MRI scanner. It was developed as a joint research project between the Department of Mechanical Engineering, University of Oulu, the Technical Research Center of Finland (VTT) and the Department of Neurosurgery at Oulu University Hospital in Oulu, Finland (Heikkilä *et al.* 2012, Koivukangas *et al.* 2012, Virtanen 2006). The kinematic structure of the robot was based on the Unimation PUMA 560, for which well-known methods for solving the inverse kinematics were available, such as those of Craig (1989). According to the classification of Madhavan *et al.* (2002), the SIRO robot can be classified as an autonomous precision localization device. The robot precisely locates a chosen surgical target based on a programmed plan.

Three joints in the robot were used for the wrist movements and three for the rest of the arm movements. The arm of the robot was 1000 mm long. The shoulder height from the base was 700 mm. Together with the arm the largest reach was 1300 mm in radius and height. The total mass of the robot was 23 kg. The mass was distributed so that the base and shoulder including the first three degrees of freedom totaled 15.5 kg and the arm and wrist 4.5 kg. The arm was balanced by attaching motors and drives for the wrist movements behind the shoulder of the robot.

The first joint counted from the base was a revolute joint with its axis coincident with the link. Power transmission system for the first DOF included bevel gears from a motor to the intermediate shaft and then worm gears to the main axis of the robot. The second and third DOFs were revolute joints with axes perpendicular to the links. Motors and ball screws were used for power transmission. The fourth DOF was a revolute joint with axis coincident with the link with power transmission including a small spur gear on the motor shaft and a large spur gear on the arm. The fifth DOF was a revolute joint with axis perpendicular to the link, and the sixth DOF a revolute joint with axis coincident with the link. These last two joints were placed at the wrist of the robot with cable drives used for power transmission from motors to the two wrist joints. Both of these joints had identical transmission systems. The motor shafts were fixed on ball screws. Cables were fixed on sliders that raced on the ball screw. The cables were also tightened on these sliders. The prototype robot (SIRO) is illustrated in Figure 8.

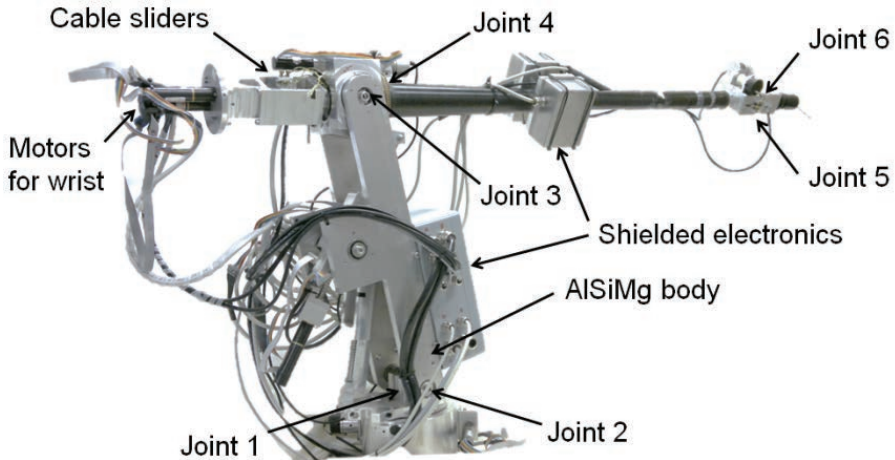


Fig. 8. The prototype surgical interactive robot developed into MRI (Koivukangas T et al. 2012, published with kind permission of Springer Science+Business Media).

Based on the MR-compatibility studies using an MR scanner (Philips Panorama 0.23 T, Philips Medical Systems MR Technologies, Vantaa, Finland), aluminum alloy AlSiMg was used as the main material of the parts (Virtanen 2006). The robot base needed to be strong and stable. As the robot base stood outside the 20 mT magnetic field line, the need for MR-compatibility for the base was low. Thus, the base structure was strengthened with an axel made of stainless steel (AISI 316). The base shaft functioned as the rotating shaft for the entire robot perpendicular to the floor. The forearm of the robot was made of carbon fiber tube. This material was verified to be MR-compatible in the tests. It was strong enough to stabilize the end effector and also lightweight (Virtanen 2006). Electric safety was achieved by shielding the electronics in MR compatible housings and by using MR compatible tubing for the cables. The safety of the instruments was also guaranteed by using MR compatible materials (Virtanen 2006).

The main reason to use intraoperative MRI during brain surgery is that image guided methods such as neuronavigation and robotic surgery require new images to be taken as the operation progresses due to changes in the surgical field, like brain shift.

However, strong static and coupling magnetic fields and radio frequency pulses produced by MR scanners produce a challenging and potentially hazardous environment. Magnetic fields exert magnetic forces and eddy currents in materials that are magnetically incompatible. This may lead to false signal

information, uncertainties in actuator control and dangerous forces acting on the robot (Madhavan *et al.* 2002, Schenck 1996). From the point of view of electromagnetic behavior and material technology, the solutions from conventional robotics are not applicable as such. In addition, there are also challenges from the conventional robotics point of view: the working space is very limited, there is limited access to this space, and results of intraoperative MR imaging need to be integrated to the work.

There has been active development of MRI compatible robotics, e.g., for biopsies of brain (Masamune *et al.* 1995), breast (Larson B *et al.* 2004) and prostate (Susil *et al.* 2003) lesions. Robots have also been under development for specific types of working space depending on the design of the MR scanner (Chinzei & Miller 2001, Tsekos *et al.* 2005). In addition, development towards a general purpose device for use within the MR scanner has been reported (Tsekos *et al.* 2008). Still, technology remains at the development phase involving prototypes few of which have been tested in clinical conditions (Gassert *et al.* 2008, Sutherland *et al.* 2008).

2.1.4 Medical imagers

Medical imaging has become a vital component of a wide range of medical applications (Hill *et al.* 2000). For IGS procedures, medical images are the main source of information (Taylor & Kazanzides 2007). Thus the advancement of the image scanners was a key step in the development of IGS systems. As imaging technologies have improved, they have been adapted from clinical diagnostic settings to preoperative surgery planning and intraoperative surgical procedures. Especially the preoperative images are used commonly for several purposes.

In pre-surgical planning, the images are necessary data. Pre-surgical planning is a key step in (I) understanding the patient's anatomy and the patient's disease, and (II) developing the desired surgical procedure path and treatment approach. The pre-surgical images are also used as the basic data in the actual IGS procedure. The use of imaging technologies has improved the quality of patient treatment significantly (Hill *et al.* 2000, Hosoda *et al.* 2011, Kubben *et al.* 2011, McGirt *et al.* 2009, Nimsky 2011, Sanai & Berger 2008).

Since IGS procedures rely largely on image data, it needs to be of high-quality to provide excellent differentiation between normal and abnormal tissues especially in preoperative planning. In the actual IGS guided procedure, the

image data also needs to provide accurate representation of the patient (Holmes III *et al.* 2008).

The imaging modalities are divided into two main categories: anatomical and functional-metabolic.

- Anatomical modalities, i.e., depicting primarily morphology, include the most commonly used techniques such as X-ray, CT, US and MRI. Some of the techniques have been developed further for new applications. Such modalities are for example: CTA (computed tomography angiography), DTI (diffusion tensor imaging), MRA (magnetic resonance angiography) and MRS (magnetic resonance spectroscopy).
- Functional or metabolic modalities, i.e., depicting primarily information on the function or metabolism of the underlying anatomy, include fMRI (functional magnetic resonance imaging), PET (positron emission tomography), SPECT (single photon emission computed tomography) and TMS (transcranial magnetic stimulation). Also a wide range of other techniques can be named under functional modalities.

The most often used imaging methods are computed tomography (CT) and magnetic resonance imaging (MRI) (Grunert *et al.* 2003). CT imaging is based on the absorbance of X-rays in the object. Thus, it is mostly used for generating a 3D image volume of patient tissue densities. CT imaging is a common imaging modality especially for spinal orthopedic procedures, skeletal anatomy in general, and with injected contrast material also vascular structure visualization (Holmes III *et al.* 2008, Goldman 2007, Zannoni *et al.* 1997). In preoperative planning, CT images have been reported to be used in nearly all disciplines of interventional procedures (Holmes III *et al.* 2008). These disciplines include cardiology (Budoff *et al.* 2006), neurosurgery (Haydel *et al.* 2000), radiation oncology (Lattanzi *et al.* 2004, Spencer 2001) and orthopedic surgery (Lattanzi *et al.* 2004). MR imaging is based on the spin effect of the hydrogen atom and thus it is mostly used for soft tissue imaging, e.g., brain imaging (Hendee & Morgan 1984). The basic phenomenon of MRI is utilized in human anatomy imaging by measuring the emission of RF energy within the varying magnetic field (Holmes III *et al.* 2008, Katisko 2012, Schenck 1996).

Specifically, the intraoperative 3D CT scanning system that was studied in this thesis, the O-arm (Medtronic Navigation Inc., Louisville, CO, USA) is a surgical, mobile 2D/3D x-ray imaging system optimized for spinal and orthopedic surgery. Scanning is based on a flat panel detector and cone-beam technology

producing 196 slices in 13 seconds in the standard mode. Pixel size is 0.415×0.415 mm with a slice thickness of 0.833 mm. The size of the scanned cylindrical 3D volume is 21 cm \times 16 cm (diameter \times length).

2.2 Accuracy assessment of surgical guidance devices

This section reviews the definitions of accuracy and the assessment of the accuracy of surgical guidance devices, concluding with the theory of instrument tracking error applied in this thesis.

2.2.1 Definition of accuracy of surgical guidance devices

“Accuracy: An unmeasurable quantity that everyone has a number for, nobody knows how they got it, and everyone wants more of.”

Neil Gossip & Richard Hu

As the use of surgical guidance devices and robotics has seen an increase in minimally invasive surgery (MIS) (Howe & Matsuoka 1999, Stiehl *et al.* 2011, Zoppi *et al.* 2010), also the need for the accuracy assessment of the IGS systems has been realized. In present operating rooms standard procedures for assuring safety have been adopted and standardized to most disciplines of medicine and engineering. Today, organizations such as the International Organization for Standardization (ISO) and the International Electrotechnical Commission (IEC) in Europe, and the Institute of Electrical and Electronics Engineers (IEEE), the American National Standards Institute (ANSI) and the American Society for Testing Materials (ASTM) are among major organizations involved in setting standards also for medical equipment. Since IGS crosses the disciplines of electrical engineering, computer science, mechanical engineering and metrology and the research is conducted transnationally, there is a lack of unified standards for the accuracy assessment of surgical guidance devices.

When assessing the accuracy of surgical guidance devices, it is important to define the terms “accuracy”, “precision” and “bias”. Also, it is important to broaden the definition of these terms when applied to different devices and applications of the guidance devices such as surgical navigators and surgical robots. Accuracy in the current literature of surgical devices reflects different attributes of a particular measurement. It may mean the standard deviation of a number of measurements from a fixed object or it may relate to the closeness of

an instrument's mean value compared to the known position. The most often used standard in validating the accuracy of surgical guidance devices are the ISO 5725-1:1994 "Accuracy (trueness and precision) of measurement methods and results" (ISO 5725) and the ISO 9238 "Manipulating industrial robots – Performance criteria and related test methods" (ISO 9238), which define accuracy as the closeness of agreement between a test result and the accepted reference value.

Repeatability is an accuracy analysis method for robots. Repeatability is defined as the ability of the robot to perform the planned motion and finish at the same point. This term reflects the precision of the machine, but not the accuracy of the system (Stiehl *et al.* 2007). Precision is a term defining a number of measurements whose standard deviation is relatively small, although the mean of these measurements is not necessarily close to the true value. Bias is the number indicating the difference of the true value and the precision value. Thus, if the mean of the precision corresponds to the true value, the system is unbiased.

Figure 9 illustrates the differences in the terms accuracy and precision. On the first image on the left, the points are scattered on the edge of the target. Thus, the system is neither accurate nor precise. On the second image the points are well grouped on the outer edge of the target. This shows that the system is precise but not accurate. On the third image, the points are accurately close to the center of the target, but there is high scatter between the points. The system is thus accurate but not precise. On the last image the points are grouped well in the center of the target. This system is accurate and precise. This Figure set illustrates the basic principles of accuracy assessment of surgical guidance devices.

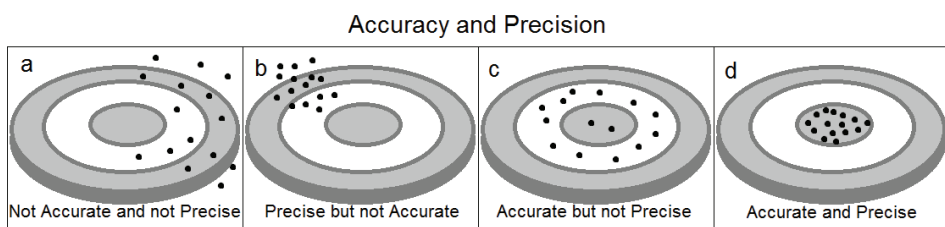


Fig. 9. An illustration of the different aspects of accuracy terms used in IGS.

For surgical navigators, only the absolute position accuracy is considered relevant. In surgical robotics also repeatability is considered as a main application accuracy indicator (Mooring & Pack 1986). For robots in general, usually the repeatability is higher than the absolute position accuracy.

In surgical navigation and robotics, the term “accuracy” needs to be divided into three types of accuracies with the following arrangement: (Alakuijala 2001, Grunert *et al.* 2003, Haidegger *et al.* 2010)

1. Technical accuracy (typically 0.1–0.6 mm)
2. Registration accuracy (typically 0.2–3 mm)
3. Application accuracy (typically 0.6–10 mm).

Technical accuracy indicates the reliability of the navigational device’s own placement definition. It applies to the surgical guidance device’s mechanical accuracy and describes the average error of the given component in operational use (Grunert *et al.* 2003). Technical accuracy takes into account also the random errors such as mechanical and electrical compliances, friction and hardware problems, and inadequate control that may all result in lower technical accuracy. Technical accuracy is thus highly affected by the mechanical quality of the used devices. These errors and limitations are the compliances of the overall accuracy that may be improved by engineers before using the devices for surgical procedures. For these reasons, the technical accuracy of the navigational devices should be higher than the registration accuracy (Grunert *et al.* 2003).

Registration accuracy is related to the coordinate transformation of the object to the navigator image set. Registration accuracy is highly affected by the technical accuracy of the device together with imaging device restrictions, the type and form of markers used, displacement of the markers and determination of the center of the markers. The accuracy is also affected by the resolution of the used medical images, movement of the patient in the scanner gantry, the type of imaging method used and the slice thickness of the image data. These are aspects that should be taken into account when setting up the operational procedure. By using the correct imaging parameters and by choosing the applicable registration technique, the registration errors may be decreased (Grunert *et al.* 2003, Stiehl *et al.* 2007).

Image artefacts can affect the diagnostic quality by decreasing the spatial accuracy making them useless for diagnosis and thus for use in IGS procedures (Barrett & Keat 2004, Erasmus *et al.* 2004). It is necessary to understand possible causes for image artefact and also to have useful tools for inspecting the spatial accuracy. Image artefact is a term applied to any systematic difference between the images and the scanned object; some affect the diagnostic quality and some may be confused with pathology (Barrett & Keat 2004, Erasmus *et al.* 2004). The origin of different artefact of CT imaging may be categorized into: (I) physics-

based resulting from the physical process in the acquisition of CT data, (II) patient-based artefact including patient movement and metallic objects in the patient or in the close proximity, (III) scanner-based artefact resulting from the imperfections in the scanner, and (IV) helical, multi-section and cone beam artefact produced by image processing (Barrett & Keat 2004). Magnetic resonance imaging (MRI) may also be affected by a number of different artefacts. In particular, MRI is sensitive to spatial inaccuracies. The inaccuracy may originate from the structure of the object, eddy currents in conductive objects and scanner structures and other susceptibility issues of the scanned object caused by air-tissue interface and water-fat interface (chemical artefact) (Schenk 1996).

MR artefacts are classified as (I) sequence artefact, (II) reconstruction algorithm artefact, (III) field artefact and (IV) noise artefact. All of these four main artefact sources originate either from the device hardware or from the patient or as a total sum of both (Bellon *et al.* 1986). Most common artefacts are radiofrequency (RF) related, external magnetic field related and gradient field related. Other artefacts include surface coil, bounce point and asymmetrical brightness artefacts. External magnetic field (B_0) inhomogeneity artefacts occur when an object is brought inside the scanner. The result of B_0 artefact is seen as different tissues mismapping in the images. This is caused by the difference in the magnetic field and the object homogeneity (Erasmus *et al.* 2004).

Application accuracy includes the overall error of the entire procedure. This accounts for the technical accuracy of the device and the registration accuracy. It shows how reliably the pointer tip of guidance device in physical space corresponds to the anatomic position in the medical images during an operation. It answers also to the loss of correspondence between the images and the anatomical structure during procedures. Application accuracy limitations are due to technical inaccuracy, registration inaccuracy, and deformations in the anatomy of the patient during operation, such as brain shift. Application accuracy is the most unpredictable type of accuracy in guidance device aided procedures. For improving the application accuracy, while using more accurate guidance devices, medical imagers and registration techniques, other techniques have been introduced. A model updating method based on gravity-induced brain deformation was introduced by Miga and co-workers (Miga *et al.* 1997). The experiments showed that the error accounted for by brain-shift was improved from 5.7 mm to 1.2 mm. One of the more recent operational techniques is to use intraoperative MRI, CT or US images and replace or match these images with the pre-operative data sets (Koivukangas *et al.* 1993, Mösges & Schlöndorff 1998). This helps to

take into account the deformations in the anatomical structures and thus provides more accurate locations of the structures to be removed and the locations of the critical anatomical structures surrounding the disorder (Grunert *et al.* 2003).

A special case of OTS guided interventional procedure has been introduced by Ruohonen & Karhu (2010). The OTS was used as a guidance device for transcranial magnetic stimulation, the Nexstim eXimia NBS system (Nexstim Oy, Helsinki, Finland). They reached a total application accuracy of the system of 5.7 mm. In the experiment, they found that the OTS accuracy was 1.6 mm.

Widmann *et al.* (2012) have also recently written a comprehensive review article based on a PubMed literature search from 1995–2010 regarding application accuracy of IGS devices. Mean total errors ranged between 4.4–5.4 mm for brain biopsies and 2.0–3.2 mm for depth electrode placements. However, application accuracy is outside of the scope of the present study which centered on technical accuracy. The latter must be assured as one of the physical bases of application accuracy.

In accuracy assessment of surgical guidance devices, technical accuracy is the segment of accuracy that can be improved solely by better equipment. By developing devices that have higher standard components and more confident operation, the accuracy of the device may be improved dramatically. Technical accuracy is also possible to be assessed and improved before the actual operation. Registration accuracy may be improved by correct imaging modality and optimal imaging parameters. Also the decision of registration technique affects the overall accuracy. The acceptable range of error and tolerable accuracy of a device depends on the procedures for which surgical guidance devices are used (Alakuijala 2001). The tolerable error range is naturally affected by the surgical scene and possible devices and instruments used. For example, if the neurosurgeon has a clear view of the operation zone and the object operated, the need for accuracy of the guidance devices is lower than in the case of an object deep in the brain. Also, if endoscopic cameras are used, the accuracy requirement may be considered to be lower. Thus, it is unnecessary to give a number for accepted application accuracy in millimeters. However, the accuracy of the devices is intended to be improved and maintained in general. To improve the accuracy of the surgical guidance devices and thus make the IGS procedures safer, Nolte and coworkers have listed usability requirements for a position sensing and tracking device (Alakuijala 2001, after Nolte *et al.* 1994):

1. Established surgical procedures should be principally preserved
2. The existing surgical tool set should remain the same
3. The system's technical accuracy should be at least one order of magnitude better than the desired overall accuracy
4. The positioning system should be fast enough to allow real-time instrument control and visualization in the medical image.

These are basic rules under which the IGS will remain under high standards and the operation will remain safe. The rules also state the most important factors that define the accuracy of surgical guidance devices. In general 3–5 mm RMS accuracies for indirect IGS are considered acceptable, but for IG neurosurgery the recommendation is 2 mm. For direct IGS assisted with a robot, the recommendation for the RMS accuracy is less than one millimeter (Grunert *et al.* 2003).

In the current literature and publications of accuracy assessment for IGS systems, there is a wide variety of experimental result analyses. This was realized already at the CAOS International Society annual meeting held in Chicago in 2004 where a group of leading engineers and physicians began the process of writing standardization guidelines (Clarke *et al.* 2008, Haidegger *et al.* 2010, Kroneif *et al.* 2011, Stiehl *et al.* 2007, Wiles *et al.* 2004). International organizations such as the American Society for Testing and Materials (ASTM) and other international organizations are making efforts on standardizing IGS devices accuracy assessment (Haidegger *et al.* 2010, Kroneif *et al.* 2011, Stiehl *et al.* 2007, Zoppi *et al.* 2010). As a result of the CAOS annual meeting in Chicago, ASTM initiated a standards committee (ASTM F04.05) in 2004 under the title "*Standards Practice for Measurement of Positional Accuracy of Computer Assisted Surgical Systems (CAOS)*" with the goal of developing an international standard for metrology, validation and performance of CAOS systems (Clarke *et al.* 2008, Haidegger *et al.* 2010, Stiehl *et al.* 2007). In 2007 ASTM F04.05, a committee initiated by the ASTM for standardizing positional accuracy of computer assisted orthopedic surgical systems (CAOS), defined and developed a draft generic measurement board. Later, multi-institutional technical committees have presented white papers and articles calling for tools for standardizing many applications and areas of IGS and CAS (Chiao *et al.* 2008, Haidegger *et al.* 2010, Kazanzides 2006, Kroneif *et al.* 2011). The first draft, presented in 2007, deals with the localizer functions of navigation systems of OTS, EMTS and mechanical digitizers.

Based on the efforts and with support from the ASTM, a multi-national technical committee presented a white paper calling for the standardization of many areas of IGS (Clarke *et al.* 2008, Haidegger *et al.* 2010). The areas for need of standardization include especially the following areas of medical devices, which are also studied in this thesis:

- Computer assisted navigation and surgery
- Surgical robotics
- Medical imaging.

This process of standardizing the accuracy assessment of the IGS devices led to the ASTM standard F2554-10 that was approved and published in 2011 (ASTM 2011). As the standard focuses on orthopedic procedures and mainly in spinal navigation, the proposed phantom is roughly planar. Thus there remain open questions regarding accuracy assessment of IGS systems in general. In the standard, a phantom is presented, but the design of the used phantom was left for consideration as normative information to investigators. The draft phantom consisted of a 150x150x20 mm base plate with two additional levels with a single level at a 30° slope (Nebraska University phantom, Figure 10). Thus, the proposed phantom may be suitable for spinal procedures accuracy assessment, but since the basis of the phantom is a board, volumetric analysis is difficult to perform.

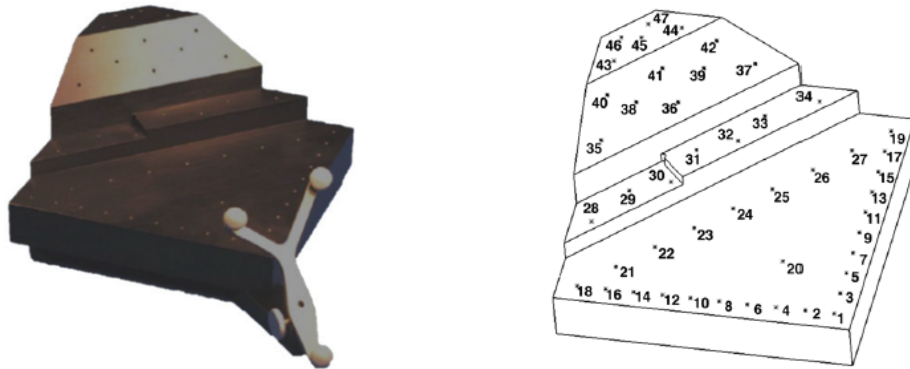


Fig. 10. The draft phantom in the ASTM F2554-10 (ASTM 2011).

The accuracy assessment holes of the Nebraska phantom were machined using a vertical computer numerical controlled (CNC) machine to the depth of 1.2 mm. As the phantom was machined from stainless steel with a total of 47 accuracy assessment points, there are limitations for its application as a universal accuracy

assessment tool for IGS devices. The phantom cannot be used for comprehensive volume or depth analysis due to the limited spatial arrangement of the holes. Also, the material chosen, namely stainless steel is not ideal for assessing the accuracy of medical imagers.

In this thesis, the ISO 5725-1 standard is applied for the accuracy analysis of surgical navigators and these standards together with ISO 9238 for the accuracy assessment of the prototype surgical robot. Accuracy relates to the terms absolute position accuracy and repeatability. Absolute position accuracy is a measure of the device's pointer tip in space with respect to the calculated coordinates and is defined as the qualitative assessment of the measured value to the true measured value. Thus, the use of a verified phantom with known coordinates for accuracy assessment is accepted as a method of verification of the overall accuracy analysis. The ASTM F2554-10 was used as a comparative tool in the analysis of the presented methods.

2.2.2 Accuracy assessment of surgical guidance devices

Accuracy assessment of medical devices has been a vital part of the product development of surgical guidance devices. The accuracy of the used surgical guidance device during operations has to be verified. The surgeon needs to know if the navigator is still as accurate as when the device was built or how much the accuracy has decreased and in which direction, i.e. horizontal or vertical. This gives the surgeon a more comfortable state of mind and makes the operation safer. To address this issue surgical navigator companies give a range of error in which the navigator operates (Frantz *et al.* 2003, Wiles *et al.* 2004). To make the understanding of the accuracy of the surgical guidance devices even better, accuracy assessment phantoms and protocols for special purposes have been developed. (ASTM 2011, Clarke *et al.* 2008, Linte *et al.* 2010, Masood *et al.* 2002, Moretti *et al.* 2000, Yamura *et al.* 2005). A phantom is an object used for a variety of purposes to replace a human in the development of new techniques and methods in the medical and surgical field. All of the above errors can be solved with more precise manufacturing and better understanding of mechanics and software. For this reason, a variety of phantoms as presented in the current literature have been developed to better understand the error caused by the navigational modalities and thus help improve the performance of future surgical navigators. If the surgeon and the technical staff know the error caused by the

navigational device, they can take this into account when performing an operation, giving a better basis for successful surgery.

The devices are calibrated before they enter the market. When the navigator leaves the factory, the accuracy is tested and assessed by the navigational device company e.g. BrainLab GMB (Munich, Germany), Medtronic Inc. (Louisville, CO, USA) and Stryker Inc. (Kalamazoo, MI, USA). The navigator's accuracy can be degraded due to many factors while in use in the hospital. For example rough handling may decrease the accuracy (Wiles *et al.* 2004). Thus a post-industrial phantom and an accuracy assessment protocol are needed (ASTM 2011, Haidegger *et al.* 2010, Stiehl *et al.* 2007, Wiles *et al.* 2004). Recent issues presented also in the MAUDE database with accuracy errors encountered in the routine use of surgical guidance devices serve to emphasize the need for periodic accuracy assessment of these devices as a part of quality assurance (MAUDE 2012). The MAUDE database is an online portal of the FDA, where all medical device users and manufacturers post errors encountered with medical devices. When browsing the database for injuries caused by stereotactic guidance devices, which in this database search are navigators and robots, a total of 203 cases can be found within the last five years. All of these error cases were encountered during a surgical procedure.

Stiehl *et al.* (2007) and Heidegger *et al.* (2010) have addressed the issue of the different accuracy analysis methods and results. They listed two significant issues regarding the analysis found in the literature. According to their review, there is serious lack of consistency both in terminology and validation methods used in the statistical measurements of the accuracies of the guidance devices. Wiles *et al.* (2004) also discussed the difficulty in comparing different accuracy assessment results, and claimed that a large variety of spatial measurement technologies and expected applications was the reason why manufacturers have not agreed on standardized methods for surgical guidance device accuracy assessment. They also suggested that users of these surgical navigators should periodically check the accuracies and called for development of user oriented and developed accuracy assessment tools and protocols for 'real world' use (Wiles *et al.* 2004).

In the field of IGS, a variety of accuracy assessment phantoms and protocols has been presented. As stated in the Introduction (Section 1.2), even though an early stage standardized method and tool for periodic assessment for these guidance devices was recently published, a number of open questions remain unanswered. The ASTM F2554 standard focused on orthopedic procedures and

thus a lack of common standardization has led to a variety of accuracy assessment analysis and different aspects of results have been published.

Wiles *et al.* have presented methods for assessing the accuracy of the commercial OTS, the NDI Polaris (NDI Medical, Waterloo, ON, Canada) (Wiles *et al.* 2004). They covered aspects regarding the entire volume covered by the optical camera pair. Their study also contained comparison between the so-called active and passive optical tracking. They found that the accuracy of OTS does not depend on the tracking method. In their experiment the mean accuracy of an OTS was 0.255 mm and the RMS error was 0.193 mm, with standard deviation (SD) of 0.167 mm. 95% CI was found to be 0.451 mm. The presented study was highly industrial and involved special accuracy assessment equipment that does not necessarily suit the analysis done in a hospital setting. Instead, the analysis was done in the factory and thus the methods were limited to analysis involving laboratory and experts in accuracy assessment. Other research groups have also assessed the accuracy of different navigators using the OTS in laboratory experiments. Hassfeld & Mühligh reported a mean accuracy of 0.8 mm with 0.8 mm SD (Hassfeld & Mühligh 2000). Mascott (2005) analyzed the application accuracy of an OTS during routine surgical procedures and published a mean error of 1.4 mm with 0.8 mm SD. Ringel *et al.* (2009) have also reported an accuracy of 0.7 mm as the mean target point deviation using the VarioGuide (BrainLAB, Feldkirchen, Germany). Wittmann *et al.* (2011) reported an accuracy of the Navigation Panel Unit (NPU) (Karl Storz GmbH & Co, KG, Tuttlingen, Germany) in the surgical scene at 1.44 mm with SD of 0.09 mm and in ideal conditions at 0.63 mm with SD 0.035 mm. Simon (1997) and Alakuijala (2001) compared the difference between the different tracking methods, finding the accuracy of the OTS to be in the range of 0.1–0.5 mm depending on the accuracy assessment method.

The other widely used tracking method is EMTS as presented in Section 2.1.2 in this thesis. In the literature there are some studies of analysis done for this tracking, but as with the OTS, no single standardized method has been presented. Thus the analysis results are not totally comparable but they give a range in which the accuracy has been reported. Frantz *et al.* from the NDI covered the analysis in detail containing different methods presented in the literature. They published the accuracy of the EMTS to be within 1.1 mm (Frantz *et al.* 2003). Hummel (2006) reported the EMTS mean accuracy to be 0.17 mm with 0.19 mm SD. Schneider & Stevens (2011) found a mean accuracy of 0.46 mm (-1.03 mm) for the EMTS. Mascott (2005) compared the application accuracies of the OTS and the EMTS in

his paper and found the accuracy of the EMTS to be 1.4 mm with 0.6 mm SD. In a recent study, de Lambert *et al.* (2012) also reported a mean error of 1.3 mm using the Aurora Magnetic Tracking System (NDI Digital Inc., ON, Canada). In the comparison tables of Simon and Alakuijala, the accuracy of the EMTS was shown to vary within 1 to 5 mm. Accuracies of the other modalities in the field of IGS have been reported to be in the range of 1 mm for acoustic tracking and 0.1 to 2.5 mm for mechanical arm based navigators (Alakuijala 2001, Simon 1997).

Earlier research results on the accuracy analysis of commercial robots have been published (Grunert *et al.* 2003, Drake *et al.* 1993, Kwartowitz *et al.* 2006). Haidegger *et al.* (2010) collected the accuracy analyses of the most widely used commercial robots (The Puma 200, the ROBODOC, the NeuroMate and the da Vinci) with the following results: technical accuracy had been reported in the range of 0.5–1.35 mm with a repeatability of 0.05–0.15 mm. Ringel *et al.* (2012) published a study comparing the accuracy of placement of lumbar and sacral pedicle screws using the SpineAssist robot and conventional freehand screw implantation. The results showed that in fact in this special case, the freehand implantation was superior compared to the robot assisted procedure. They showed that in 93% of cases freehand implantation was within the desired accuracy range while the range was achieved in 85% of the cases when assisted by the robot. This is a study that clearly shows that the use of robots in particular should be evaluated and the accuracy of the systems assessed.

The total number of MIS procedures worldwide has been estimated at 3 million cases annually (MaRS 2010). The use of the presented IGS devices has a share of 6% of the total number. Thus, roughly 180 000 procedures are guided using these devices annually and the use of these devices is clearly increasing (MaRS 2010).

As can be seen in the reports on accuracy analysis in the literature, there is a range of accuracy analysis methods and thus deviation in the results. The fact that there are no standardized methods for accuracy assessment of surgical guidance devices and navigators in detail has led to broad definitions and analysis methods for surgical guidance device accuracy assessment. The aspects regarding the importance of assessing the accuracy of surgical guidance devices have been published by many international research groups (Clarke *et al.* 2008, Haidegger *et al.* 2010, Kroneif *et al.* 2011, Stiehl *et al.* 2007, Wiles *et al.* 2004).

This thesis addresses the issues regarding the different terminologies, validation methods and results analysis by evaluating the used surgical guidance devices using the same accuracy assessment phantoms and protocols. The results

are also presented in a uniform manner providing tools for quick and comprehensive comparison between the different IGS devices.

2.2.3 Instrument tracking error theory

Instrument tracking error is an important component of IGS systems and the focus of this thesis. The main source of this error lies in the technical accuracy of the system. Depending on the used IGS system, instrument tracking error may be derived from the localization of fiducial markers (OTS), the localization of the coils (EMTS), or the kinematic construction of the device (surgical robots). The common subject with these IGS systems is that the tip or axis of the used instrument is mapped in space with respect to the object tracked. The used instrument is calibrated to the object using registration techniques.

The instrument tracking error has been divided into three main categories (Fitzpatrick *et al.* 1998, Haidegger *et al.* 2010, West & Maurer 2004):

1. Fiducial Localization Error (FLE)

- FLE is the error resulting from the misalignment of the fiducial positions. FLE is the calculated distance between the true positions of the fiducials and the measured positions. FLE gives the localization error in the precise point within the fiducial. The FLE may be calculated using (1).

$$FLE = \frac{1}{n_{Trial} * n_{Fiducial}} \sum_{i=1}^{n_{Trial}} \sum_{j=1}^{n_{Fiducial}} \varepsilon(i, j), \quad (1)$$

where ε is the error measured at each fiducial.

2. Fiducial Registration Error (FRE)

- FRE is a commonly used fiducial marker localization error. This is the number that most of the IGS devices return after the registration of the object to the reference coordinate system. In the ideal case, the FRE equals zero and the connection between the FRE and FLE has been shown to follow (2) (Fitzpatrick *et al.* 1998):

$$\langle FRE \rangle = \sqrt{\left(1 - \frac{1}{2n}\right) \langle FLE^2 \rangle}, \quad (2)$$

where n is the number of fiducials used during the registration.

3. Target Registration Error (TRE)

- TRE is the error of misalignment of the fiducials that results from the registration error. The TRE may be calculated using (3):

$$\langle TRE^2(r) \rangle = \frac{\langle FLE^2 \rangle}{n} \left(1 + \frac{1}{3} \sum_{k=1}^3 \frac{d_k^2}{f_k^2} \right), \quad (3)$$

where n is the number of fiducial markers, d_k is the distance of the target, and f_k is the RMS distance of the fiducials from the principal axis k .

3 Development of advanced materials and methods based on statistical formulation for the region of surgical interest

In this section, the advanced accuracy assessment phantoms and protocols developed in the present work are introduced as methods and tools for periodic “real world” analysis of surgical guidance devices in the region of surgical interest (ROSI). The tools and methods for accuracy assessment were utilized in all of the present experiments. The process of development was begun already in 2008 when the need for these types of accuracy assessment tools was realized.

The purpose of the phantoms was to function as tools for assessing the accuracies of surgical guidance devices, namely neuronavigators using OTS and EMTS and a surgical robot. Due to the routine use of the guidance devices and possible rough handling, the accuracy of the devices can decrease over time. To periodically check the accuracy, a model with accurately machined accuracy assessment points was needed. Together with material selection, the main criterion given for the phantom was the need to provide more than one surface for measurement points in the ROSI. The solution for these criteria was a phantom designed to have three separate levels with accurately machined beveled calibration holes to render a sufficient volume for testing and to make the phantom volume easily accessible. The levels also needed to be easily disassembled to reach the calibration holes on the lower levels. The first task in the development process was to determine the volume of the ROSI. The approximate size of the human head was chosen as the volume for the ROSI.

3.1 Accuracy assessment tools

The accuracy assessment tools included two phantoms and protocols. The developed phantoms and protocols are a response to the suggestion by industry for “real world” methods for routine hospital use (Stiehl *et al.* 2007, Wiles *et al.* 2003).

Accuracy assessment phantoms

The design process of the first phantom started with understanding of the MR imaging principles and scanner system architecture. In navigation the most

commonly used MR image protocol is the 3D-T1 weighted sequence (Katsko 2012). This method shows liquid in gray and acrylic material in black. For this reason the first phantom (Phantom I) needed to be filled as completely as possible with liquid to discriminate between liquid and plastic. The result was to design separate levels containing calibration pegs so that these pegs were visible in black against the gray background of the liquid. The second phantom (Phantom II) had similar criteria, but as this phantom was intended for CT imaging, there was no need for liquid use. Thus, the phantom was designed so that the accuracy assessment points were machined directly on the surface of 40 mm thick accuracy assessment levels.

Acrylic plastic (PMMA - polymethylmethacrylate) was used as the material for both phantoms. PMMA has been used for a variety of products since the 1930's. It is an amorphous thermoplastic, which can be used as a replacement for glass. PMMA has eight times greater shock resistance than glass. PMMA is easily machined and has very strong weather resistance. The temperature range in which PMMA can be used without deformation is -40°C to +70°C (MatWeb 2012). Since the linear coefficient of thermal expansion of PMMA at -30 to 30°C is $6 \times 10^{-5}/^{\circ}\text{C}$ (ASM International 1988), the deformation of the phantoms in controlled experimental testing is marginal. PMMA has very good environmental characteristics and only strong acids and esters may cause deformation (ASM International 1988). PMMA has also been shown to cause hardly noticeable image abnormality on either spin-echo or gradient-echo MR imaging (Schenck 1996). It has also been commonly used for CT image artefact studies (Barrett & Keat 2004). To prevent possible deformation issues, the phantoms should be stored in dry and clean premises.

Both phantoms were machined using a NC-machine (Yasda Precision, Okayama, Japan) at the University of Oulu Mechanics Laboratory (Phantom I) and at a commercial machining company (KL Mechanics, Kempele, Finland; Phantom II). The phantom levels contained beveled holes industrially machined with a verified ± 0.015 mm displacement error and used as the accuracy assessment points. The displacement errors of the accuracy assessment points of the phantoms were verified by Oulu PMC (Oulu, Finland), a company specializing in 3D accuracy analysis, using the Mitutoyo Strato 9166 (Mitutoyo Corp., Kawasaki, Japan) coordinate measuring machine (CMM).

The points were machined identically forming a 7x7 matrix giving 49 accuracy assessment points on each level. The total volume approximated the dimensions of the human head which was chosen as the ROSI target volume.

Specifically, the first phantom (Phantom I, Fig. 11, left) was designed as a tool with three 10 mm thick levels on which were placed 6 mm diameter accuracy assessment pegs on top of which the beveled holes were machined. As this phantom would later also be used to assess the image quality of the MRI scanner, the phantom was designed so that it could be placed inside a container that could be filled with liquid. As the basic principle of MR imaging is based on the spin effect of the proton of the hydrogen atom (Hendee W & Morgan C 1984), the phantom was designed so that as much liquid as possible could be added into the container with the phantom for image scanning. The use of pegs made it possible to fill the container with enough liquid to make the accuracy assessment points visible in the image data sets. In the experiments regular tap water with dish washing solvent (Sodium Laureth Sulphate, $\text{CH}_3(\text{CH}_2)_{10}\text{CH}_2(\text{OCH}_2\text{CH}_2)_n\text{OSO}_3\text{Na}$) was used as the liquid. Water can be used as a substitute liquid for human tissue, as both materials are similarly MRI compatible and produce hardly noticeable torques or forces; negligible image distortion occurs even close to the imaged region in the human anatomy (Schenck 1996). Human tissue is also considered to have the same MR susceptibility parameters as water. The dependence of water susceptibility and temperature has been shown to be marginal in controlled conditions and thus no real image degradation will be detected (Schenck 1996). The assessment points were machined at 22 mm intervals in lateral and longitudinal directions in planes set at 50 mm intervals vertically. This gave the phantom an accuracy assessment volume of 132x132x100 mm³ (Koivukangas *et al.* 2009).

The second phantom (Phantom II, Fig. 11, right) was designed as a tool containing levels of 40 mm thickness on which the accuracy assessment points were machined directly. This phantom would also be used for image quality assessment of CT scanners. As the basic principle of CT imaging is based on X-ray being absorbed by the object (Goldman 2007), the phantom was designed to have suitable material for making the accuracy assessment points visible on the image data. The accuracy assessment points were machined at 20 mm intervals in lateral and longitudinal directions in planes set at 50 mm intervals vertically, giving a total accuracy assessment volume of 120x120x100 mm³ (Koivukangas & Katisko 2010).

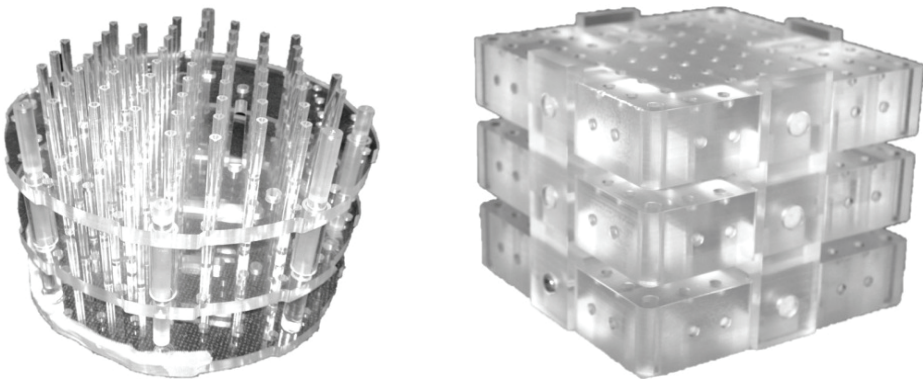


Fig. 11. Phantom I (left) and Phantom II (right) with the three accuracy assessment levels combined.

Accuracy assessment protocols

The accuracy assessment protocol and the shape of each level are illustrated in Fig. 12. Numbers 1 to 49 show the accuracy assessment points that were touched in the corresponding order. Data was collected from each point and analyzed to see the error trend and the accuracy of the surgical navigator in the analyzed volume. The optical camera in the OTS assessment and the magnetic field generator in the EMTS assessment together with the patient trackers of the navigators were placed in a typical surgical configuration as indicated by the navigator software.

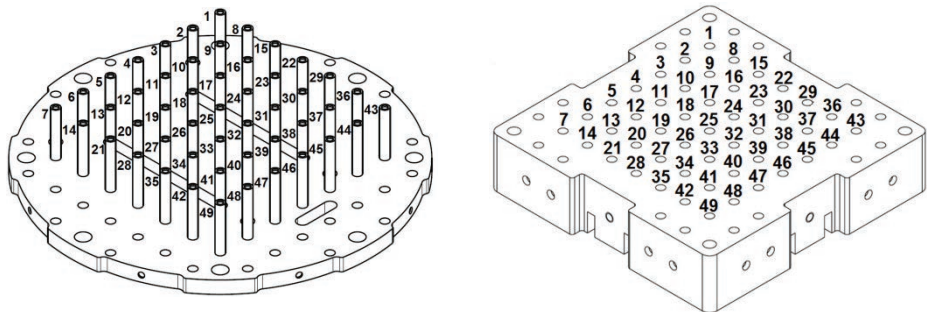


Fig. 12. Phantom I (left) and Phantom II (right) CAD models of the accuracy assessment levels of the phantoms with accuracy assessment protocol numbers indicating the accuracy assessment points.

The accuracy assessment experiments were done according to two protocols based on the common accuracy assessment phantoms forming the ROSI. The two protocols were:

- I The basic protocol for the entire ROSI volume contains all 49 accuracy assessment points on each level, thus providing a total of 147 points. In this protocol the accuracy assessment was done in 22 mm increments with phantom I and in 20 mm increments with phantom II. This protocol shows the accuracy in detail with the goal of detecting deviation and error trend within the ROSI volume. This protocol is illustrated in Figure 12.
- II The modified accuracy assessment protocol for the ROSI contains 17 points on each phantom level, providing a common accuracy assessment volume with 51 assessed points. With this protocol, the assessment was done in 40 mm increments using phantom II. The assessments were verified by five experiments according to this protocol when the results under protocol I showed no significant deviation (I.e. $E_{MEAN} < 0.50$ mm). As the environment for accuracy assessment was specified to be the hospital premises, quick yet accurate and reliable methods were needed. The 40 and 44 mm increments of the phantoms proved to be adequate as shown above for performing the accuracy assessment of the IGS devices. This protocol was utilized as the single method in assessing the SIRO robot since the method proved to be suitable in earlier experiments with the commercial navigators. This protocol is illustrated in Figure 13.

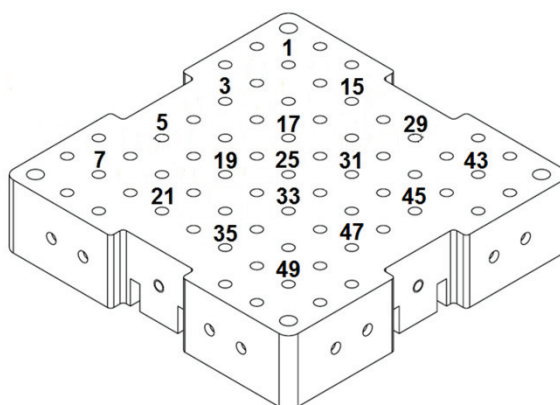


Fig. 13. A modified accuracy protocol for accuracy assessment in the ROSI.

Figure 14 illustrates the common accuracy assessment protocol and order of tracking each point. The Figure illustrates each assessed point on each corresponding level. The order of assessment was started at the bottom level, at the furthest corner from the observer and concluded at the closest corner to the observer on the top level.

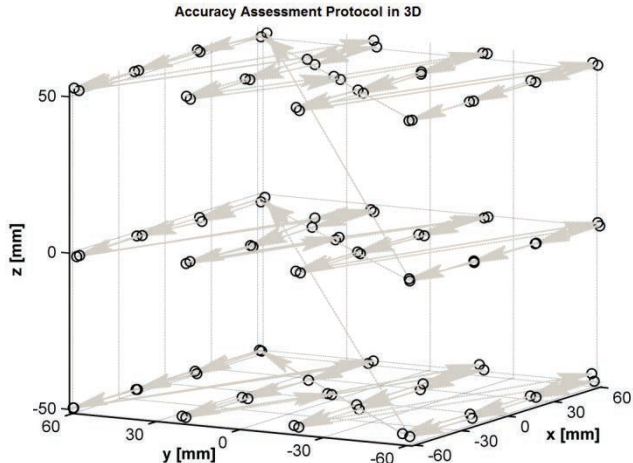


Fig. 14. Accuracy assessment protocol for the experiments. The Figure represents the assessment protocol used to reach each point throughout the ROSI volume. The arrows illustrate the order of assessment from point number 1 on the bottom level at the furthest corner from the observer at (60, 60, -50) to point number 49 at the closest corner of the top level at (-60, -60, 50).

3.2 Accuracy assessment analysis

The data was collected according to the accuracy assessment protocol and the middle point (accuracy assessment point 25) of the middle level on the phantom was chosen as the reference point of origin. The collected data from the navigators and the robot for each accuracy assessment point and the true points on the phantom were compared to point number 25. The data analysis for the accuracies of the navigators was based on the ISO 5725-1 (ISO 5725) standard and the robot also on the ISO 9238 (ISO 9238), and their fundamental requirements. The accuracy in the study refers to trueness according to the standards. The error was calculated as the displacement error between the known phantom points and the collected data from the surgical guidance devices. Figure 15 illustrates the procedure for the accuracy assessment.

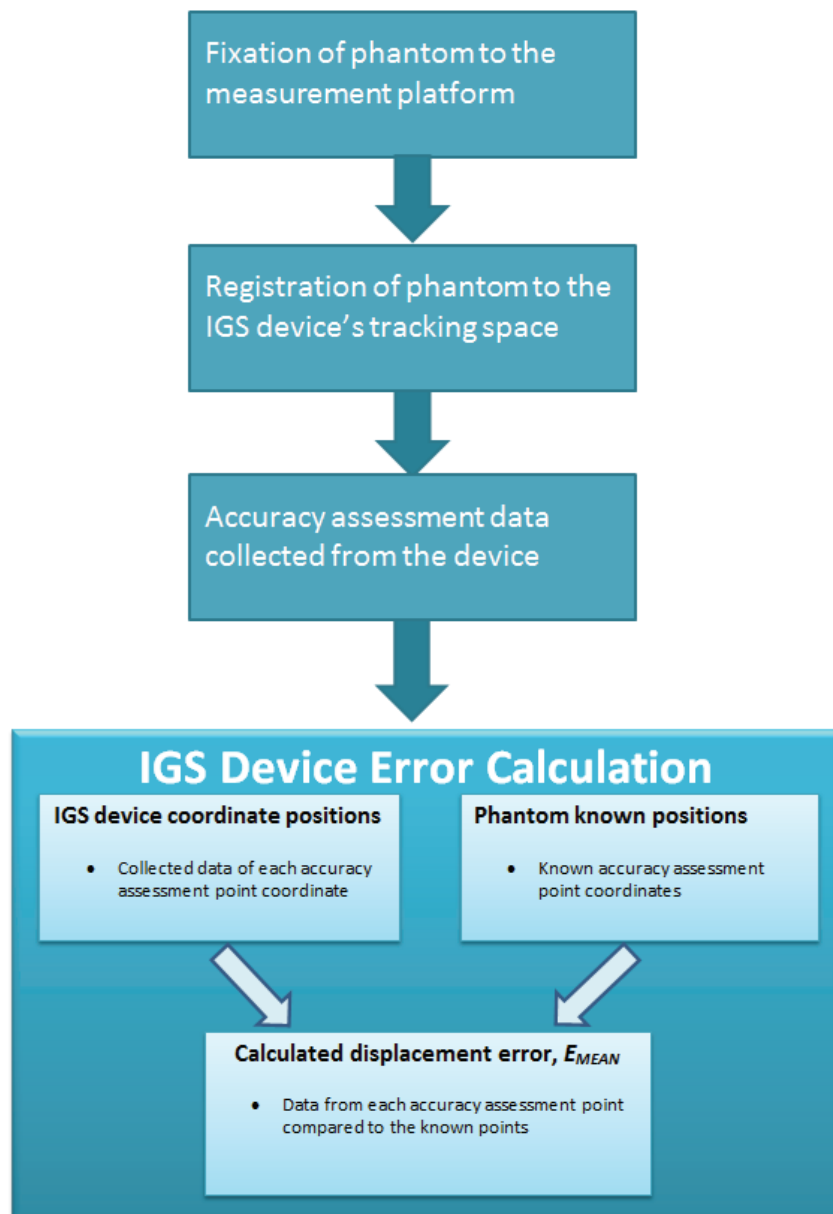


Fig. 15. The utilized method for error calculation.

The results analysis was done using Matlab for the 3D error surface representations and the numerical analysis representation was done using Microsoft Excel 2010. The robot analysis included also the Robotics Toolbox for Matlab (Corke P 1996). Figure 16 illustrates the corresponding directions used in the analysis.

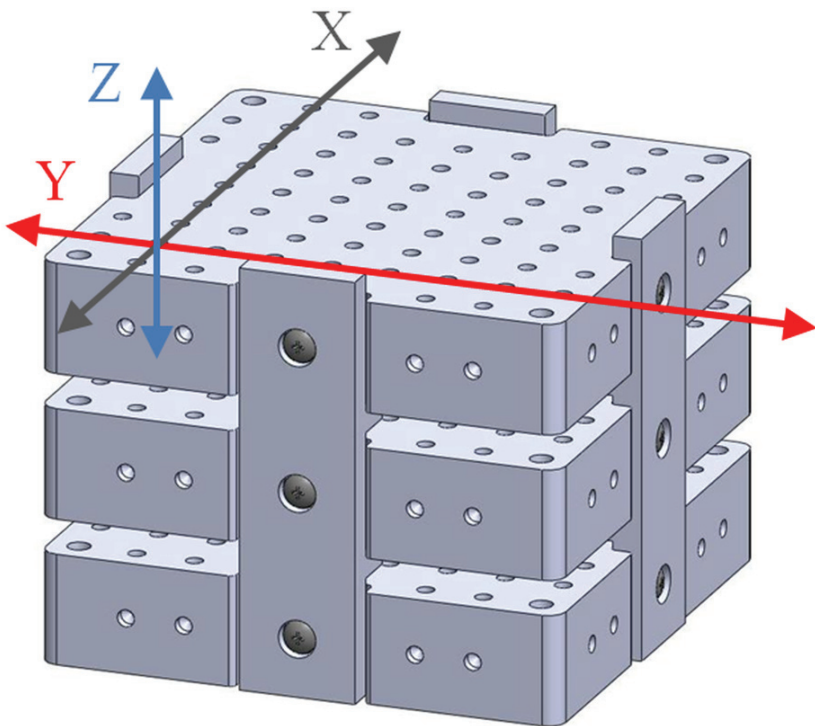


Fig. 16. A 3D CAD model of Phantom II and the error analysis directions used in the experiments: the X-direction represents the lateral displacement on the phantom, the Y-direction represents the longitudinal distance from the IR camera and Z-direction the vertical displacement with respect to the IR camera in the OTS assessment. Correspondingly, the Y-direction is the direction from the EMTS field generator to the phantom in the EMTS assessment and similarly the direction from the robot base to the phantom in the SIRO assessment.

Mathematical theory applied in this thesis

The errors mentioned in Section 2.2 (FLE, FRE, and TRE) occur both in image and each tracking modality space. However, as this work presents universal methods for periodic assessment of the IGS devices, the analysis covers the technical accuracy within the ROSI. Thus, the mathematical analysis used in this thesis was modified from these published IGS device error representations.

For each accuracy assessment point, the error E_{ij} was calculated using (4) (Koivukangas *et al.* 2009):

$$E_{ij} = \sqrt{\left(X_{M,ij} - X_{M,R}\right)^2 + \left(Y_{M,ij} - Y_{M,R}\right)^2 + \left(Z_{M,ij} - Z_{M,R}\right)^2} - \sqrt{\left(X_{ij} - X_R\right)^2 + \left(Y_{ij} - Y_R\right)^2 + \left(Z_{ij} - Z_R\right)^2}, \quad (4)$$

where X_{ij} , Y_{ij} and Z_{ij} are the ‘true’ values on the phantom and $X_{M,ij}$, $Y_{M,ij}$ and $Z_{M,ij}$ are the i -th accuracy assessment point coordinates measured on the phantom and j corresponds to the analyzed level on the phantom, $i \in [1,49]$, $j \in [1,3]$. R corresponds to the chosen reference point of origin on the phantoms.

The technical accuracy was calculated as the mean of the displacement errors (E_{MEAN}) using (5). The root mean square (RMS) error, ϵ , was obtained using (6). In the equations, the E_{ij} are considered positive. The 95% CI was used as a statistical method for the accuracies of the different guidance systems to cover the total technical accuracy and the effect of high errors in the assessed region (7).

$$E_{MEAN} = \frac{1}{n} \sum_{k=1}^n (E_{ij})_k, \quad (5)$$

$$\epsilon = \sqrt{\frac{1}{n} \sum_{k=1}^n (E_{ij})_k^2}, \text{ and} \quad (6)$$

$$95\% \text{ CI} = E_{MEAN} + 2\sigma, \quad (7)$$

where E_{ij} indicates the mean error at each corresponding accuracy assessment point gained using (4), n indicates the number of assessed points and σ indicates standard deviation.

4 Results of accuracy assessment

In this chapter, the developed tools and methods are utilized in accuracy assessment of the IGS devices. Section 4.1 concentrates on optical tracking system (OTS) accuracy analysis with the error trends and possible sources for this phenomenon. Section 4.2 contains the accuracy assessment of the electromagnetic tracking system (EMTS). Section 4.3 presents a comparison study of the OTS and the EMTS modalities. Section 4.4 shows the results of accuracy analysis of the surgical robot (SIRO). Finally, Section 4.5 is a study of the spatial accuracy of a surgical 3D CT scanner within the common ROSI.

Section 2.2.2 presented the different accuracy assessment methods and accuracy results for the surgical guidance devices that have been published. This has resulted in a comprehensive, but also complicated description of the accuracy of the devices. Depending on the setting and analysis methods, the results of similar cases vary extensively. Chapter 3 introduced the present tools and methods for quick and reliable accuracy assessment of surgical guidance devices in the hospital setting. They were used to analyze the technical accuracies of the devices in a uniform manner, so the results are comparable and adequate.

4.1 Accuracy assessment of OTS

This section concentrates on the OTS accuracy assessment of two commercial surgical navigators. The navigators used were the StealthStation Treon plus (Fig. 17) and the StealthStation S7, both manufactured by Medtronic Inc. (Louisville, CO, USA). The analysis was done using both of the designed phantoms for a comprehensive evaluation of the accuracies. The data was collected from both navigators as the position of the tip of the instrument in x, y and z directions. The results were collected and analyzed in four separate OTS experiment sets and then combined to see the trends of error:

Experiment 1: StealthStation Treon plus –navigator with phantom I

Experiment 2: StealthStation Treon plus –navigator with phantom II

Experiment 3: StealthStation S7 –navigator with phantom I

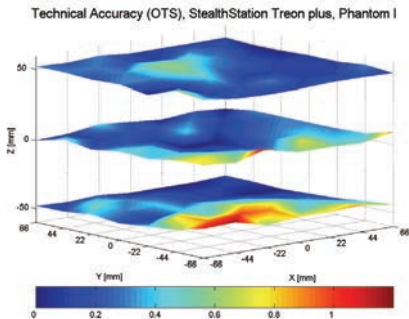
Experiment 4: StealthStation S7 –navigator with phantom II.

Both of the assessed navigators had been in routine use at the Oulu University Hospital, Oulu, Finland. The StealthStation Treon plus had been taken into use in early 2008 and the StealthStation S7 in 2010.

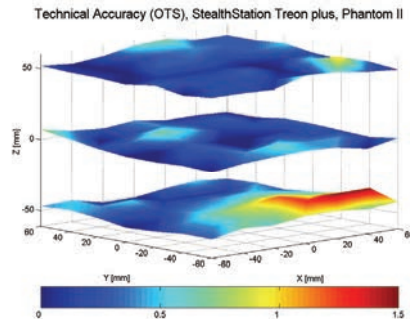


Fig. 17. The StealthStation Treon plus –navigator and the accuracy assessment setup with systems in place. (1) Accuracy assessment phantom, (2) Navigator’s optical camera, (3) Tracking instrument, (4) Patient tracker, (5) StealthStation Treon plus –navigator’s CPU, (6) Surgeon’s monitor.

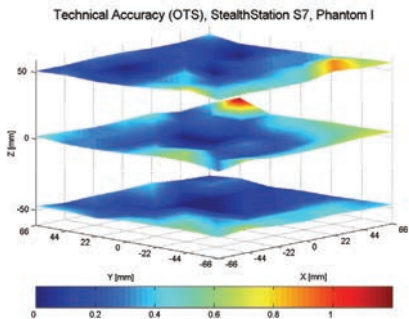
The results obtained in the four experiments using the two accuracy assessment phantoms show that the displacement error of the OTS in the surgical navigators has a tendency for growing with the distance from the center of the common field of view of the optical cameras increases. This tendency is shown in Fig. 18 as the error increase toward the edges of the navigated phantom. The figures thus show the tendency of the error to be highest at the fringes of the field of view of the OTS camera pair. Figure 19 collects the accuracy assessment data in a sequence plot representation and Figure 20 as a histogram of the experimental results.



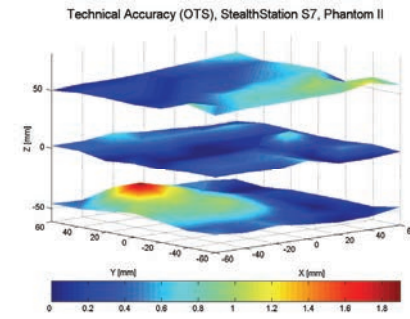
(a)



(b)



(c)



(d)

Fig. 18. (a) illustrates the results of Experiment 1, (b) the results of Experiment 2, (c) the results of Experiment 3 and (d) the results of Experiment 4, respectively. In the figures, the orientation of the phantom levels is such that accuracy assessment point 25 is in the center of the grid at each level. Point number 1 is in the back corner and number 49 is closest to the observer. The color bars can be used as tools to see the error in millimeters. Point number 1 is in the back corner and number 49 is closest to the observer.

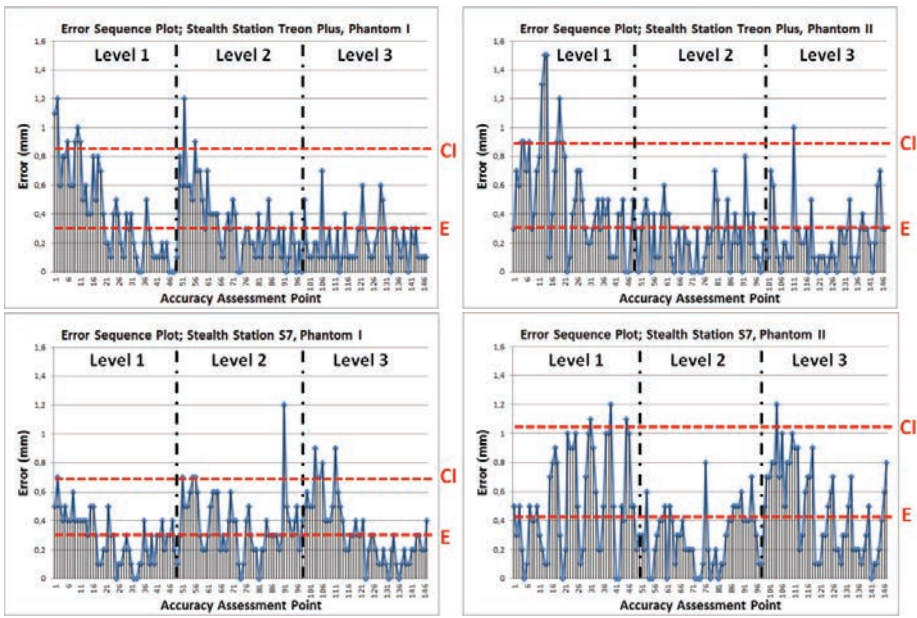


Fig. 19. The error sequence plot of Experiment 1 (top left), the error sequence plot of Experiment 2 (top right), the error sequence plot of Experiment 3 (bottom left) and the error sequence plot of Experiment 4 (bottom right). The first point in the sequence diagrams represents the first accuracy assessment point and point number 147 the 147th, respectively. The dotted lines divide the diagrams into three areas labeled 1, 2, and 3. These areas represent the errors on each phantom level in such way that area 1 is the bottom, area 2 is the middle and area 3 the top levels, respectively. On each graph, the error scale is from 0 to 1.60 mm. The dashed lines with labels 'E' and 'CI' represent the mean position error and 95 % confidence interval (CI), respectively.

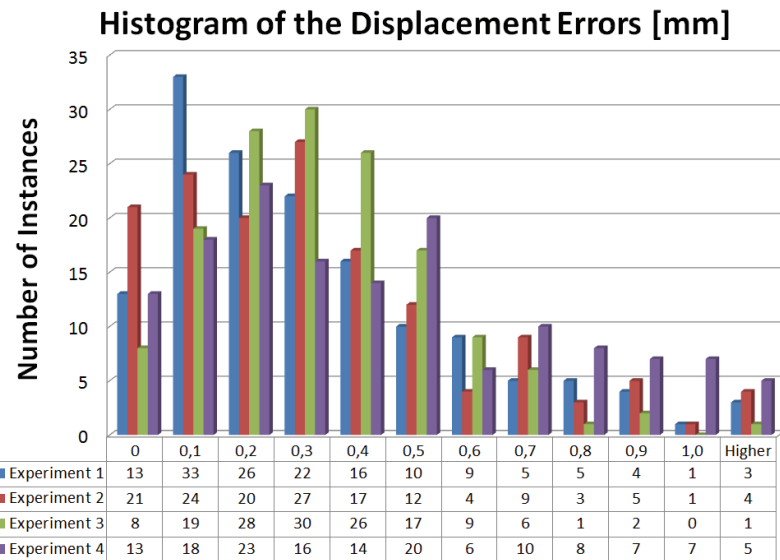
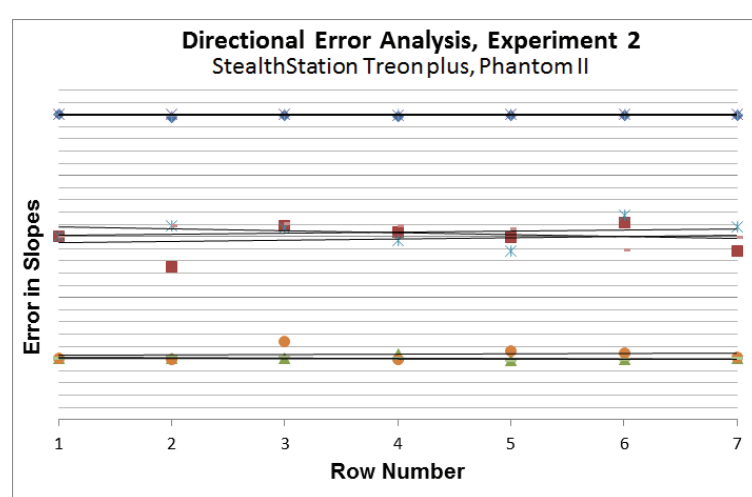
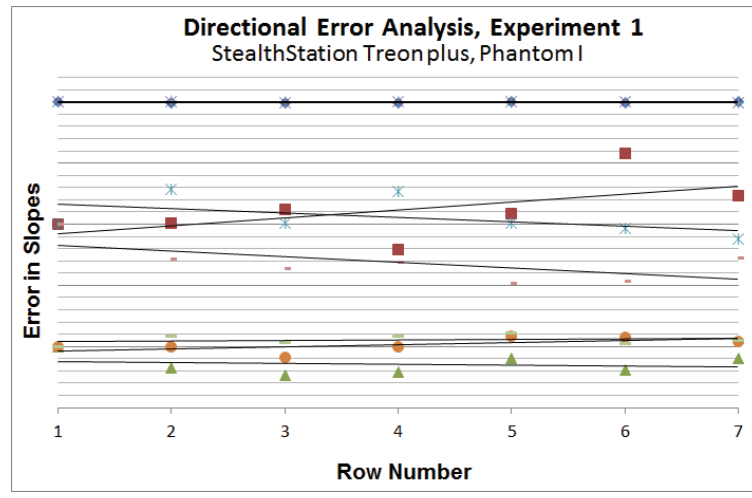


Fig. 20. A histogram of the displacement errors. The first bar indicates the results of Experiment 1 and the fourth indicates Experiment 4, respectively.

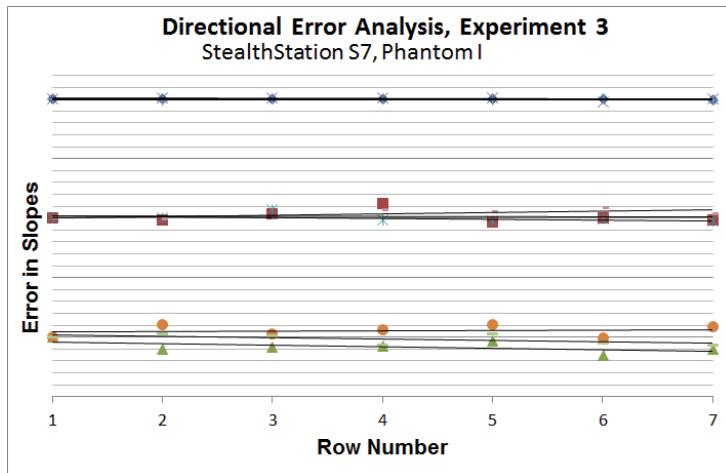
Directional analysis was done by evaluating the total area covered using the accuracy assessment points of each accuracy assessment level. The obtained data was evaluated in the x-, y-, and z- directions. As the assessment was done for a phantom with the shape of a square, the plotted data should also form a square with straight lines, each containing seven plots, with accuracy assessment points separated by 22 or 20 mm depending on the accuracy assessment phantom used as illustrated in the accuracy assessment protocols.

A regression line was calculated for each seven-point line on the accuracy assessment levels and the slopes of the lines were collected. The value of the slope on the first line was standardized to 1 by dividing the slope's value by itself. The other lines' slope values were then compared to this initial value. These results are displayed on directional error analysis diagrams. The dispersion of the values from 1 shows the actual error in each direction. The same method was used for both navigators evaluated with both phantoms. The corresponding directions illustrated in the 3D CAD model of phantom II in Figure 16 were utilized in this study. Figure 21 illustrates the directional error analysis. In the Figure, each experiment set is analyzed in its own error chart. The top row of each graph represents the x-direction, the middle row presents the y-direction, and the bottom row the z-direction respectively.

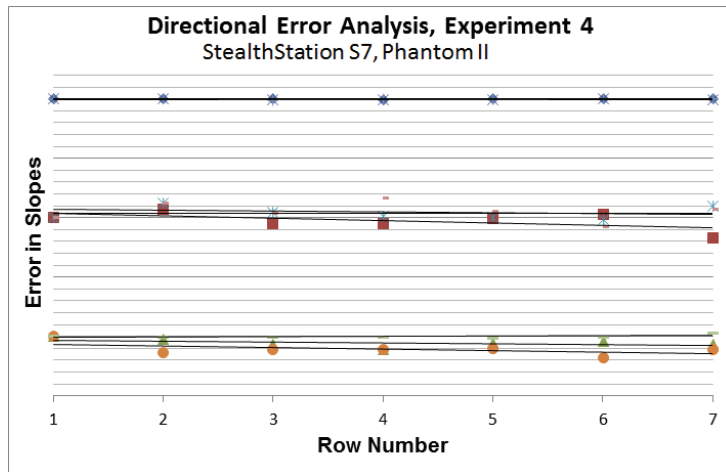


- ◆ X-Direction, Bottom Level
- ✗ X-Direction, Middle Level
- + X-Direction, Top Level
- Y-Direction, Bottom Level
- ✖ Y-Direction, Middle Level
- Y-Direction, Top Level
- ▲ Z-Direction, Bottom Level
- Z-Direction, Middle Level
- ▬ Z-Direction, Top Level

Fig. 21. (a) illustrates the directional analysis results of experiment 1 with Phantom I and StealthStation Treon plus –navigator, (b) illustrates the directional analysis results of experiment 2 with Phantom II and StealthStation Treon plus –navigator.



(c)



(d)

- | | | |
|-----------------------------|-----------------------------|-----------------------------|
| ◆ X-Direction, Bottom Level | ■ Y-Direction, Bottom Level | ▲ Z-Direction, Bottom Level |
| ✗ X-Direction, Middle Level | ✖ Y-Direction, Middle Level | ● Z-Direction, Middle Level |
| + X-Direction, Top Level | - Y-Direction, Top Level | - Z-Direction, Top Level |

Fig. 21. (c) illustrates the directional analysis results of experiment 3 with Phantom I and StealthStation S7 –navigator, and (d) illustrates the directional analysis results of experiment 4 with Phantom II and StealthStation S7 –navigator.

A significant dependence of the displacement error was found in the y direction. This was a systematic error and it was found in all experiments. The phenomenon is illustrated in Figure 21. This is a finding that should be taken into account when setting up the operating room when surgical navigators using OTS devices are present. The present study shows also that the other component that has systematic error for the overall accuracy is the vertical, z-direction. Moreover, it can be seen from the Figure that the vertical direction error is present at all experiments, but the major error occurs when the distance from the camera pair is not optimal. This is seen especially in Figure 21 (a), where the y-component has an extensive deviation.

The results obtained in the four experiments using the two accuracy assessment phantoms gave a displacement error of 0.30 to 0.45 mm as shown in Table 2. The results also show that the displacement error of the OTS in surgical navigators has a tendency for growing as the distance from the center of the common field of view of the optical cameras increases. There is also a tendency for error increase toward the edges of the navigated phantom. These errors remained small, however, because the volumes of the present phantoms mimicked that of the region of surgical interest as compared to the larger volumes studied by a manufacturer of OTS (NDI 2012, Wiles *et al.* 2004). Also, the phantoms were placed in optimal positions indicated by the navigator.

Table 2. A table of the accuracy results of the OTS.

Experiment Results*	1	2	3	4
Mean Error, E_{MEAN}	0.32	0.34	0.33	0.43
RMS Error, ϵ	0.42	0.45	0.39	0.53
95% CI	0.84	0.94	0.74	1.05
Standard Deviation, σ	0.26	0.30	0.20	0.31
Variance, μ	0.07	0.09	0.04	0.10
Maximum Error, E_{MAX}	1.20	1.50	1.20	1.20

*Units in mm, Experiment 1: StealthStation Treon plus –navigator with phantom I, Experiment 2: StealthStation Treon plus –navigator with phantom II, Experiment 3: StealthStation S7 –navigator with phantom I, Experiment 4: StealthStation S7 –navigator with phantom II.

4.2 Accuracy assessment of EMTS

This section presents the accuracy assessment analysis for the EMTS modality of the two surgical navigators, the StealthStation Treon plus and the StealthStation S7. The analysis was done using phantom II and the data was collected from both

navigators as the position of the tip of the instrument in x, y and z directions (Figure 22).

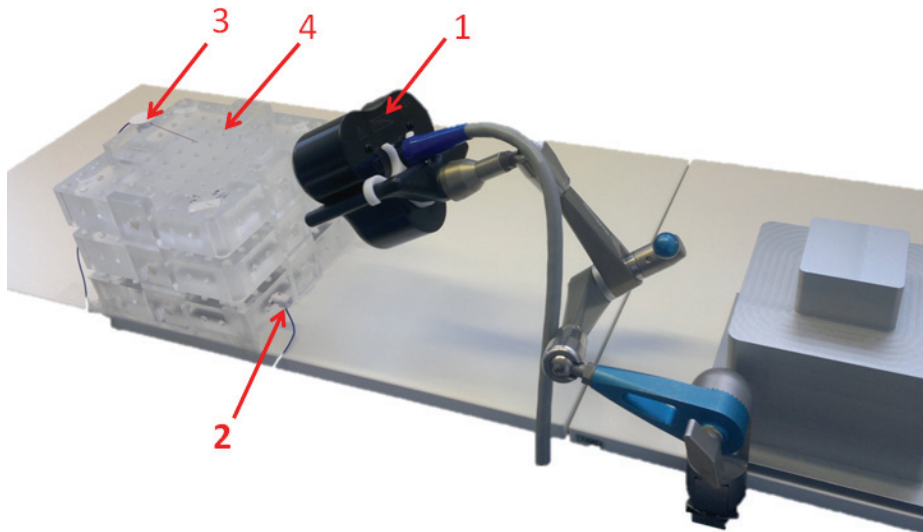


Fig. 22. Accuracy assessment setup of the Stealth Station S7 EMTS modality. (1) EMTS field generator, (2) Patient tracker, (3) tracking instrument, (4) accuracy assessment phantom.

The results obtained in the EMTS experiments show that the displacement error was quite scattered. This noticeable tendency is seen clearly in the 3D representations (Fig. 23) and in the histogram (Fig. 24). It is also seen that there are more relatively high outlier errors especially with the StealthStation Treon plus experiments with the EMTS at the furthest edges of the ROSI (Fig. 23, top). The reason for this phenomenon is that the furthest accuracy assessment points are located in the outmost range for the EMTS field generator and the produced magnetic field does not have enough strength for sensing the coils on the instrument. This furthest range of approximately 35 cm from the field generator should thus be avoided when performing IGS operations with the present EMTS.

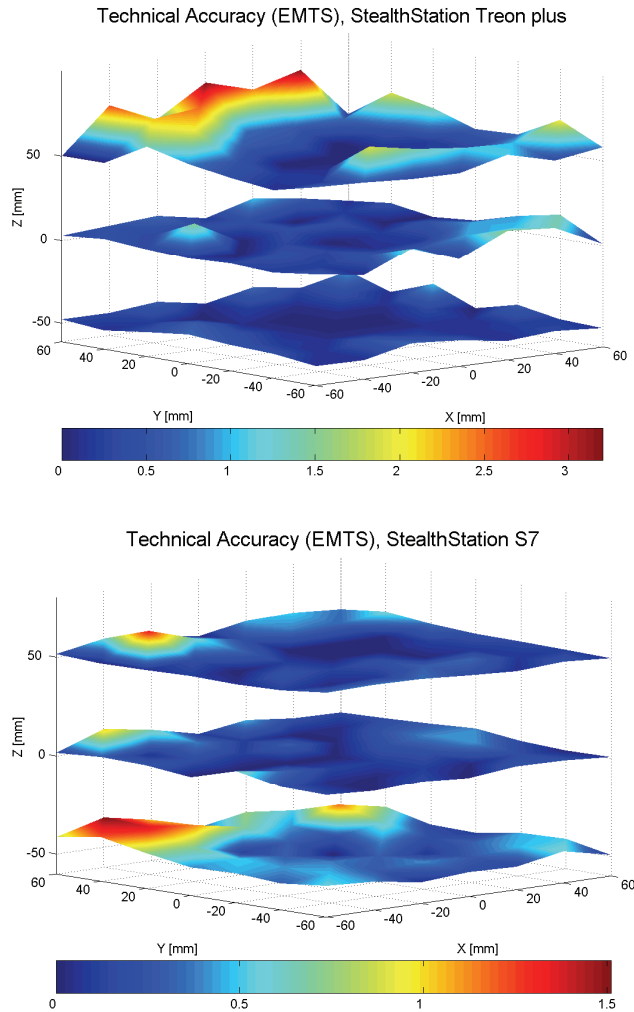


Fig. 23. The error representation in 3D surfaces. The top figure illustrates the results of the StealthStation Treon plus navigator's EMTS, and the bottom figure the results of the StealthStation S7 navigator's EMTS. In the figures the orientation of the phantom levels is such that, respectively, in the middle level the center coordinate point (0,0,0) corresponds to accuracy assessment point 25, coordinate point (60,60,0) to assessment point number 1 and coordinate point (-60,-60,0) to assessment point number 49. The color bars can be used as tools to see the error in millimeters.

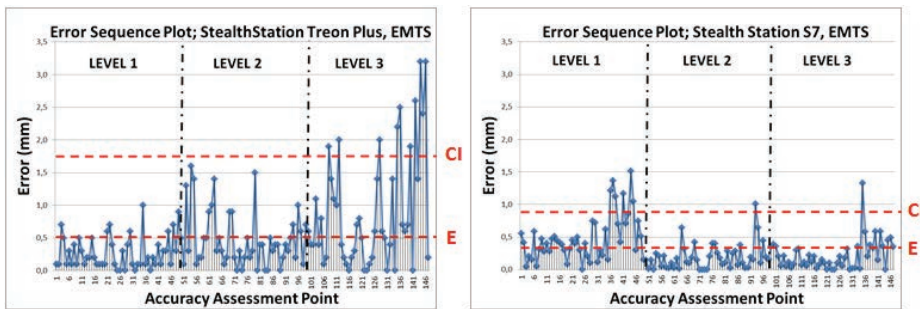


Fig. 24. The error sequence plot of the results of the StealthStation Treon plus navigator's EMTS (left), and the results of the StealthStation S7 navigator's EMTS (right). The first point in the sequence diagrams represents the first accuracy assessment point and point number 147 the 147th, respectively. The dotted lines divide the diagrams into three areas labeled 1, 2, and 3. These areas represent the errors on each phantom level in such way that area 1 is the bottom, and 2 is the middle and 3 the top levels, respectively. On each graph, the error scale is from 0 to 1.40 mm. The dashed lines with labels 'E' and 'CI' represent the mean position error and 95% confidence interval (CI), respectively.

Table 3 presents the accuracy details of the assessed EMTS modalities. The technical accuracy of the EMTS was found to be 0.30–0.50 mm.

Table 3. Accuracy Assessment Results of the EMTS.

Experiment Results*	1	2
Mean Error, E	0.50	0.30
RMS Error, ϵ	0.84	0.42
95% CI	1.76	0.82
Standard Deviation, σ	0.63	0.26
Variance, μ	0.40	0.07
Maximum Error, E_{MAX}	3.20	1.50

*Units in mm. Experiment 1: StealthStation Treon plus –navigator's EMTS with phantom II, Experiment 2: StealthStation S7 –navigator's EMTS with phantom II.

In the present study, accuracy assessment done using the designed phantom and accuracy assessment protocol show that the error increased as the distance from the origin of the navigated volume grew. The results also show that the RMS displacement error is highest on the furthest edge of the assessed volume and the error increases as the function of the cubic radius of the EM field generator. The error trends are best seen in the 3D error representation (Fig. 23).

4.3 Comparison of the OTS and EMTS

The results show that the assessed navigator tracking modalities are nearly equal in their accuracies. Thus, the most suitable method of instrument tracking for surgical procedure can be chosen by criteria other than the technical accuracy. The greatest difference between the tracking modalities was found to be regarding the instruments used. For the EMTS modality, the instruments can be quite flexible. If the instruments are forced to a place so that they are subject to bending, it may result in high accuracy errors. Since the navigation is based on tracking the coils on the instrument, the relative position of the coils must not be changed.

As presented in the previous sections, the absolute technical accuracy for the StealthStation Treon Plus –navigator's OTS was found to be $0.34 \text{ mm} \pm 0.15 \text{ mm}$, with 95% CI of 0.94 mm and for the StealthStation S7 –navigator's OTS it was $0.43 \text{ mm} \pm 0.15 \text{ mm}$, with 95% CI of 1.05 mm. The absolute accuracy of the EMTS with the StealthStation Treon Plus –navigator was $0.50 \text{ mm} \pm 0.32 \text{ mm}$, with 95% CI of 1.76 mm and of the EMTS of the StealthStation S7 –navigator it was $0.30 \text{ mm} \pm 0.14 \text{ mm}$, with 95% CI of 0.82 mm. The following histogram (Figure 25) and Table 4 collects the comparison data of the OTS and the EMTS.

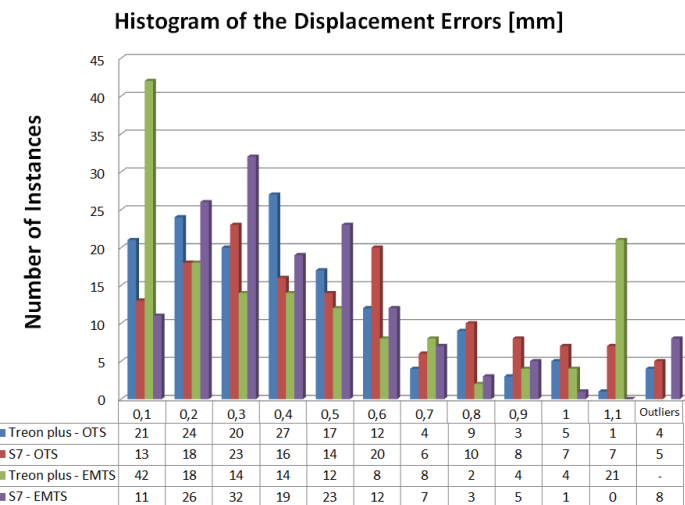


Fig. 25. A histogram of the accuracy assessment of the OTS and the EMTS of two commercial navigators.

Table 4. A comparison of the accuracies of the OTS and EMTS modalities.

Experiment Results*	1	2	3	4
Mean Error, E	0.34	0.43	0.50	0.30
RMS Error, ϵ	0.45	0.53	0.84	0.42
95% CI	0.94	1.05	1.76	0.82
Standard Deviation, σ	0.30	0.30	0.63	0.326
Variance, μ	0.09	0.10	0.40	0.07
Maximum Error, E_{MAX}	1.50	1.20	3.20	1.50

*Units in mm, Experiment 1: StealthStation Treon plus –navigator's OTS, Experiment 2: StealthStation S7 –navigator's OTS, Experiment 3: StealthStation Treon plus –navigator's EMTS, Experiment 4: StealthStation S7 –navigator's EMTS.

4.4 Accuracy assessment of the SIRO

This section presents the results of applying accuracy and repeatability assessment of the prototype surgical robot (SIRO) that was introduced in Section 2.1.3. As the position of the instrument tip in the experiments was received relative to the position of the base of the robot, this relative coordinate system needed to be matched to the absolute coordinate system of the ROSI. This matching of the coordinate systems is the basis of the position measurements in IGS (Kwartowitz *et al.* 2006). In order to accomplish the requirements, the most optimal working volume was first determined for the robot. The technical accuracy assessment in the ROSI for this study was then done in the following manner. (1) The developed accuracy assessment phantom (Phantom II) was fixed on a measurement platform in the pre-determined working volume. (2) The joint variable data from each encoder at each DOF were collected from the robot and with forward kinematics the position of the tip of the instrument was calculated using the Denavit-Hartenberg (DH) –parameters received from Matlab with the Robotics Toolbox. (3) The position at each point was compared with the known positions on the phantom. In these experiments an interval of 40 mm between the assessed points was used. A total of 17 points on each level was assessed in order from 1 to 49. Thus, a total of 51 accuracy assessment points were analyzed within each experiment according to the presented accuracy assessment protocol II. Figure 26 illustrates the wrist and the tracked instrument touching the phantom II during the accuracy assessment experiments.



Fig. 26. The wrist and the instrument of the SIRO touching an accuracy assessment point (Koivukangas T et al. 2012, published with kind permission of Springer Science+Business Media).

The repeatability of the robot was assessed in the following manner. (1) The robot was driven to the base position and, with the noted angular positions, driven back to each accuracy assessment point using the robot's software. (2) The difference between the pre-recorded position and the driven position were compared to verify the repeatability. The points chosen for the repeatability tests were 1, 7, 25, 43 and 49 on each level of the phantom according to the protocol. The test was repeated five times for each chosen point on the phantom and the mean of the results collected.

The results for the technical accuracy of the assessed SIRO are represented in the following figures. First, a 3D error surface representation (Fig. 27) shows the trend of the error within the ROSI. A sequence plot diagram (Fig. 28) shows the error in detail at each corresponding point. The histogram (Fig. 29) shows the error as number of instances within 1.0 mm increments. Fig. 30 illustrates the repeatability of the robot. Table 5 collects the data of the accuracy analysis.

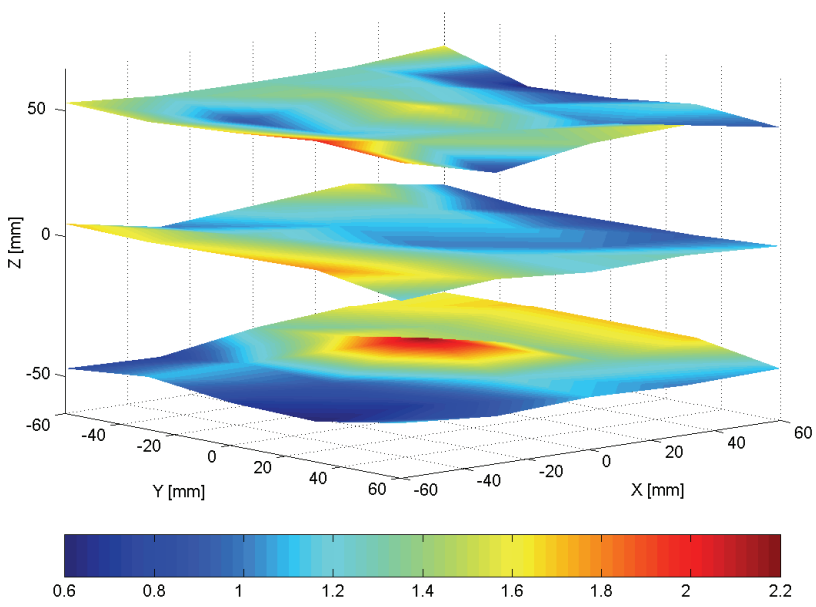


Fig. 27. An illustration of the mean error on each level of the phantom. The top surface represents the mean error on the top level, the middle surface represents the mean error on the middle level, and bottom the mean error on the bottom level, respectively. In the figure, the orientation of the phantom is such that accuracy assessment point 25 is in the center of the grid at each level. Point number 1 is in the back corner and number 49 is closest to the observer. The color bar can be used as an indicator for the error in millimeters at each point on the levels.

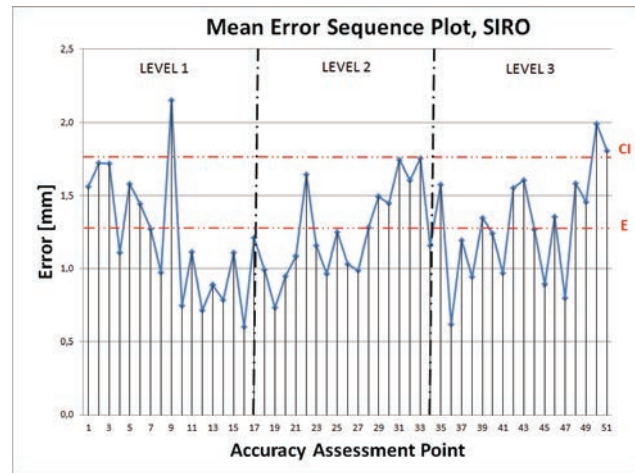


Fig. 28. A representation of the error of the SIRO as a sequence plot. The first point in the sequence diagrams represents the first accuracy assessment point and point number 51 the 51st, respectively. The black vertical dashed lines divide the diagram into three areas labeled LEVEL 1, LEVEL 2, and LEVEL 3. These areas represent the errors on each phantom level in such a way that LEVEL 1 is the bottom, LEVEL 2 is the middle and LEVEL 3 the top levels, respectively. On the graph, the error scale is from 0 to 2.50 mm. The red dashed lines with labels 'E' and 'CI' represent the mean position error and 95 % confidence interval (CI), respectively.

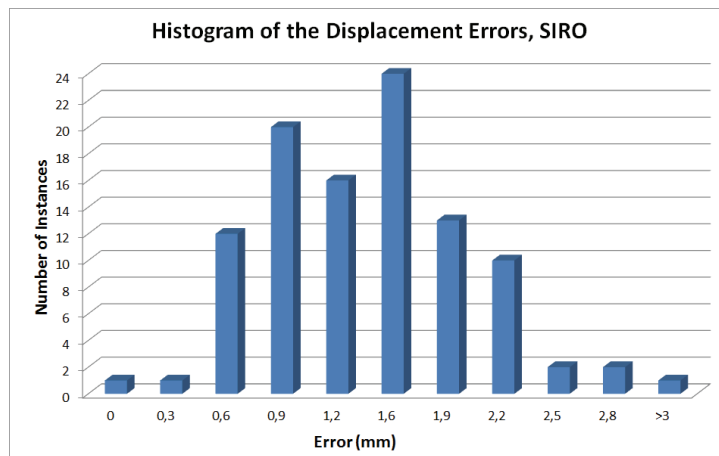


Fig. 29. A Histogram of the displacement error of the SIRO.

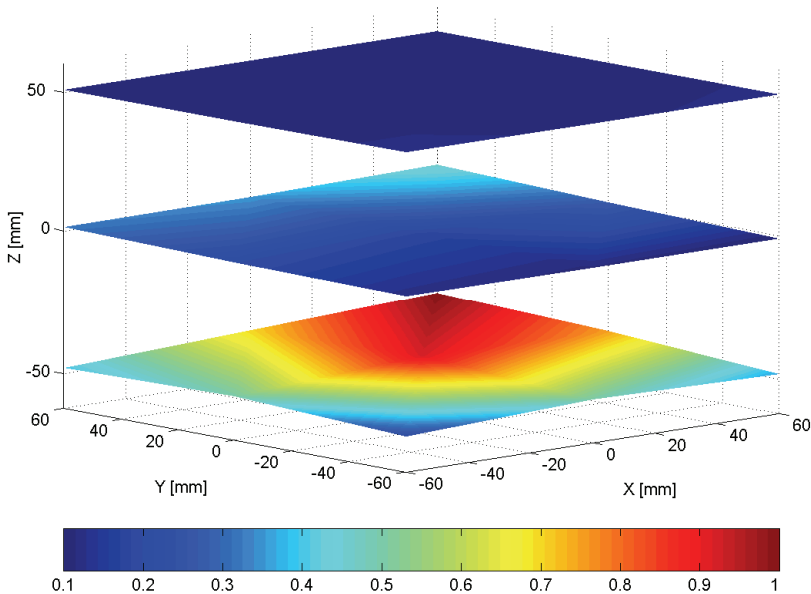


Fig. 30. A surface representation of the repeatability of the prototype SIRO. The colorbar on the bottom can be used as a tool for the repeatability error at each point on the ROSI volume. The three levels on the phantom are at their corresponding positions with a 50 mm interval between the levels.

The accuracy assessment results of the SIRO are presented in Table 5. The mean technical accuracy of the SIRO in the assessed ROSI was verified to be $1.26 \text{ mm} \pm 0.25 \text{ mm}$ with absolute position accuracy (RMS) error of 1.38 mm, 95% interval of confidence of 1.76 mm and repeatability within 0.5 mm.

Table 5. Accuracy assessment results of the SIRO.

	Error [mm]
Mean Error, E	1.26
RMS Error, ϵ	1.38
95% CI	1.76
Standard Deviation, σ	± 0.25
Maximum Error, E_{MAX}	2.30
Repeatability	< 0.50

4.5 Spatial accuracy results of the O-Arm

This section concentrates on the image quality of a surgical 3D CT scanner (O-Arm, Medtronic Inc., Louisville, CO, USA) and the possible errors in the region of surgical interest (ROSI) that should be taken into account when using this device for image acquisition.

The O-arm had been taken into routine use at Oulu University Hospital, Oulu, Finland, in 2009. Figure 31 illustrates phantom II in the gantry of the O-arm.

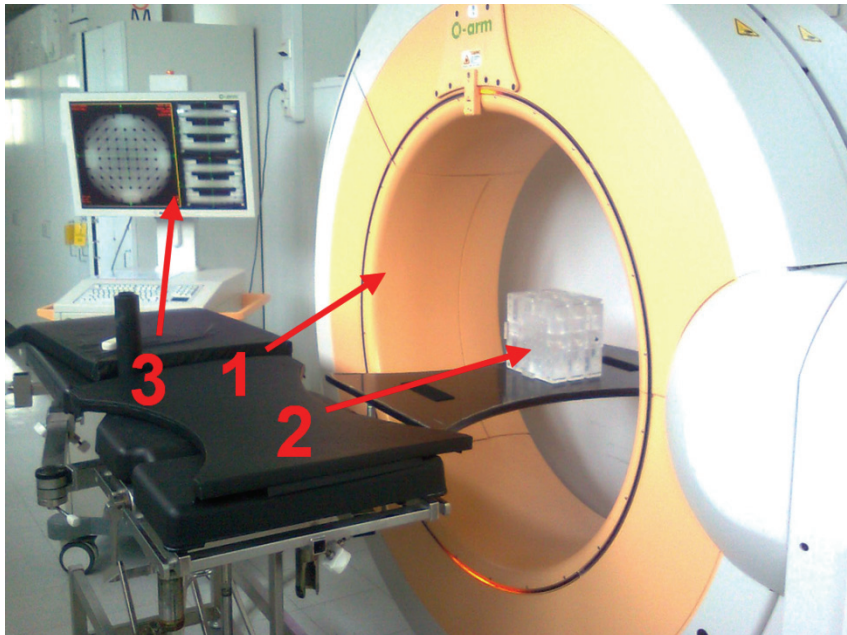


Fig. 31. Phantom II set in the gantry of the O-arm. (1) The O-Arm, (2) the phantom, (3) the surgeon's monitor.

Phantom I was scanned using the O-arm with 80 kVp voltage and 40 mA current with 160 mAs. From the O-arm software the patient parameters were chosen to be medium and spinal canal as the imaging target. Phantom II was scanned using the O-Arm with 120 kVp voltage and 40 mA current with 156 mAs and the same patient parameters as with phantom I imaging and the images retrieved for inspection.

Since the O-arm produces a conical scan, there are no gaps between the slices. The screen of the O-Arm computer unit shows the image data in coronal, sagittal

and axial views (Fig. 31). The view on the screen may be frozen so that as any of the views is scanned, the other views refresh simultaneously. This made it possible to perform the image quality assurance in the following manner:

Phantom I

- I The image data was collected using the O-arm, and screenshots of the image data were saved to the scanner's database. A screenshot was taken at approximately 25 mm intervals containing the tips of the calibration pegs and the middle layer of the calibration levels giving a total of nine slices from the phantom.
- II Visual detection of the accuracy of the images

The images were inspected by connecting lines from each corner of the calibration pegs on each image layer (Fig. 32). The angles of the connection lines were calculated (Fig. 34) and the results collected.

The screenshot images were combined in layers so that the bottom level was made red and the upper layers slightly transparent (Figures 32 and 33). Thus, the position of the accuracy assessment pegs could be seen with respect to the upper layers. Also the connection lines on the outer edges were visible and the difference in the positions could be verified by visual inspection.

By visual inspection, we can see that the image quality of the ascertained area in the ROSI volume seems to have no noticeable distortion or image artefact using the parameters for phantom I. The connection lines' perpendicular angles were at 90 ± 0.5 degrees proving that there is no cone-beam artefact or image distortion on the outer area of the ROSI volume from the center of each phantom level.

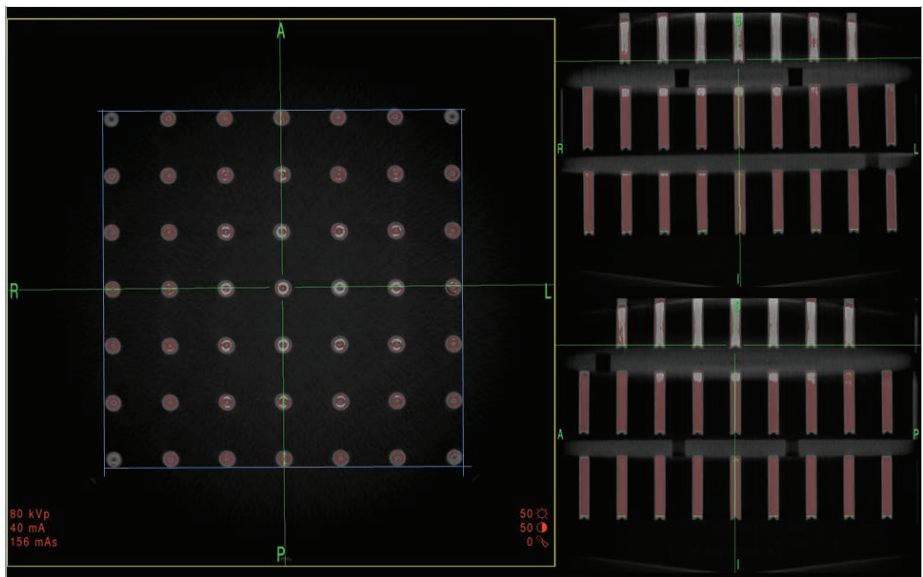


Fig. 32. Combined image data of phantom I. The red colored shading represents the bottom level slices and the slightly transparent grey shading the upper levels slices, respectively.

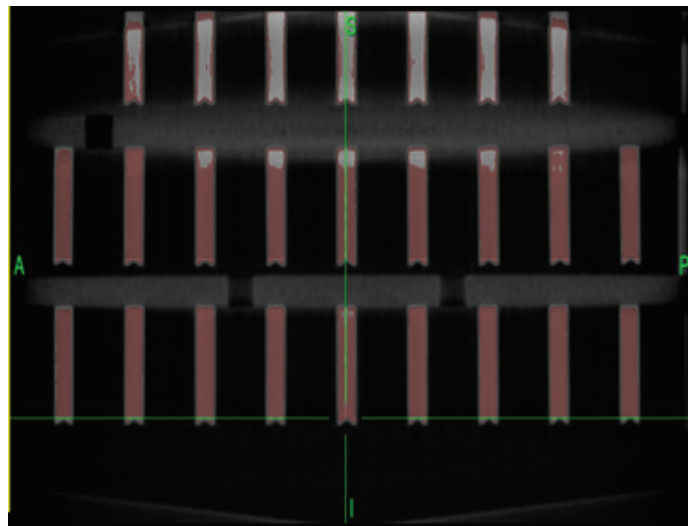


Fig. 33. Combined image data of phantom I image data with all of the images of each layer combined. This is the sagittal view from Fig. 32.

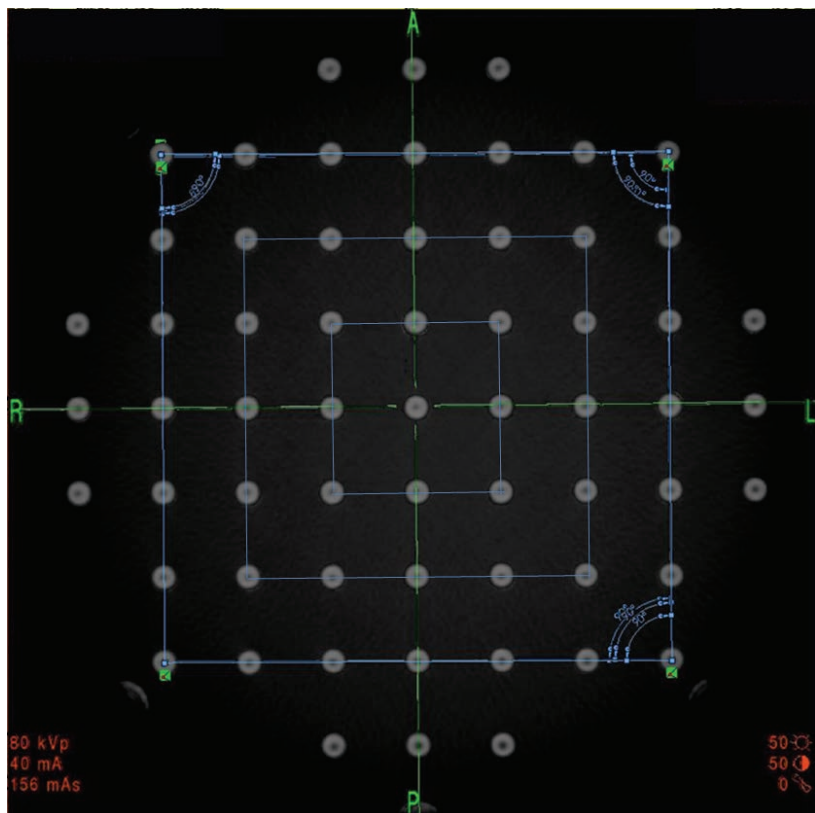


Fig. 34. A closer look at the phantom I images with the connection lines and the corresponding angles added on each of nine layers and then combined to see the possible difference in the outermost edges of the ROSI volume.

Phantom II

- I The image data was collected using the O-arm, and screenshots of the image data were saved to the scanner's database in the same manner as presented with phantom I.
- II Visual detection of the accuracy of the images
The images were inspected by drawing a red circle with a diameter equal to the accuracy assessment hole (Fig. 35 and 36). The diameter of the machined holes was verified at $6 \text{ mm} \pm 0.015 \text{ mm}$ and the image distortion can be detected as the visible black area around the red circles (Fig. 36).

On the phantom II images, with higher voltage and a more attenuating object, we can see minor cone-beam artefact at the outermost corners of the axial view. The accuracy assessment holes seem to become ellipsoidal and the pattern has distortion.

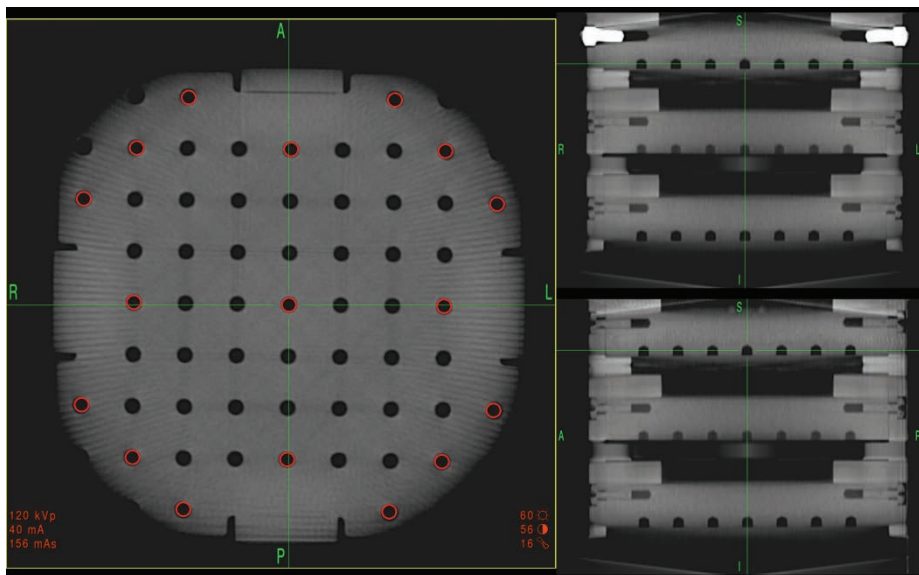


Fig. 35. Phantom II image data obtained using the O-Arm. The screenshot is taken from the bottom level of the phantom. The phantom was placed in the optimal position in the gantry, as the middle level was placed the middle of the scanner. The red circles are attached to the image to verify the accuracy of the image in the fringes of the ROSI. The image seems to have noticeable cone-beam artefact, but as the common circle is attached to the shown positions, actually there is only minor difference in the size of the accuracy assessment points. Two M6 screws made of stainless steel (AISI 316) were used and are highly visible in the sagittal image on the upper right corner.

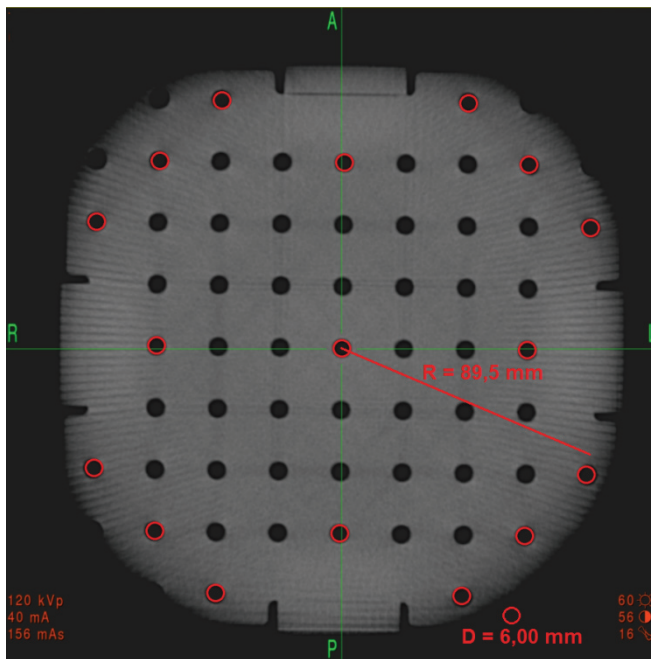


Fig. 36. A close-up image of phantom II with the slight cone-beam artefact shown using the red circles. The artefact is seen at the fringes of the phantom. This drift occurs at 89.5 mm radius from the center of the phantom.

This study presents a method for image quality inspection and detection of possible geometrical distortions due to mechanical misalignments (Barrett & Keat 2004, Henry *et al.* 1989, Kelly 1991, Zylka & Wischmann 1996) in the region of surgical interest (ROSI) (Koivukangas *et al.* 2003, Koivukangas *et al.* 2009, Koivukangas & Katisko 2010).

The method presented a quick and reliable way for image quality and spatial accuracy assessment of 3D CT scanners by inspecting the quality of O-Arm scanner images. The results show that in the pre-determined ROSI there is no visible image distortion or artefact and thus the O-Arm causes minimal error for the IGS accuracy. However, minor cone-beam artefacts were visible in the fringe-fields of scanning volume.

These results are within the range of error of the published values of 0.1 to 3 mm regarding the technical accuracy and the registration accuracy of common IGS systems. Image quality affects both the technical and registration errors of IGS systems as presented by Grunert *et al.* (2003) and Haidegger *et al.* (2010).

4.6 Summary of the research contributions

The systems and methods developed in this thesis as research contributions are:

1. The concept of accuracy testing to meet the needs of quality assurance of navigators and robots in a hospital environment based on the developed tracking error theory.
2. A ‘real world’ universal accuracy assessment phantom and protocol for periodic quality assurance of surgical guidance devices for use in the hospital setting.
 - A phantom
 - An accuracy assessment protocol based on statistical formulation
3. Accuracy analysis and evaluation of the two most widely used tracking modalities and the issues that should be taken into account when setting up the OR for IGS procedures using these navigators.
 - A method for assessing the accuracy of the navigators in the total ROSI volume
 - The dependence of accuracy on the distance from the optical camera pair to the patient in OTS
 - The dependence of accuracy on the distance from the EM field generator to the patient in EMTS
 - Based on the comparison of the results, possible new IGS procedures for the EMTS modality
4. Accuracy analysis of the surgical robot and the development of the SIRO
 - The developed accuracy analysis tools and methods utilized in accuracy assessment of surgical robots
 - Methods and development guides for a 6 DOF surgical robot for use in MRI
5. Spatial accuracy detection of the O-Arm
 - The developed tools and methods utilized in detecting spatial accuracy of a surgical 3D imager in the ROSI volume.

5 Discussion

The discussion of this thesis is divided into four sections. Section 5.1 is a discussion of the developed tools and methods that were designed for use as routine hospital accuracy assessment tools and that were utilized in the accuracy assessment of the surgical guidance devices. Section 5.2 contains the discussion of the accuracy assessment results of the studied navigators. Section 5.3 discusses the accuracy assessment of the prototype surgical robot (SIRO). Finally, Section 5.4 contains discussion of the spatial accuracy results of the studied surgical 3D CT scanner, the O-Arm.

5.1 Accuracy assessment tools and methods for periodic testing of IGS devices

In IGS surgical navigators are used as the main localization technique for instrument tracking. The most commonly used technique is the optical tracking system (OTS) (Grunert *et al.* 2003, Mascott 2005, Wiles *et al.* 2004). For the present research, accuracy assessment phantoms and protocols were developed for periodic assessment of the accuracy of surgical navigators and other IGS equipment while in routine hospital use (Koivukangas *et al.* 2009, Koivukangas & Katsiko 2010). The developed phantoms and protocols are a response to the suggestion by industry for “real world” methods for use in hospitals and designed for use in the region of surgical interest (ROSI) (ASTM 2011, Haidegger *et al.* 2010, Stiehl *et al.* 2007, Wiles *et al.* 2004). Furthermore, the method satisfies the requirements of, first, a comprehensive set of statistics representative of the accuracy and, second, a clear definition of the accuracy assessment protocol (Stiehl *et al.* 2007). As this thesis answers to the need of accuracy assessment tools and methods for periodic evaluation of IGS devices, the technical accuracy of the devices was represented as mean accuracies in the ROSI. The tools and methods for the technical accuracy assessment within the studied ROSI provide essential information for hospital users to contact the manufacturer of the device if a clear indication of inaccuracy has been detected. The purpose of the tools and methods is to verify the performance of IGS devices and to indicate the possible need for re-calibration.

Possible occurrence of image artefact of the phantoms was minimized by using the chosen material, PMMA. The phantoms were designed for commonly used surgical CT and MRI scanners, the latter producing magnetic fields between

0.15 T to 3 T, and regular tap water with common dish washing solvent was used as the liquid. Thus, heating effects and gradient field related and chemical artefacts could be minimized. Naturally increasing the MRI field strength for example, would cause these artefacts to worsen. Since the tools were utilized in a common hospital setting, this effect was considered to be outside of the scope of this thesis.

As demonstrated in the accuracy analysis done for the two commercial navigators that are in use at Oulu University Hospital, the method can be universally applied to periodically confirm the quality of IGS guidance devices such as surgical navigators and medical robots designed to function in the region of surgical interest. Furthermore, slight cone-beam artefact was detected when the phantom was scanned with the surgical 3D CT –scanner.

Due to the nature of surgical procedures, anatomic changes occur in the patient's anatomy. These changes (e.g., brain shift) in the anatomy are highly likely to occur during IGS, which is based on preoperative image data acquired before the procedure. Thus the application accuracy is not uniform within different assessments even when using common procedures and tools. Based on these facts and the accuracy assessment of several IGS devices, it can be concluded that the analysis of technical accuracy is in fact the most necessary error component that can be periodically verified and improved. Naturally the errors in the imaging scanners that are related to registration accuracy can cause significant error for the total IGS procedure, but the testing of these devices has already been standardized and is a mandatory maintenance procedure.

In the results analysis, the 3D models showed the error dependence on the location of the accuracy assessment points within the ROSI volume. The sequence plots show further in detail the error in millimeters at each point. The histograms of each modality and device show the distribution of the error as instances within certain tenths of a millimeter. The histograms are tools for seeing the dependence of the outlier errors with respect to the mean and RMS errors. These graphs by themselves may not be the best way of presenting the error since there is no real dependence factor for any other statistics, because of the nature of the error being distance values, which by definition are presented as positive numbers. These errors are shown to be systematic and similar within the different IGS devices, namely the OTS and EMTS of the navigators, and the SIRO robot. The 95% CI further clarifies the accuracy of the tested device and strengthens the mean and RMS accuracy results by showing the user the effect of highest errors on the total accuracy. This is seen especially in Figure 24, where the means of the

errors of the two EMPS navigators have a difference of 0.20 mm (0.30 mm for the S7 and 0.50 mm for the Treon plus), but the difference in the 95% CI error is 0.94 mm (0.82 mm for the S7 and 1.76 mm for the Treon plus). Naturally extensive temperature and humidity changes could cause errors to deviate even more, but the effect of these aspects was minimized by testing the IGS devices in common ambient conditions.

5.2 Accuracy assessment of surgical navigators

After operationalizing the concept of accuracy of image-guided devices, and consideration of materials and machining to fulfill these requirements, the study continued with assessment of the accuracy of surgical navigators being used in the hospital setting. The phantom accuracy assessment points were machined symmetrically and in three levels to obtain an accuracy assessment volume mimicking that of the human head, i.e. the region of surgical interest (ROSI) and specifically in the neurosurgical region (Koivukangas *et al.* 2009, Koivukangas & Katisko 2010).

Compared with previous reports, one of the features of the present study was that the phantoms and study protocol were designed to be used periodically to verify accurate functioning in the actual hospital setting during routine use of the surgical navigators. Earlier accuracy assessment studies of surgical navigators have concentrated on the overall accuracy of the system in general and on the error sources leading to inaccuracies (Ringel *et al.* 2009, Hassfeld & Müchling 2000, Kücker *et al.* 2006, Mascott 2005, Mösges & Schlöndorff 1998, NDI 2011, Simon 1997, Wiles *et al.* 2004). The present accuracy assessment results on the comparison of the two tracking modalities are in the range reported by these groups.

During this research, the accuracy of the OTS was assessed in detail using also directional analysis to find the source of error in the surgical procedure setup and the factors that need to be taken into account when placing the camera with respect to the patient. The results show that in placing the surgical navigator equipment using OTS, the most important factor for minimizing displacement error is the distance from the optical camera to the object.

The overall results for the OTS, being 0.30–0.45 mm, are clearly in the tolerable error range for safe operations. Groups assessing the OTS have reported accuracies in the range of 0.1 mm to 1.4 mm, again depending on the assessment procedure and the device assessed (Alakuijala 2001, Hassfeld & Müchling 2000,

Kücker *et al.* 2006, Mascott 2005, Mösges & Schlöndorff 1998, NDI 2011, Ringel *et al.* 2009, Ruohonen & Karhu 2010, Simon 1997, Wiles *et al.* 2004, Widmann *et al.* 2012, Wittmann *et al.* 2011). Also, a company making commercial optical cameras for surgical navigators (NDI) gives their new products, the Polaris Spectra® and Polaris Vicra® RMS accuracies of 0.25 mm with a 95% CI of 0.5 mm (NDI 2011).

The present study also showed that the direction resulting in increasing error was the distance from the optical camera pair to the navigated object. This was seen to be systematic also in the error sequence plot diagrams (Fig. 19). One possibility for this phenomenon can be seen in the basic stereo camera model (Schenenberger 2004). There is a tendency for lens distortions using the optical cameras as the tracking method (Schenenberger 2004, Weng *et al.* 1992). It has been shown that the overall technical accuracy of infrared camera based optical tracking may be influenced by the following different error components: 2D calculation of the patterns accounts for 0.02 mm of the error, residual image distortions account for 0.17 mm of the error, thermal drift with up to 0.11 mm error, scaling which accounts for 0.26 mm error and noise with an additional 0.01 mm error component, with the total error summing to 0.47 mm (Schenenberger 2004). These error components seem to explain the RMS errors obtained also in the present study.

This finding is comparable to an optical camera manufacturer's results in earlier studies in the literature (Wiles *et al.* 2004). The group assessed the accuracy of the NDI Optotrack and the Polaris measurement systems that were used in OTS and they found a notable systematic overall RMS error increase in the direction from the optical camera to the object. These results further indicate that the main factor contributing to the RMS error throughout the entire assessed volume in fact comes from the error in the longitudinal y direction (their z direction).

The technical accuracy of the EMTS was found to be 0.30–0.50 mm. Thus, the accuracy of the devices was found to be acceptable for surgical procedures. Earlier accuracy assessment of the EMTS has been reported to be in the range of 0.17 mm to 1.4 mm depending on the devices and assessment procedures (Alakuijala 2001, de Lambert *et al.* 2012, Frantz *et al.* 2003, Hummel *et al.* 2006, Mascott 2005, Schicho *et al.* 2005, Schneider & Stevens 2005, Simon 1997). The results also show that the error is highest on the furthest edge of the assessed volume and the error increases as the function of the cubic radius of the EM field generator.

Also, these results show that the assessed navigator tracking modalities were nearly equal in the accuracies. Thus, the most suitable method of instrument tracking for a particular surgical procedure can be chosen by criteria other than plain technical accuracy. The greatest difference between the tracking modalities was found to be regarding the instruments used. For the EMTS modality, the instruments are quite flexible. If the instruments are forced into a place so that they are subject to bending, it may result in high accuracy errors. Since the EMTS navigation is based on tracking the coils on the instrument, the relative position of the coils must not change.

As the difference between the accuracies of the OTS and EMTS was marginal, this study showed that EMTS is a very suitable method for surgical navigation. The possible limitations of use when compared to the OTS are in some interventional procedures. Because of the nature of EMTS tracking, this tracking method may not be suitable for iMRI procedures. On the other hand, EMTS has unique advantages compared to OTS that have received little notice in previous studies. The coils in the instruments are placed near the end of each tip. As a comparison, the sensing spheres or LED-markers on the OTS instruments are placed so that they are visible (Figure 7). This is a significant difference between the tracking methods and means that surgical navigation based on EMTS may be used more accurately and closer to the ROSI (region of surgical interest) and that the instruments may be guided closer to the sensitive structures in the human anatomy. Also, since the patient trackers are light and may be attached to the patient without for example skull clamps, the immobilization of the patient during procedures is not as critical as with OTS based navigation. Another noticeable aspect concerns small children in pediatric procedures. The use of EMTS makes navigation possible even for babies as rigid immobilization is not necessarily required.

Based on the experimental analysis of the navigator accuracies it was shown that EMTS is very suitable for a variety of surgical procedures and its use may be extended to specialties in which OTS may not be as suitable.

5.3 Accuracy assessment of the SIRO

The accuracy assessment results of the prototype surgical robot (SIRO, Heikkilä *et al.* 2012, Koivukangas *et al.* 2012, Virtanen 2006) were within the range of error accepted in the literature (Grunert *et al.* 2003) and also within the range of error of commercial robots in the surgical field (Haidegger *et al.* 2010). Thus, the

robot's performance is clearly tolerable and promising for further study and enhancement. The accuracy assessment protocol together with the phantom also proved to be a suitable way of accuracy analysis of a surgical robot in the region of surgical interest (ROSI).

A total of 51 points on the phantom were localized in both of the two experiment sets with the robot according to the accuracy assessment protocol, and the mean error of each corresponding point analyzed. The distances measured from a fixed origin with the robot were compared to the known phantom accuracy assessment point distances on the phantom giving the mean error for the robot within the ROSI. The repeatability was assessed by using the collected angular data of the robot to drive the tip of the instrument from base position back to each pre-determined accuracy assessment point. The mean difference in the location between the five experiments on each point is considered as the repeatability.

The mean technical accuracy for the SIRO in the assessed ROSI was verified to be $1.26 \text{ mm} \pm 0.25 \text{ mm}$ with absolute position accuracy (RMS) error of 1.38 mm, 95% interval of confidence of 1.76 mm and repeatability within 0.5 mm. In the 3D representation of the results we can see that the error tends to be systematic at the furthest area of the studied ROSI. Also the systematic error in the vertical direction could be seen (Koivukangas *et al.* 2012).

The reason for this phenomenon is that the cables on the transmission of DOF 5 and 6 crept slightly due to the tension during the long test drives of the accuracy assessment. Another reason for the systematic error may have been that the robot base level slightly differed from that of the phantom level. Also, the basic error sources in the mechatronic construction of robots in general have an effect on the total and systematic error. These error sources include possible instrument errors due to the encoders, elasticity in the structure and the measurement errors in joint positions. Joint position measurement errors have a tendency of multiplying through the DH-chain (Kwartowitz *et al.* 2006, Shiakolas *et al.* 2002). As presented, the construction of the present robot, SIRO, was intended to be used in the MRI environment. This objective naturally set restrictions in using common technologies and components; thus a number of these parts were designed and developed during the research project solely for this purpose. The technical error is thus partially affected by these components.

The results presented in this study reflect these basic phenomena of accuracy and sources of error of robotic systems. The error trends shown in 3D surfaces demonstrated that the error increases as the distance from the robot base increases. Thus, the farther the joint is from the base, the larger is the localization error.

It has been shown that the largest effect on robot accuracy is based on its mechanical construction (Shiakolas *et al.* 2002). The encoder resolutions of the joints on the SIRO were 0.006 degrees (joint 1), 0.09 degrees (joint 2), 0.09 degrees (joint 3), 0.006 degrees (joint 4), 0.06 degrees (joint 5), and 0.0125 degrees (joint 6). Based on these resolutions of the encoders, the repeatability of the position of the tip of the tool is at the level of ± 0.26 mm, ± 0.24 mm, and ± 0.37 mm in x, y and z directions, respectively (Heikkilä *et al.* 2012).

Based on the requirements for RMS accuracy of IGS, 3–5 mm is generally considered acceptable as is 2 mm for neurosurgical IGS (Grunert *et al.* 2003). Also, submillimetric error has been recommended for robot assisted IGS procedures (Grunert *et al.* 2003, Haidegger *et al.* 2010).

Earlier research results have been published with similar findings of commercial robots (Grunert *et al.* 2003, Drake *et al.* 1993, Kwartowitz *et al.* 2006). Haidegger *et al.* collected the accuracy analysis of the most widely used commercial robots (The Puma 200, the ROBODOC, the NeuroMate and the da Vinci) with the following results: technical accuracy has been reported in the range of 0.5–1.35 mm and repeatability of 0.05–0.15 mm (Haidegger *et al.* 2010). Bell *et al.* (2012) recently reported an accuracy of 0.56 mm ± 0.41 mm for a robot that was specially built for stereotactic cochlear implantation by their group at the ARTOG Center, University of Bern, Switzerland. Also, Song *et al.* (2009) and Yong *et al.* (2010) reported accuracies of 0.89 mm (Song *et al.* 2009) and 1.77 mm (Yong *et al.* 2010) for their custom built surgical robots.

The accuracy assessment may seem to have been done with rather compact data containing two experiment sets of 51 analyzed points from which the analysis error was done. However, since there was no noticeable deviation within data received in the experiment sets, and since the repeatability tests of a total of 15 points driven five times each gave such remarkable results, it was concluded that the accuracy tests were extensive enough for the accuracy assessment of the robot. Also, as the SIRO robot is a prototype platform, a goal for the accuracy assessment was to collect information on the maneuverability and limiting factors of such a construction for future research. Thus, the lack of more extensive data for the accuracy assessment was justified.

After these encouraging accuracy and repeatability results, future work will include enhancement of the link and joint power transmission of the current robot. Especially, the cable driven power transmission for the wrist movements (5th and 6th DOF) are under study with the goal of a more rigid, MR compatible, and affordable technique for replacing the current cable drives.

The accuracy assessment exercise using the SIRO, a prototype surgical robot, also demonstrated the flexibility of the present phantom and protocol, whose original intents also included quality assurance of surgical guidance devices invented and developed in research groups.

5.4 Spatial accuracy of the O-Arm

Image artefacts can decrease the spatial accuracy of CT images making them useless for diagnosis and thus for use in IGS procedures (Barrett & Keat 2004). It is necessary to understand possible causes for image artefact and also to have useful tools for inspecting the spatial accuracy.

It can be seen that using a less attenuating phantom (i.e., less material) with relatively low imaging parameters, there was no noticeable image distortion or other image artefact that could result in a noticeable decrease in the accuracy of IGS procedures. On the other hand, using a more attenuating phantom (i.e., more material) with higher voltage, the cone-beam artefact became visible at fringes of the imaged volume.

Thus, the object being scanned should be taken into account when choosing parameters and positioning the object in the gantry for image acquisition using a CT-scanner.

Future research on image quality inspection contains evaluation of the accuracy assessment of the surgical navigators using the image data acquired with the O-Arm using direct registration. Also, other sources of image artefact will be studied using surgical instruments such as retractors and implantable fixation screws commonly used in orthopedic procedures.

6 Conclusions

The process of developing reliable tools and methods for accuracy assessment of IGS devices for this study began in early 2008. At that time there were no standardized methods available and the research was begun by understanding and determining the region of surgical interest. As this research arose from the needs of neurosurgeons and scientists at the Neurosurgical Research Unit in Oulu University Hospital, Oulu, Finland, the region of surgical interest was chosen to roughly mimic the size of a human head.

As stated in the introduction and literature review, the multi-national committee led by the ASTM began their work in standardizing tools and methods for accuracy assessment of IGS devices. Their scope was to publish a preliminary standard with orthopedic procedures as the main field of application. This process led to the ASTM F2554-10 standard that was accepted in December 2010 and published as a standard practice in 2011. This preliminary standard however left open questions in other fields e.g. neurosurgery. The standard states that the practice provides recommendations for the processes of accuracy assessment. The open questions that may lead to subsequent standards will address the IGS system along with any necessary imaging modality. Additional standards are also needed for specialty specific procedures and surgical specialties such as neurosurgery, including brain tumor biopsy and so forth.

The present study was focused on IGS systems in neurosurgical procedures. The specified and developed tools and methods were utilized in accuracy assessment of two commercial navigators, both enabling the OTS and EMTS modalities, and a prototype surgical robot (SIRO). The developed tools and methods are intended for periodic accuracy assessment to verify the device performance, rather than for actual re-calibration. Thus, the mathematical representation of the technical accuracy was determined as the mean accuracy in the ROSI. Also, a study on the spatial accuracy of a commercial, surgical 3D CT scanner (the O-Arm) was performed using both developed phantoms. It is clear that the accuracy assessment of the IGS devices in the pre-determined ROSI could be performed and the total ROSI volume analyzed. The 3D error surfaces show the trend of error of each tracking system in the overall volume. If the assessment was done in a single surface, the error trend could have been dramatically different. This is the main difference between this study and the abovementioned standardized method. Furthermore, since the present phantoms were made of PMMA, the spatial accuracy of the imager could also be evaluated.

Finally, as the phantoms were developed as three level devices, the volumetric assessment in the ROSI could be reliably assessed.

The results indicate that the two most used tracking modalities in the fields of IGS, namely the OTS and EMTS, have nearly identical accuracy. Since these tracking methods are based on different physical phenomena, also the surgical setups of both modalities are unique and the error dependence on placing the systems was demonstrated. Based on this fact, suggestions were made in placing the devices for surgical procedures. Also, suggestions on using either modality for special cases were discussed. It was found that OTS accuracy was highly dependent on the distance from the optical camera pair array to the navigated object. On the other hand, the EMTS magnetic field generator and patient tracker placement with respect to the navigated object was shown to be critical. The accuracy assessment results and performance of the SIRO robot showed the dependence on the placement of the robot base with respect to the object being critical. The detection of the spatial accuracy of the O-Arm showed noticeable image artefact in the fringes of the scanned phantom.

The accuracy assessment phantom and protocol satisfied the need expressed in the literature for a way to periodically check the accuracy of surgical navigators, robots and other IGS guidance devices, especially those functioning within a defined region of surgical interest (ASTM 2012, Haidegger *et al.* 2010, Kazanzides 2006, Kroneif *et al.* 2011, Kwartowitz *et al.* 2006). The importance of assessing IGS devices and evaluating the performance of robots in particular was also stressed by Ringel *et al.* (2012). They showed that for example in some cases free-hand assisted pedicle screw implantation may be more accurate than that assisted by the robot.

Recently, the growing number of issues related to the accuracy and functionality of surgical image-guided devices underscores the need for methods that can be routinely used to assess the accuracy of these devices in the hospital setting (MAUDE 2012). Had the accuracy of the devices been assessed routinely, probably a great number of these errors could have been detected pre-surgically.

The presented methods for accuracy assessment of surgical guidance devices could be utilized in the following cases:

1. When the IGS guidance device is taken into routine use
2. Periodically for quality assurance
3. When the device indicates accuracy decrease
4. When the user suspects accuracy decrease

5. In all clinical research environments in which new IGS technology is being developed.

The accuracy assessment was done to verify the error in the region of neurosurgical interest (ROSI). Thus, the assessed volume was limited to mimic the size of the human head. Increasing the ROSI volume may result in greater deviation in the results.

References

- Adams L, Knepper A, Meyer-Ebrecht D, Rüger R & van der Brug W (1996) Image guided surgery – Optical position measurement for brain surgery. *IEEE Computer* 29(1): 48–54.
- Alakuijala J (2001) Algorithms for modeling anatomic and target volumes in image-guided neurosurgery and radiotherapy. PhD dissertation, Univ Oulu, Dept Electrical Engineering, Oulu, Finland.
- Alexander E III, Moriarty T, Kikinis R & Jolesz F (1995) Innovations in minimalism: intraoperative MRI. *Clinical Neurosurgery. Proceedings of the Congress of Neurological Surgeons*, San Francisco, CA, USA 43: 338–352.
- ASM International (1988) Engineered materials handbook Volume 2: Engineering plastics. ASM International, Metals Park, OH, USA.
- Barrett J & Keat N (2004) Artifacts in CT: Recognition and Avoidance. *RadioGraphics* 24: 1679–1691.
- Beaulieu A, Shepard T, & Ellis R (2008) A process control system model for interactive image guided surgery. *Proceedings of the 2nd SysCon 2008 - IEEE International Systems Conference*, Montreal, Canada: 1–8.
- Bell B, Stieger C, Gerber N, Arnold A, NEuer C, Hamacher V, Kompis M, Nolte L, Caversaccio M & Weber S (2012) A self-developed and constructed robot for minimally invasive cochlear implantation. *Acta Oto-Laryngology* 132(4): 355–60.
- Birkenfeller W, Watzinger, F, Wanschitz F, Ewers R & Bergmann H (1998) Calibration of tracking systems in a surgical environment. *IEEE Trans Med Imaging* 17(5):737–742.
- Chiao J, Goldman J, Heck D, Kazansides P, Peine W, Stiehl J, Yen D & Dagalakis N (2008) Metrology and standards needs for some categories of medical devices. *J Res Natl Inst Stand Technol* 113(2): 121–129.
- Chinzei K & Miller K (2001) MRI guided surgical robot. *Proceedings of the Australian Conference in Robotics and Automation*, Sydney, Australia: 50–55.
- Chung A, Edwards P, Deliganni F & Yang G-Z (2004) Freehand cocalibration of optical and electromagnetic trackers for navigated bronchoscopy. *MIAR 2004, LNCS* 3150: 320–328.
- Clarke J, Deakin A, Picard F & Nicol A (2008) Technical evaluation of the positional accuracy of computer assisted surgical systems. *Proceedings of the 8th Annual Meeting of CAOS - Int Proc*: 333–335.
- Cleary K & Nguyen C (2001) State of the art in surgical robotics: Clinical applications and technology challenges. *Comp Aid Surg* 6(6): 312–328.
- Corke PI (1996) A Robotics toolbox for MATLAB. *IEEE Rob Aut Mag* 3(1): 24–32.
- de Lambert A, Esneault S, Lucas A, Haigron P, Chinquin Ph & Magne JL (2012) Electromagnetic tracking for registration and navigation in endovascular aneurysm repair: A phantom study. *Eur J Vasc Endovasc Surg* 43(6): 684–9.
- Drake JM, Joy M, Goldenberg A & Kreindler D (1991) Computer- and robot-assisted resection of thalamic astrocytomas in children. *Neurosurg* 29(1): 27–33.

- Drake JM, Prudencio J & Holowka S (1993) A comparison of a PUMA robotic system and the ISG Viewing Wand for neurosurgery. In: Maciunas R (ed) Interactive Image-guided Neurosurgery. Amer Assoc Neurol Surgeons, USA: 121–133.
- Fischer GS (2005) Electromagnetic tracker characterization and optimal tool design (with application to ENT surgery). MSc thesis. John Hopkins Univ, Dept Mech Eng. Baltimore, MD, USA.
- Fitzpatrick JM, West JB & Maurer CR Jr. (1998) Predicting error in rigid-body, point based registration. IEEE Trans Med Imaging 17: 694–702.
- Frantz DD, Wiles AD, Leis S & Kirsch S (2003) Accuracy assessment protocols for electromagnetic tracking systems. Phys Med Biol 48: 2241–51.
- Galloway RL, Berger MS, Bass A & Maciunas RJ (1993) Registered intraoperative information: electrophysiology, ultrasound, and endoscopy. In: Maciunas R (ed) Interactive image-guided neurosurgery. Amer Assoc Neurol Surgeons, USA: 247–258.
- Gassert R, Burdet E & Chinzei K, (2008) MRI-compatible robotics. A critical tool for image-guided interventions, clinical diagnostics, and neuroscience. IEEE Eng Med Biol Mag 3: 12–14.
- Glauser D, Fankhauser H, Epitaux M, Hefti JL & Jaccottet A (1995) Neurosurgical robot Minerva: first results and current developments, J Image Guid Surg 1: 266–272.
- Graig J (1986) Introduction to robotics, mechanics & control. Reading, MA, USA, Addison-Wesley: 35–42, 114–119.
- Grunert P, Darabi K, Espinosa J, & Filippi R (2003) Computer aided navigation in neurosurgery. Neurosurg Rev 26: 73–99.
- Goldman L (2007) Principles of CT and CT technology. J Nucl Med Tech 35(3): 115–128.
- Haidegger T, Kazandides P, Rudas I, Benyó B & Benyó Z (2010) The importance of accuracy measurement standards for computer-integrated interventional systems. EURON GEM Sig Workshop on The Role of Experiments in Robotics Research at IEEE ICRA: 1–6.
- Haidegger T & Virk GS (2012) International Standardization Efforts in Medical Robotics. A presentation at the ICRA 2012 Workshop on: Modular Surgical Robotics: how can we make it possible? Theme: Robots and Automation: Innovation for Tomorrow's Needs. 2012 IEEE International Conference on Robotics and Automation. St. Paul, MN, USA. URI: http://www.eurosurge.eu/c/document_library/get_file?uuid=754447a3-6fa0-4b42-acef-9547b592912f&groupId=13342/. Cited 2012/6/1.
- Hassfeld S & Müchling J (2000) Comparative examination of the accuracy of a mechanical and an optical system in CT and MRT based instrument navigation. Int J Oral Maxillofac Surg 29: 400–407.
- Hendee W & Morgan C (1984) Magnetic resonance imaging: Part I – physical principles (medical progress). The Western J Med 141: 491–500.

- Heikkilä T, Yrjänä S, Kilpeläinen P, Koivukangas J & Sallinen M (2012) An assistive surgical MRI compatible robot - first prototype with field tests, explicative cases of controversial issues in neurosurgery. In: Signorelli F (ed), ISBN: 978-953-51-0623-4. InTech. URI: <http://www.intechopen.com/books/explicative-cases-of-controversial-issues-in-neurosurgery/an-assistive-surgical-mri-compatible-robot-first-prototype-with-field-tests/>. Cited 2012/6/29.
- Hill DLG, Batchelor PG, Holden M & Hawkes DJ (2001) Medical image registration. Topical Review. *Phys Med Biol* 46: R1–45.
- Holmes D III, Rettmann M & Robb R (2008) Visualization in image-guided interventions. In: Peters TM & Cleary KR (ed) Image-guided interventions: technology and applications. Springer Science+Business Media, LLC, New York, NY, USA: 45–80.
- Hosoda T, Takeuchi H, Hashimoto N, Kitai R, Arishima H, Kodera T, Higashino Y, Sato K & Kikita K (2011) Usefulness of intraoperative computed tomography in surgery for low-grade gliomas: a comparative study between two series without and with intraoperative computed tomography. *Neurologia Medico-Chirurgica* 51: 490–495.
- Hummel J, Figl M, Birkenfellner W, Bax M, Shahidi R, Maurer Jr. C & Bergmann H (2006) Evaluation of a new electromagnetic tracking system using a standardized assessment protocol. *Phys Med Biol* 51: N205–210.
- ISO 5725-1:1994(E) (1994) Accuracy (trueness and precision) of measurement methods and results: Part 1. General principles and definitions. The International Organization for Standardization, Geneva, CH.
- ISO 9283 (1998) Manipulating industrial robots-performance criteria and related test methods. The International Organization for Standardization, Geneva, CH.
- Katisko J (2004) Optisesti neuronavigoitu ultraäänikuvaus intraoperativisessa magneettikuvausympäristössä. Lic. thesis. Univ Oulu, Dept Physics and Neurosurgery and Oulu University Hospital, Oulu, Finland.
- Katisko J (2012) Intraoperative imaging guided delineation and location of regions of surgical interest – feasibility study. Ph.D. dissertation, Faculty of Medicine, Institute of Clinical Medicine, Dept Neurosurgery, and Faculty of Medicine, Institute of Diagnostics, Dept Diagnostic Radiology, Univ Oulu, Oulu, Finland.
- Kazanzides P (2006) Surgical robots and phantom (artefact) devices. In: Proceedings of the ASTM workshop on medical devices metrology and standards. ASTM, NIST, NCI, FDA and UT. Arlington, Atlanta, USA.
- Khatib O, Craig J & Lozano-Pérez T (ed) (1992) The Robotics Review 2. The MIT Press. Cambridge, MA, USA.
- Knappe P, Gross I, Pieck S, Wahrburg J, Kuenzler S & Kerchblaumer F (2003) Position control of a surgical robot by a navigation system. Proceedings of the International Conference on IEEE/RJS Conference on Intelligent Robots and Systems, Las Vegas. Nevada, USA, 3: 3350–3354.
- Koivukangas J (1984) Ultrasound imaging in operative neurosurgery: An experimental and clinical study with special reference to ultrasound holographic B (UHB) imaging. PhD dissertation. Univ Oulu, Dept Neurosurgery, Oulu, Finland.

- Koivukangas J, Louhisalmi Y, Alakuijala J & Oikarinen J (1993) Ultrasound-controlled neuronavigator-guided brain surgery. *J Neurosurg* 79: 36–42.
- Koivukangas J, Katisko J, Yrjänä S, Tuominen J, Schiffbauer H & Ilkko E (2003) Successful neurosurgical 0.23T intraoperative MRI in a shared facility. *Neurosurg* 2003, Monduzzi Editore Medimond: 439–444.
- Koivukangas T, Katisko J, Louhisalmi Y, Nevala K, & Koivukangas J (2009) Development of an accuracy assessment phantom for surgical navigators. Proceedings of the 31st Annual International Conference of the IEEE Engineering in Medicine and Biology Society, Minneapolis, MN, USA: 1517–1520.
- Koivukangas T & Katisko J (2010) Accuracy assessment phantom for surgical devices. Proceedings of the 5th Cairo International Conference on Biomedical Engineering, Cairo, Egypt: 57–60.
- Koivukangas T, Makkonen T, Louhisalmi Y & Nevala K (2012) Accuracy assessment of a prototype surgical interactive robot developed for the MRI environment. *Int J CARS* 7(Suppl 1): S215–S216.
- Kroneif G, Ptacek W, Kornfeld M & Fürst M (2011) Evaluation of robotic assistance in neurosurgical applications. *J Rob Surg* 1(6): 33–39.
- Kubben PL, ter Meulen KJ, Schijns OE, ter Laak-Poort, van Overbeeke JJ & van Santbrink H (2011) Intraoperative MRI-guided resection of glioblastoma multiforme: a systematic review. *The Lancet Oncology* 12(11): 1062–1070.
- Kücker J, Xu S, Viswanathan A, Shen E, Glossop N & Wood B (2006) Clinical evaluation of electromagnetic tracking for biopsy and radiofrequency ablation guidance. *Int J CARS* 1: 169–187.
- Kwartowitz D, Herrell S, Galloway R (2006) Toward image-guided robotic surgery: Determining intrinsic accuracy of the daVinci robot. *Int J CARS* 1: 157–165.
- Larson BT, Erdman AG, Tsekos NV, Yacoub E, Tsekos PV & Koutlas IG (2004) Design of an MRI-compatible robotic stereotactic device for minimally invasive interventions in the breast,” *J Biomech Eng* 126: 458–465.
- Madhavan G, Thanikachalam S, Krukenkamp I & Saltman A (2002) Robotic surgeons. *IEEE Potentials* 21(3): 4–7.
- Madritsch, F (1996) CCD-camera based optical tracking for human computer interaction. *IJVR* 2007: 161–170.
- MaRS 2010. Market Insight. Life Sciences – Minimally-Invasive Medical Technologies, September 2010, MaRS Discovery District, Toronto ON, CA. URI: <http://www.profoundmedical.com/images/MinimallyInvasive.pdf/>. Cited 2012/6/1.
- Masamune K, Kobayashi E, Masutani Y, Suzuki M, Dohi T, Iseki H & Takakura K (1995) Development of an MRI-compatible needle insertion manipulator for stereotactic neurosurgery. *J Image Guid Surg* 1: 242–248.
- Mascott C (2005) Comparison of magnetic tracking and optical tracking by simultaneous use of two independent frameless stereotactic systems. *J Neurosurg* 57(4): 295–301.
- Masood S, Gao J & Yang G-Z (2002) Virtual tagging: Numerical considerations and phantom validation. *IEEE Trans Med Imaging* 21(9): 1123–1131.

- MAUDE 2012. The Manufacturer and User Facility Experience Database. URI: <http://www.accessdata.fda.gov/scripts/cdrh/cfdocs/cfMAUDE/search.cfm/>. Cited 2012/5/18.
- McGirt MJ, Chaichana KL, Gathinji M, Attenello FJ, Than K, Olivi A, Weingart JD, Brem H & Quiñones-Hinojosa AR (2009) Independent association of extent resection with survival in patients with malignant brain astrocytoma. *J Neurosurg* 110(1): 156–162.
- Miga IM, Paulsen KD, Kennedy FE, Hoopes PJ, Hartov A & Roberts DW (1997) A 3d brain deformation model experiencing comparable surgical loads. Proceedings of the 19th Annual International Conference of the IEEE Engineering in Medicine and Biology Society, Chicago, IL, USA: 773–776.
- Mooring BW & Pack TJ (1986) Determination and specification of robot repeatability. Proceedings of 1986 IEEE International Conference on Robotics and Automation, San Francisco, CA, USA: 1017–1023.
- Moretti B, Fadili L, Ruan S, Bloyet N & Mazoyer B (2000) Phantom-based performance evaluation: Application to brain segmentation from magnetic resonance images. *Med Image Anal* 4: 303–316.
- Mösges R, Schlöndorff G (1998) A new imaging method for intraoperative therapy control in skull base surgery. *Neurosurg Rev* 11: 245–247.
- Nakajima S, Kikinis R, Black PM, Atsumi H, Leventon ME, Hata N, Moriarty TM, Alexander III E & Jolesz FA (1997) Image-guided neurosurgery at Brigham and Women's Hospital. *Computer-Assisted Neurosurgery*: 144–162.
- NASA (2012) The official homepage of the National Aeronautics and Space and Administration. URI: <http://science.hq.nasa.gov/kids/imagers/ems/xrays.html/>. Cited 2012/3/7.
- Ng WS, Davies BL, Hibberd RD & Timoney AG (1993) Robotic surgery – a first hand experience in transurethral resection of the prostate. *Eng Med Biol* 12(1): 120–125.
- NDI Digital (2012). URI: <http://www.ndigital.com/medical/technology-optical.php/>. Cited 2012/4/11.
- Nimsky C (2011) Intraoperative MRI in glioma surgery: proof of benefit? *The Lancet Oncology* 12(11): 982–983.
- Nolte LP, Zamorano LJ, Jiang Z, Wang Q, Langlotz F, Arm E & Visarius H (1994) A novel approach to computer assisted spine surgery. Proceedings of the 1st Int Symp MRCAS: 323–328.
- Polaris Spectra & Polaris Vicra Technical Specifications, Northern Digital Inc. Waterloo, ON, Canada, 2011, URI: <http://www.ndigital.com/medical/polarisfamily-techspecs.php/>. Cited 2012/4/11.
- Ringel F, Stürer C, Reinke A, Preuss A, Behr M, Auer F, Stoffel M & Meyer B (2012) Accuracy of robot-assisted placement of lumbar and sacral pedicle screws: a prospective randomized comparison to conventional freehand screw implantation. *Spine* 37(8): E496–501.
- Ringel F, Ingerl D, OTT S & Meyer B (2009) VarioGuide: a new frameless image-guided stereotactic system - accuracy study and clinical assessment. *Neurosurg* 64(5 Suppl 2): 365–371.

- Riviere CN & Khosla PK (1997) Augmenting the human-machine interface: improving manual accuracy. Proceedings of IEEE Robotics & Automation, Albuquerque, NM, USA. (5): 3546–3550.
- Riviere CN, Rader RS & Khosla PK (1997) Characteristics of hand motion of eye surgeons. Proceedings of the 19th Annual International Conference of the IEEE Engineering in Medicine and Biology Society, Chicago, IL, USA: 1690–1693.
- Ruohonen J & Karhu J (2010) Navigated transcranial magnetic stimulation. Review. Clin Neurophys 40: 7–17.
- Russell T & Joskowicz L (2009) Computer-integrated surgery and medical robotics. In: Kurtz M (ed) Standard Hand-book of Biomedical Engineering and Design. McGraw-Hill 14: 391–437.
- Roberts DW, Strohbehn JW, Hatch JF, Murray W & Kettenberger H (1986) A frameless integration of computerized tomographic imaging and the operating microscope. J Neurosurg 65(4): 545–549.
- Sanai N & Berger MS (2008) Glioma extent of resection and its impact on patient outcome. Neurosurg 62(4): 753–764.
- Schenck J (1996) The role of magnetic susceptibility in magnetic resonance imaging: MRI magnetic compatibility of the first and second kinds. Med Phys 13(6): 815–850.
- Schicho K, Figl M, Donat M, Birkfellner W, Seemann R, Wagner A, Bergmann H & Ewers R (2005) Stability of miniature electromagnetic tracking systems. Phys Med Biol 50: 2089–2098.
- Schiffbauer H (1997) Neuronavigation in brain tumor surgery; clinical beta phase of the Neuronavigator System. PhD dissertation. Univ Oulu Depart Neurosurgery, Oulu, Finland.
- Schneberger M (2004) Infrared optical tracking systems mathematical and operational principles. Lecture: Intra-operative Imaging & Visualization URI: <http://campar.in.tum.de/twiki/pub/Chair/TeachingWs04IOIV/09StereoCameraTracking.pdf>. Cited 2012/4/11.
- Schneider M & Stevens C (2011). Development and testing of a new magnetic-tracking device for image guidance. URI: <http://www.asscension-tech.com/>. Cited 2011/11/22.
- Shiakolas P, Conrad K & Yih T (2002) On the accuracy, repeatability, and degree of influence of kinematics parameters for industrial robots. Int J Model Simul 22(3): 1–10.
- Simon D (1997) Intra-operative position sensing and tracking devices. Proceedings of the First Joint Conference on Computer Vision, Virtual Reality and Robotics in Medicine and Medical Robotics and Computer Assisted Surgery, CVRMed/MRCAS, Grenoble, France: 62–64.
- Song Y, Gang A & Zhang J (2009) Positioning accuracy of a medical robotic system for spine surgery. Proceedings of the 2nd International Conference of the Biomedical Engineering and Informatics, Tianjin, China: 1–5.

- Stiehl J, Bach J & Heck D (2007) Validation and metrology in CAOS. In: Stiehl J, Konermann W, Haaker R & DiGioia A (eds) *Navigation and MIS in Orthopedic Surgery*. Springer Medizin Verlag, Heidelberg, Germany. ISBN 978-3-540-36690-4: 68-78.
- Sutherland GR, Latour I & Greer AD (2008) Integrating an image-guided robot with intraoperative MRI. *IEEE Eng Med Biol Mag* 27(3):59–65.
- Susil RC, Krieger A, Derbyshire JA, Tanacs, Whitcomb LL, Fichtinger G, Atalar E (2003) System for MR image-guided prostate interventions: Canine study. *Radiology* 228: 886–894.
- Taylor RH & Kazanzides P (2007) Medical robotics and computer-integrated interventional medicine. In: Feng DD (ed) *Biomedical Information Technology*. Academic Press, Burlington, MA, USA: 393–415.
- Tronnier VM, Wirtz CR, Knauth M, Lenz G, Pastry O, Bonsanto MM, Albert FK, Kuth R, Staubert A, Schlegel W, Sartor K & Kunze S (1997) Intraoperative diagnostic and interventional magnetic resonance imaging in neurosurgery. *Neurosurg* 40(5): 891–901.
- Tsekos NV, Ozcan A & Christoforou E (2005) A prototype manipulator for MR-guided interventions inside standard cylindrical MRI scanners. *J Biomech Eng* 127: 972–980.
- Tsekos N, Christoforou E & Özcan A (2008) A general-purpose MR-compatible robotic system - Implementation and image guidance for performing minimally invasive interventions. *IEEE Eng Med Biol Mag* 3: 51–58.
- Vahala E, Ylihautala M, Tuominen J, Schiffbauer H, Katisko J, Yrjänä S, Vaara T, Enholm G & Koivukangas J (2001) Registration in interventional procedures with optical navigator. *JMRI* 13: 93–98.
- Virtanen J (2006) Enhancing the compatibility of surgical robots with magnetic resonance imaging. PhD thesis. Univ Oulu, Dept Mechanical Engineering.
- Watanabe E, Watanabe T, Manaka S, Mayanagi Y & Takakura K (1987) Three-dimensional digitizer (neuronavigators): New equipment for computed tomography-guided stereotactic surgery. *Surg Neurosug* 27(6): 543–547.
- Wells PNT (1977) Ultrasonics in medicine and biology. Review Article. *Phys Med Biol* 22(4): 629.
- Weng J, Cohen P & Herniou M (1992) Camera calibration with distortion models and accuracy evaluation. *IEEE Trans Pattern Anal and Mach Intell* 14(10): 965–990.
- West JB & Maurer CR Jr. (2004) Designing optically tracked instruments for image-guided surgery. *IEEE Trans Med Imaging* 23(5): 533–545.
- Widmann G, Schullian P, Ortler, M & Bale R (2012) Frameless stereotactic targeting devices: technical features, targeting errors and clinical results. *IJCARS* 8: 1–16.
- Wiles A & Peters T (2009) Real-time estimation of FLE statistics for 3-D tracking with point-based registration. *IEEE Trans Med Imaging* 28(9): 1384–1398.
- Wiles A, Thompson D, & Frantz D (2004) Accuracy assessment and interpretation for optical tracking systems. *Medical Imaging 2004: Visualization, Image-Guided Procedures, and Display*. In: (ed) Galloway R. Proc SPIE 5367: 421–432.

- Wittmann W, Wenger T, Loewe E & Lueth TC (2011). Official measurement protocol and accuracy results for an optical surgical navigation system (NPU). Proceedings of the 33rd Annual International Conference of the IEEE Engineering in Medicine and Biology Society, Boston, MA, USA: 1237–1240.
- Wood BJ, Zhang H, Durrani A, Glossip N, Sohan R, Lindisch D, Elliott L, Banovac F, Borgert J, Krueger S, Kruecker J, Anald V & Cleary K (2005). Navigation with electromagnetic tracking for interventional radiology procedures: A feasibility study. *Laboratory Investigations. J Vasc Interv Radiol* 16: 493–505.
- Yamura M, Hirai T, Korogi Y, Ikushima I, & Yamashita Y (2005) Quantitative evaluation of measurement accuracy for three-dimensional angiography system using various phantoms. *Radiat Med* 23(3): 175–181.
- Yang L, Wen R, Qin J, Chui C-K, Lim K-B & Chang S (2010) A robotic system for overlapping radiofrequency ablation in large tumor treatment. *IEEE/ASME Trans Mechatr* 15(6): 887–897.
- Zannoni C, Viceconti M, Pierotti L & Capello A (1997) Evaluation of CT accuracy in orthopaedic implants geometry reconstruction. Proceedings of the 19th Annual International Conference of the IEEE Engineering in Medicine and Biology Society, Chicago, IL, USA: 1862–1864.
- Zoppi M, Khan M, Schäfer F & Molfino R (2010). Toward lean minimally invasive robotic surgery. *Robotica* 28: 185–197.

ACTA UNIVERSITATIS OULUENSIS
SERIES C TECHNICA

411. Arvola, Jouko (2011) Reducing industrial use of fossil raw materials : Techno-economic assessment of relevant cases in Northern Finland
412. Okkonen, Jarkko (2011) Groundwater and its response to climate variability and change in cold snow dominated regions in Finland: methods and estimations
413. Anttonen, Antti (2011) Estimation of energy detection thresholds and error probability for amplitude-modulated short-range communication radios
414. Neitola, Marko (2012) Characterizing and minimizing spurious responses in Delta-Sigma modulators
415. Huttunen, Paavo (2012) Spontaneous movements of hands in gradients of weak VHF electromagnetic fields
416. Isoherranen, Ville (2012) Strategy analysis frameworks for strategy orientation and focus
417. Ruuska, Jari (2012) Special measurements and control models for a basic oxygen furnace (BOF)
418. Kropsu-Vehkaperä, Hanna (2012) Enhancing understanding of company-wide product data management in ICT companies
419. Hietakangas, Simo (2012) Design methods and considerations of supply modulated switched RF power amplifiers
420. Davidyuk, Oleg (2012) Automated and interactive composition of ubiquitous applications
421. Suutala, Jaakko (2012) Learning discriminative models from structured multi-sensor data for human context recognition
422. Lorenzo Veiga, Beatriz (2012) New network paradigms for future multihop cellular systems
423. Ketonen, Johanna (2012) Equalization and channel estimation algorithms and implementations for cellular MIMO-OFDM downlink
424. Macagnano, Davide (2012) Multitarget localization and tracking : Active and passive solutions
425. Körkkö, Mika (2012) On the analysis of ink content in recycled pulps
426. Kukka, Hannu (2012) Case studies in human information behaviour in smart urban spaces

Book orders:
Granum: Virtual book store
<http://granum.uta.fi/granum/>

UNIVERSITY OF OULU P.O.B. 7500 FI-90014 UNIVERSITY OF OULU FINLAND

A C T A U N I V E R S I T A T I S O U L U E N S I S

S E R I E S E D I T O R S

A SCIENTIAE RERUM NATURALIUM

Senior Assistant Jorma Arhipainen

B HUMANIORA

Lecturer Santeri Palvainen

C TECHNICA

Professor Hannu Heusala

D MEDICA

Professor Olli Vuolteenaho

E SCIENTIAE RERUM SOCIALIUM

Senior Researcher Eila Estola

F SCRIPTA ACADEMICA

Director Sinikka Eskelinen

G OECONOMICA

Professor Jari Juga

EDITOR IN CHIEF

Professor Olli Vuolteenaho

PUBLICATIONS EDITOR

Publications Editor Kirsti Nurkkala

ISBN 978-951-42-9903-2 (Paperback)

ISBN 978-951-42-9904-9 (PDF)

ISSN 0355-3213 (Print)

ISSN 1796-2226 (Online)

UNIVERSITY of OULU
OULUN YLIOPISTO

